SYSTEMATIC INVESTIGATION OF MODELS OF HELICOPTER WITH A SLUNG LOAD

by

B. L. Nagabhushan

Dissertation submitted to the Graduate Faculty of the
Virginia Polytechnic Institute and State University
in partial fulfillment of the requirements for the degree of

DOCTOR OF PHILOSOPHY

in

Aerospace Engineering

APPROVED:

E. M. Cliff, Chairman

F. H. Lutze

L. Meirovitch

T. A. Weisshaar

H. L. Johnson

February, 1977
Blacksburg, Virginia

ACKNOWLEDGEMENT

I sincerely thank my advisor, Professor Eugene M. Cliff for his guidance, encouragement and criticisms during this research work. His insight into complex physical systems through simple analytical models has been very helpful in this study.

I am grateful to Professor Frederick H. Lutze for his valuable suggestions and comments which have enhanced this accomplishment.

I wish to thank Professor Terrance A. Weisshaar, Professor Leonard Meirovitch and Professor James A. Cochran for serving on my advisory committee and for helping in the final documentation of this thesis.

I express my gratitude to Professor Joseph A. Schetz and the Department of Aerospace and Ocean Engineering for providing financial assistance to pursue my graduate studies.

The author is indebted to Mrs. Lois Heising for her meticulous typing and thanks Goodyear Aerospace Corporation, Akron, Ohio, for helping in the preparation of this dissertation.

This work is dedicated to my loving parents Lakshminarayana Swamy and Subbagowramma.

CONTENTS

CONTENTS [Cont'd]

LIST OF FIGURES

LIST OF FIGURES [CONT'D]

LIST OF TABLES

LIST OF TABLES [CONT'D]

NOMENCLATURE

a	Slope of the lift curve (rad.$^{-1}$)
A	Area (m^2)
b	Number of blades
B	Tip loss factor
c	Chord length (m)
C	Force or Moment Coefficient
D	Aerodynamic drag (N) Rotor diameter (m)
e	Hinge-offset distance from rotor shaft (m)
F	External Force (N)
g	Acceleration due to gravity (m/s^2)
h	Rotor shaft length (m)
h_p	Vertical location of the load suspension point from vehicle center of mass (m)
i	Imaginary number = $\sqrt{-1}$ Unit vector in x-direction
I	Moment of Inertia (kg.m^2)
j	Unit vector in y-direction
k	Unit vector in z-direction
K_v, K_L	Drag constant of vehicle and load respectively
K_G	Glauerts factors
ℓ	Length of suspension cable (m)
ℓ_t	Tail length (m)
ℓ_{tr}	Horizontal distance between tail rotor axle and vehicle center of mass (m)

NOMENCLATURE [Cont'd]

ℓ_p	Horizontal distance between suspension point and vehicle center of mass (m)
L	Lagrangian, Rolling moment (N.m) Lift (N)
m	Mass (kg)
M	Pitching moment (N.m)
n	Unit normal
N	Yawing moment (N.m)
p	Roll velocity of the vehicle (rad./s)
q	Pitch velocity of the vehicle (rad./s) Generalized coordinate
Q	Non-potential force, Rotor torque (N.m)
r	Yaw velocity of the vehicle (rad./s)
R	Rotor blade radius (m), Resultant force (N)
S	Surface area (m^2), Eigenvalue
t	time (s)
T	Thrust (N)
u	Velocity component in the direction of x-axis (m/s)
U	Total Velocity (m/s), Control matrix
v	Velocity component in the direction of y-axis (m/s)

NOMENCLATURE [Cont'd]

w	Velocity component in the direction of z-axis (m/s)
W	Weight (N)
X	Column matrix of state variables
z_{tr}	Vertical distance between the tail rotor axle and vehicle center of mass (m)

Greek

α	Angle of attack (rad.)
β	Blade flapping angle (rad.)
γ	Rotor blade Lock number
ζ	Rotor blade lag angle (rad.)
η	Chordwise distance of blade element from the hinge
θ	Pitch angle (rad.)
λ	Rotor inflow ratio, Azimuthal displacement of the load from x-axis of the Local Horizon System [see Figure 2.1]
μ	Rotor advance ratio
ξ	Spanwise location of a blade element from the hinge
ρ	Air density (g/m^3)
σ	Rotor blade solidity ratio, Modal damping
ϕ	Roll angle (rad.)
ψ	Rotor blade azimuth angle (rad.)
ω	Modal frequency (rad./s)

Greek

Ω	Rotor angular velocity (rad./s)

Subscripts and Superscripts

$( )_v$, $( )^v$	Vehicle
$( )_L$, $( )^L$	Load
$( )_e$, $( )^e$	Steady state value
k, l, m	Dummy indices
$( )_I$	Inertial coordinate
$( )_P$	Suspension point
$( )_S$	System, shaft
$( )_t$	Tail
$( )_{tr}$	Tail rotor
$( )^f$	Fuselage
$( )_f$	Freestream
$( )_i$	Induced
$( )_{R,D}$	Rotor, Disc, respectively
$( )_B$	With reference to blade
$( )_T$	Of Thrust
$( )_H$	With reference to hub
$(\hat{})$	Nondimensional quantity
$( )_n$	Normal component

Subscripts and Superscripts [Cont'd]

$(\bar{\ })$	Column vector
$(\underline{\ })$	Matrix
$(\dot{\ })$	Derivative with respect to time

Abbreviations

KE	Kinetic Energy
PE	Potential Energy
np	non-potential
cm	center of mass
PMM	Point Mass Model
PVDR	Point mass Vehicle Disc Rotor
RVDR	Rigid body Vehicle Disc Rotor
RVAR	Rigid body Vehicle Articulated Rotor
RVARQ	Rigid body Vehicle Articulated Rotor Quasi-statics
(XY2) (XY2, Page 10)	Indicates reference to a book or a publication. The alphabets refer to the first two letters of the authors last name. The number indicates the sequence in the present reference.
$1 \leq \ell \leq 64 (*4)$ $0.1 \leq \hat{m} \leq 1.5 (0.4)$	The variation in parameter values is abbreviated as follows: ℓ varies from 1m to 64m in multiples (*) of 4. $\hat{m}$ varies from 0.1 to 1.5 in steps of 0.4.

CHAPTER I

INTRODUCTION

1.1 Statement of the Problem

In efforts to conserve our natural resources and effectively utilize the current technology in meeting our demands, there is a growing need for transporting large and bulky objects to remote areas which may not be accessible to conventional aircrafts and land or sea vehicles. Often the cargos are too big to be carried internally. Consequently, a new generation of VTOL [Vertical Take-Off and Landing] vehicles, particularly helicopters, with heavy lift capabilities are presently being considered for development. These vehicles would carry the cargo externally. In order to realize the full potential of such a vehicle, it is essential that the motion of the vehicle-load configuration be analyzed to determine its stability characteristics. In this thesis the flight mechanics and control of a configuration that consists of a helicopter carrying a singly tethered load is analyzed, using several mathematical models that describe the dynamics of the system in varying complexity. The simpler models of the helicopter/load system are utilized, wherever possible, for better understanding of the system dynamics described by more complex models developed subsequently. One of the objectives

of this work is to determine the validity of using these simple models for stability analyses, for a given design and flight conditions. In the present analysis the system stability in uniform translation and in a steady turn is analyzed. The effect of varying some of the principal parameters of the configuration, on the inherent motion of the helicopter as well as that induced by the load are determined. Using a sixth order model of the helicopter a stability augmentation scheme is designed, which is then modified for application to a more complex model [fifteenth order] of the vehicle.

1.2 Previous Analyses and Related Studies

Albeit VTOL vehicle dynamics has been extensively studied in the past, it has not been analyzed in a configuration, such as considered here, till recently. Substantial work has been done on aerodynamic instabilities of a suspended object where the vehicle motions have not been considered. Poli (PO1) and Etkin (ET1) have examined the aerodynamic stability of towed objects but have neglected the vehicle-load interaction. Although these and similar analyses are helpful in curing the aerodynamic instabilities of the load, they are insufficient to ensure a stable configuration. The present analysis reveals that this interaction is an important factor in determining the stability

of the system.

Recently several studies have been made in which the stability and control of a helicopter-load system was analyzed in some detail. Abzug (AB1) derived the perturbation equations of motion for a configuration in which both the helicopter and load are modeled as rigid bodies connected by two inextensible tethers. The modes of motion were obtained in the absence of aerodynamics. Subsequently Liu (LI1) extended Abzug's analysis to include aerodynamics and analyzed the stability of a CH-47 helicopter carrying several typical loads. Lucassen (LU1) studied vertical plane motion of a helicopter/load configuration in hover while Dukes (DU1) analyzed the system stability in typical maneuvers. Gupta (GU1) examined the stability and control of a helicopter with a slung load in a case where the vehicle is hovering near ground. Clift (CL1) determined the dynamic stability in forward flight using a point mass model of the helicopter and load. Although these analyses have resulted in a better insight into the dynamics of a vehicle-load system it would perhaps be naive to utilize these predictions without a systematic study that would reveal the validity of some of the approximations and simplifications made in them as well as provide a better understanding of the vehicle-load motion.

Flight test results of a helicopter with a slung load have been reported by Gabel (GA1) and Hutto (HU1). Boeing Vertol Company (BO1) has demonstrated the use of active controls to stabilize the load induced motion of the helicopter/load system in flight. These results are more appropriate for evaluation than prediction.

1.3 Contributions of this Study

Several mathematical models that describe the dynamics of a helicopter-load configuration in varying complexity have been systematically analyzed to determine the stability characteristics of the vehicle and load motion.

The simplest model [seventh order] consists of a point mass helicopter which has a thrust force acting on it. The load is also assumed to be a point mass and is suspended from the helicopter by a rigid link. Stability of the system in forward flight has been determined for the cases where (a) the thrust vector is fixed in the inertial space, (b) the thrust vector is fixed with respect to the vehicle velocity vector. The dynamic stability of the system in a steady coordinated turn is also examined by using this model.

A more realistic model [twelfth order] of this configuration is developed by considering the helicopter to be a

rigid body that has an actuator disc for a rotor, which is connected to the fuselage by a rigid shaft. The rotor disc has pitch and roll degrees of freedom with respect to fuselage and responds to fuselage pitch and roll velocities, like a real articulated rotor. This model also includes the conventional helicopter components like tail rotor and stabilizer. The load is assumed to be a point mass and is suspended from the fuselage in its plane of symmetry. Using this representation of the vehicle-load system, nonlinear equations of motion are derived and linearized about a steady level flight condition. These equations are utilized to examine the dynamic stability of the system in uniform translation. The effects of varying some of the principal parameters of the configuration on the system stability have been determined.

Subsequently the disc rotor is replaced by a real articulated rotor with rigid blades that are hinged at an offset. General equations of motion of a single rotor blade (HA1) have been specialized to consider only the out of plane motion of the blades which is described by the blade flapping equation. Using an approximate flapping angle, the flapping equation is linearized about an equilibrium point corresponding to steady level flight of the helicopter. These perturbation equations are combined with

corresponding equations of the fuselage-load system to obtain the complete system [eighteenth order] equations. The stability characteristics of the system, as predicted by this model, have been determined and compared with similar results obtained from simpler models.

In order to augment the stability of the vehicle/load motion, a regulator is designed for the helicopter in forward flight by using a lower order model [sixth] of the vehicle that has a disc rotor. This time invariant control law is subsequently adapted to the helicopter models that include an articulated rotor as well. Closed loop stability of the helicopter in the presence of a suspended load has been examined for various design and flight conditions.

Finally the adequacy and limitations of each of the above models in a particular analysis of the configuration are indicated.

1.4 Organization of this Thesis

In Chapter II a simple model of the helicopter-load system is considered in which both the vehicle and load are assumed to be point masses connected by a rigid link. The vehicle has a thrust force acting on it. The only aerodynamic forces considered are the drag of the vehicle and

load. The nonlinear equations of motion are linearized about a steady level flight condition as well as about a steady turning flight condition and the corresponding stability of the system are determined. The effect of vehicle thrust orientation on the vehicle/load stability is examined for the cases where (a) the thrust vector is fixed in space (b) the thrust vector is fixed relative to the helicopter velocity vector.

Chapter III presents more complex models of the system where the vehicle thrust is assumed to be generated by a rigid rotor disc that has pitch and roll degrees of freedom with respect to a Local Horizon System. This model of the rotor is first included in the point mass model considered in Chapter II and the stability characteristics observed here are compared with corresponding results obtained previously. Subsequently the vehicle is assumed to be a rigid body with conventional helicopter components like tail rotor and stabilizer. The main rotor, which is modeled as a rigid disc, is connected to the fuselage by a rigid shaft at the vehicle center of mass. The load is again assumed to be a point mass and is suspended from the fuselage from a point in its plane of symmetry. The dynamical equations for this model of the system are derived by Lagrange's method. Forward flight stability of the system

is examined for various values of principal parameters of the configuration.

In Chapter IV the equations of motion of an articulated rotor blade, used by Hall (HA1), are specialized to consider only the out of plane motion of the blades, which is described by the blade flapping equation. Using an approximate flapping angle, given by its constant and first harmonic content, the flapping equation is linearized about an equilibrium point corresponding to steady level flight of the helicopter. The average aerodynamic forces generated by an articulated rotor are evaluated and expressed as components along the vehicle axes.

In Chapter V the results obtained in Chapter IV are applied to the fuselage and load system discussed in Chapter III to form a complete set of perturbation equations of motion of rotor-fuselage-load system, about an equilibrium point corresponding to uniform translation. Using these equations the stability of the system is examined as before and compared with those predicted previously. A lower order model of the system that consists of a quasi-static rotor is also analyzed to determine the effect of rotor dynamics on the system stability in forward flight.

From these analyses it is found that the inherent

motion of the vehicle could become unstable in the presence of a load and that the dynamics of the load induces additional oscillatory motion of the helicopter which may or may not be stable. Consequently in Chapter VI a stability augmentation system is designed to realize satisfactory stability characteristics of the vehicle-load configuration in forward flight. For the purpose of this design a simple model of the helicopter that has a rigid body fuselage and a disc rotor is used. Only forward, lateral, pitching and rolling motion of the vehicle are considered in this case. A relation between a set of controls of the rotor disc and collective and cyclic pitch angles of an articulated rotor is developed and used to obtain an equivalent steady state control law apt for application to a helicopter model with a real articulated rotor. The closed loop performance of the helicopter with this regulator, in the presence of a suspended load, is examined for various design and flight conditions.

Chapter VII presents the principal conclusions of this study and recommendations for further analyses.

CHAPTER II

SYSTEM MODEL WITH POINT MASSES (PMM)

2.1 Introduction

A simple model of the helicopter load system is derived by assuming both the vehicle and load to be point masses connected by a rigid, massless link. The forces acting on the helicopter include its weight, aerodynamic drag and a thrust force. Also, the weight and aerodynamic drag of the load are considered. The system equations of motion are derived by using Lagrange's method. Stability of the system in steady, level flight and turning flight conditions are analyzed by linearizing the nonlinear equations about the correspondingly chosen equilibrium points. The effect of vehicle thrust orientation on the system stability is examined for the following cases,

(a) The thrust vector is fixed in space

(b) The thrust vector is fixed relative to the vehicle velocity vector.

2.2 Equations of Motion

Figure 2.1 shows the model of the helicopter-load system. The motion of the helicopter is described in terms of the Local Horizon System (LHS) (MI 1, page 43) whose origin is at the center of mass of the vehicle, while motion of the

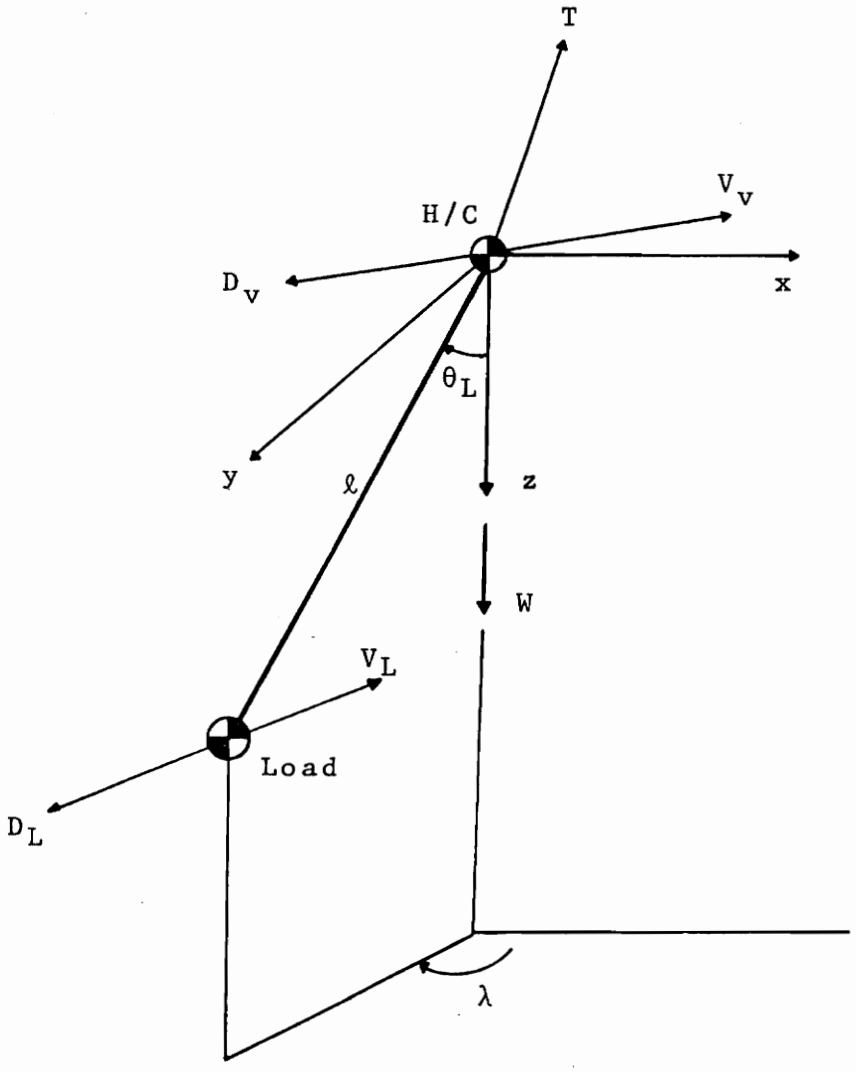

Figure 2.1 - Helicopter-Load Point Mass Model

load, relative to the vehicle, is described by polar angle θ_L and azimuth angle λ. A thrust force T acts on the vehicle as shown. The only aerodynamic forces considered are the drag of the vehicle and load which are evaluated by square speed law ($D = KV^2$). In order to derive the Lagrange's equations of motion of the system, the Lagrangian L is evaluated in terms of the system coordinates as

$$L = T - V \tag{2.1}$$

where

$$T = \tfrac{1}{2} m_v V_v^2 + \tfrac{1}{2} m_L V_L^2$$

$$= \tfrac{1}{2} m_v [\dot{x}^2 + \dot{y}^2 + \dot{z}^2] +$$

$$\tfrac{1}{2} m_L [(\dot{x} + \ell\dot{\theta}_L \cos\theta_L \cos\lambda -$$

$$\ell\dot{\lambda} \sin\theta_L \sin\lambda)^2 + (\dot{y} +$$

$$\ell\dot{\theta}_L \sin\lambda \cos\theta_L + \ell\dot{\lambda} \sin\theta_L \cos\lambda)^2$$

$$+ (\dot{z} - \ell\dot{\theta}_L \sin\theta_L)^2]$$

and

$$V = -(m_v + m_L)\, gz - m_L g \ell \cos\theta_L$$

this should be $V = (m_v + m_L)\, gz - m_L g \ell \cos\theta_L$ (typo)

In general, the Lagrange's equations of motion of an n degree of freedom system, described by generalized coordinates q_k, k = 1, 2, ... n, are in the form [ME 1, page 76]

$$\frac{d}{dt}\left(\frac{\partial L}{\partial \dot{q}_k}\right) - \frac{\partial L}{\partial q_k} = Q_{k_{np}}$$

Using this formulation and Equation 2.1, the following equations of motion are obtained:

$$(m_v + m_L)\,\dot{u} + m_L\,[\ell\dot{q}_L \cos\theta_L \cos\lambda - \ell\dot{r} \sin\theta_L \sin\lambda - \ell\,(q_L^2 + r^2) \sin\theta_L \cos\lambda - 2\ell q_L r \cos\theta_L \sin\lambda] = Q_x \qquad (2.2)$$

$$(m_v + m_L)\,\dot{v} + m_L\,[\ell\dot{q}_L \cos\theta_L \sin\lambda + \ell\dot{r} \sin\theta_L \cos\lambda + 2\ell q_L r \cos\theta_L \cos\lambda - \ell(q_L^2 + r^2) \sin\theta_L \sin\lambda] = Q_y \qquad (2.3)$$

$$(m_v + m_L)\,\dot{w} - m_L \ell q_L^2 \cos\theta_L - m_L \ell \dot{q}_L \sin\theta_L - (m_v + m_L)g = Q_z \qquad (2.4)$$

$$m_L \ell \cos\theta_L \cos\lambda\,\dot{u} + m_L \ell \cos\theta_L \sin\lambda\,\dot{v} - m_L \ell \sin\theta_L\,\dot{w} + m_L \ell^2 \dot{q}_L - m_L \ell^2 r^2 \sin\theta_L \cos\theta_L + m_L g \ell \sin\theta_L = Q_{\theta_L} \qquad (2.5)$$

$$m_L \ell^2 \sin^2\theta_L\,\dot{r} + 2m_L \ell^2 \sin\theta_L \cos\theta_L\, q_L r - m_L \ell \sin\theta_L \sin\lambda\,\dot{u} + m_L \ell \sin\theta_L \cos\lambda\,\dot{v} = Q_\lambda \qquad (2.6)$$

(Note: In the above equations, $u = \dot{x}$, $v = \dot{y}$, $w = \dot{z}$, $q_L = \dot{\theta}_L$ and $r = \dot{\lambda}$.)

The nonpotential forces, Q_x, Q_y ... Q_λ, due to the aerodynamic drag of the vehicle and load and vehicle thrust are derived in terms of the system coordinates by using the principle of virtual work [ME 1, page 59] and are given by

$$Q_x = T_x - K_v V_v u - K_L V_L (u + \ell q_L \cos\theta_L \cos\lambda - \ell r \sin\theta_L \sin\lambda)$$

$$Q_y = T_y - K_v V_v v - K_L V_L (v + \ell q_L \cos\theta_L \sin\lambda + \ell r \sin\theta_L \cos\lambda)$$

$$Q_z = T_z - K_v V_v w - K_L V_L (w - \ell q_L \sin\theta_L)$$

$$Q_{\theta_L} = K_L V_L (u\ell \cos\theta_L \cos\lambda + v\ell \cos\theta_L \sin\lambda - w\ell \sin\theta_L + \ell^2 q_L)$$

$$Q_\lambda = - K_L V_L (-u\ell \sin\theta_L \sin\lambda + v\ell \sin\theta_L \cos\lambda - \ell^2 r \sin^2\theta_L)$$

where K_v and K_L are the drag constants of the helicopter and load respectively.

2.3 Stability and Control in Forward Flight

The equations of motion (2.2 - 2.6) are nonlinear and are coupled in the vehicle-load dynamics. Stability analysis of the system in uniform translation requires that the general equations of motion be linearized about a steady forward flight condition. Consequently, the equilibrium point is chosen to be level flight ($u = u^e$, $v^e = w^e \equiv 0$) where the load and the vehicle are in the same vertical plane ($\lambda^e = \pi$). The perturbation equations are put in the form

$$\underline{B}\dot{\overline{X}} = \underline{A}\overline{X} + \overline{F} \qquad (2.7)$$

where the state vector, $\overline{X}^T = (u\ w\ \theta_L\ q_L\ v\ \lambda\ r]$ and forcing function, $\overline{F}^T = [T_x\ T_z\ 0\ 0\ T_y\ 0\ 0]$.

In Equation 2.7 additional kinematic equations,

$$\dot{\theta}_L - q_L = 0,\ \dot{\lambda} - r = 0$$

have been introduced. Matrices A and B are given in Appendix A. Note that the perturbations of the variables are given by the same symbols as the original variables. The perturbations in thrust components T_x, T_y and T_z are, in general, functions of the perturbations in the vehicle states and are dependent on the thrust vector representation in the model.

Case (a) Thrust Vector Fixed in Space

In case (a) the vehicle thrust vector is assumed to be constant at its equilibrium value, such that the perturbations in its components along LHS are zero. Consequently in Equation 2.7 $\overline{F} = 0$, and hence, it is observed that the linearized equations are uncoupled in longitudinal and lateral motion, which are described by corresponding equations.

Longitudinal Motion:

$$\dot{\overline{X}}_{LG} = \underline{A}_{LG}\, \overline{X}_{LG},\ \overline{X}_{LG}^{T} = [u\ w\ \theta_L\ q_L]$$

Lateral Motion:

$$\dot{\overline{X}}_{LT} = \underline{A}_{LT}\, \overline{X}_{LT},\ \overline{X}_{LT}^{T} = [v\ \lambda\ r]$$

where $\underline{A}_{LG}$ and $\underline{A}_{LT}$ are upper and lower diagonal blocks respectively, in the matrix $\underline{B}^{-1}\underline{A}$, evaluated from Equation 2.7. The stability of the system is examined by determining the eigenvalues of the longitudinal and lateral system matrices. As a typical example, a helicopter of mass 3000 kg and flying at 20 m/s is considered. The load is assumed to have a mass of 1500 kg ($\hat{m} = 0.5$) and has drag coefficient $C_{D_L} = 1$, equivalent to that of a conex box of dimensions 2.44m × 2.44m × 6.09m (P01). It is suspended by a cable of length 4m. [These parameter values are used as nominal values in

the subsequent analysis.] Table I shows the corresponding modes and modeshapes of the system [see Appendix B]. It is observed that the lateral and longitudinal oscillatory modes [S_1, S_2, respectively] are stable and involve coupled motion of the vehicle and load. The ratio of changes in the lateral component of the linear momentum of the helicopter to that of the load in mode S_1 is found to be

$$\left(\frac{p_H}{p_L}\right)_Y = \frac{m_v v}{m_L (v - \ell \sin\theta_e r_L)} = 1.0039 \underline{/-178°}$$

Physically this may be construed as the motion of the vehicle and load being such, that they move in opposite directions with velocities inversely proportional to their masses so that the center of mass of the system remains stationary. Similar observations are also made with reference to horizontal and vertical motions predicted in mode S_2. The real roots correspond to the convergence of helicopter velocity components.

Case (b) Thrust Vector Fixed in Wind Axes System [WAS]

In this case the thrust vector is assumed to be fixed relative to the helicopter velocity vector. Consequently, the perturbations of the components of the thrust in the directions of the flight path, normal to the flight path in the vertical and horizontal planes [e_t, e_n, e_o] are assumed

Table I - PMM Case(a): Modes and Mode Shapes [Nominal Parameter Values]

EIGENVALUES AND EIGENVECTORS

$S_1 = -0.0184 \pm 1.922i$

v = 0.131 (0)
λ = 0.520 (90)
r_L = 1.000 (-1)

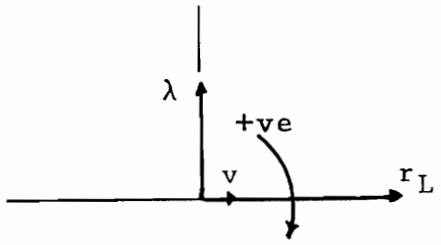

$S_2 = -0.0367 \pm 1.922i$

u = 1.000 (0)
w = 0.099 (-1)
θ_L = 0.391 (89)
q_L = 0.753 (-2)

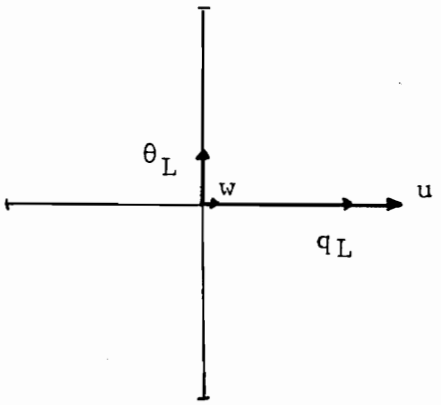

$S_3 = -0.0507$

u = 1.00 (0)
w = 0
θ_L = 0.466E-02(0)
q_L = 0.236E-03(180)

$S_4 = -0.0254$

v = 1.00 (0)
λ = 0.238E-01(0)
r_L = 0.604E-03(0)

$S_5 = -0.0254$

w = 1.0
u = 0.218E-04(0)
θ_L = 0.230E-03(0)
q_L = 0

to be zero. Equation 2.8 gives the coordinate transformation from the LHS to the WAS in terms of vehicle flight path angle γ and heading angle ψ. Since the vehicle is in uniform

$$\begin{Bmatrix} e_t \\ e_n \\ e_o \end{Bmatrix} = \begin{bmatrix} \cos\gamma\cos\psi & \cos\gamma\sin\psi & -\sin\gamma \\ \sin\gamma\cos\psi & \sin\gamma\sin\psi & \cos\gamma \\ \sin\psi & -\cos\psi & 0 \end{bmatrix} \begin{Bmatrix} e_x \\ e_y \\ e_z \end{Bmatrix} \tag{2.8}$$

translation, it is assumed that $\gamma^e = \psi^e = 0$. Correspondingly, the steady state values of the thrust components in WAS and their perturbations about the equilibrium point are respectively

$$T_t{}^e = T_x{}^e,\ T_n{}^e = T_z{}^e,\ T_o{}^e = -T_y{}^e$$

$$T_t = T_x + T_y{}^e\psi - T_z{}^e\gamma$$

$$T_n = T_x{}^e\gamma + T_z$$

$$T_o = T_x{}^e\psi - T_y$$

It is now required that $T_t = T_n = T_o \equiv 0$ which yields the equivalent thrust perturbations in LHS. Similarly, using Equation 2.8, the perturbations in γ and ψ are obtained

in terms of the corresponding perturbations in the helicopter velocity components in LHS as

$$\psi = \left(\frac{1}{u_e} \right) v$$

$$\gamma = \left(-\frac{1}{u_e} \right) w$$

Combining the above results the equivalent thrust perturbations in the LHS are

$$\begin{aligned} T_x &= [(m_v + m_L)\ (g/u_e)]w \\ T_y &= [(K_v + K_L)\ u_e]v \\ T_z &= [(K_v + K_L)\ u_e]w \end{aligned} \qquad (2.9)$$

Introducing Equation 2.9 in 2.7 the equations are rearranged in the normal form $\dot{\overline{X}} = \underline{A}\overline{X}$ where $\overline{X}$ has already been defined in Equation 2.7. It is observed that these linearized equations are also uncoupled in longitudinal and lateral motion.

A detailed stability analysis of this model can be found in reference (CL 1) where criteria for dynamic and static stability of the system have also been derived. For the same nominal parameter values as considered in case (a) the system modes predicted by this model are given in Table

II. Modes S_1 and S_2, respectively, correspond to the lateral and longitudinal oscillatory motion of the system. The damping ratio of these modes are found to be smaller compared to that predicted in case (a). S_3 corresponds to helicopter forward speed convergence. One of the zero eigenvalues (S_4) corresponds to rigid, lateral motion of the system in the horizontal plane, indicating lack of preferred heading. The other zero eigenvalue (S_5) indicates rigid, longitudinal motion of the system in the vertical plane.

The damping ratios and frequencies of the oscillatory modes of the system are found to vary considerably with values of the parameters $\hat{m}$, u^e and ℓ. It is observed that increasing $\hat{m}$ or decreasing u^e tends to decrease the dampings of these modes [Figure 2.2, 2.3]. This may be explained by noting that in either case the acceleration due to drag is decreased and hence the damping decreases. The increase in frequencies of oscillation due to increase in $\hat{m}$ is easily interpreted by considering a simple example where a mass m_L is suspended from another mass m_V, which is free to move in the horizontal plane [Figure 2.4]. The frequencies of oscillation of this system are given by $[(1 + \hat{m})\ g/\ell]^{\frac{1}{2}}$, which explains the previous observation. It is also observed that increasing ℓ decreases the frequencies of these modes [Table III]. The aperiodic motion of the system is

Table II - PMM Case(b): Modes and Mode Shapes [Nominal Parameter Values]

EIGENVALUES AND EIGENVECTORS

$S_1 = -0.0121 \pm 1.922i$

$v = 0.131\ (0)$

$\lambda = 0.520\ (89)$

$r_L = 1.000\ (-1)$

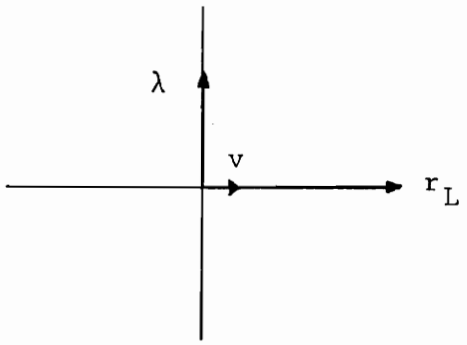

$S_2 = -0.0246 \pm 1.921i$

$u = 1.000(0)$

$w = 0.098(-2)$

$\theta_L = 0.392(0)$

$q_L = 0.752(-3)$

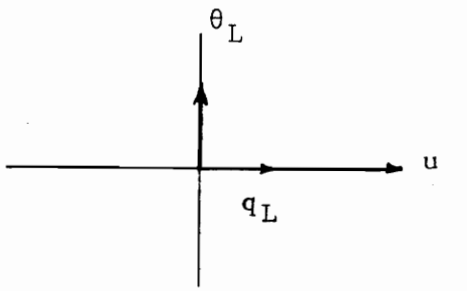

$S_3 = -0.0507$

$u = 1.000(0)$

$\theta_L = 0.466E-02(0)$

$q_L = 0.236E-03(180)$

$S_4 = 0$

$v = 1.000(0)$

$\lambda = 0.049(0)$

$S_5 = 0$

$u = 1.000(0)$

$w = 0.103(0)$

$\theta_L = 0.978E-02(0)$

$q_L = 0$

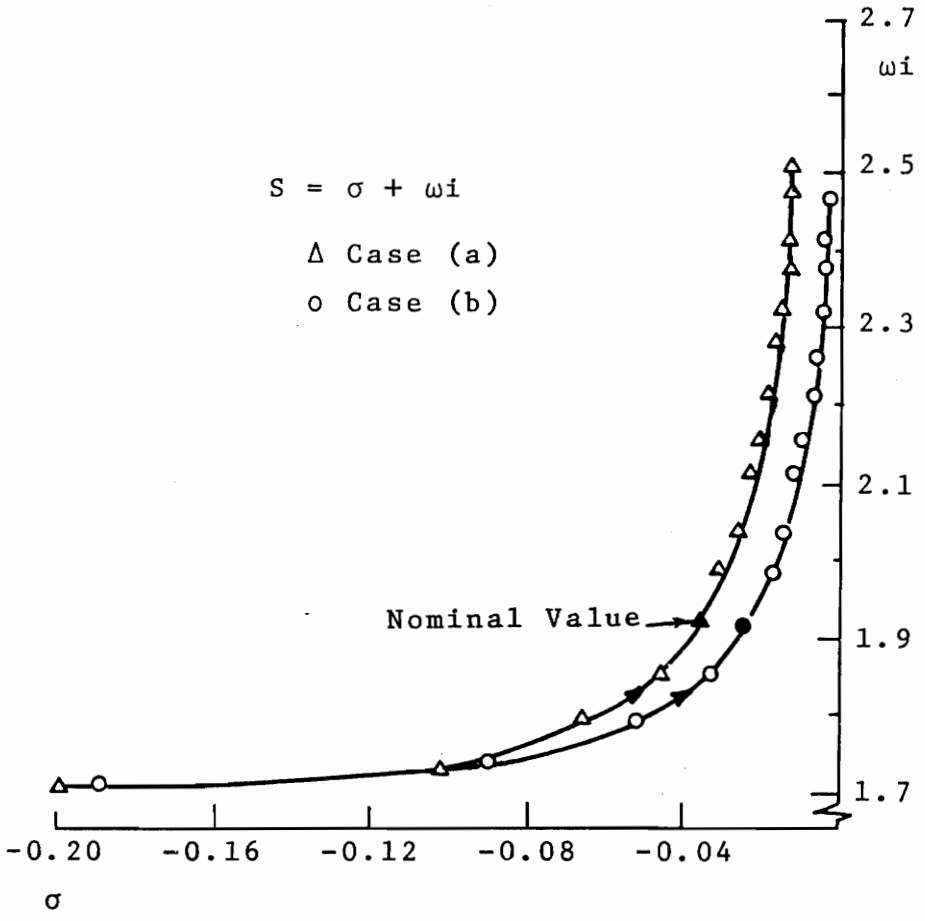

Figure 2.2 - PMM: Effect of $\hat{m}$ on Longitudinal Oscillatory Mode [$0.1 \leq \hat{m} \leq 1.5(0.1)$]

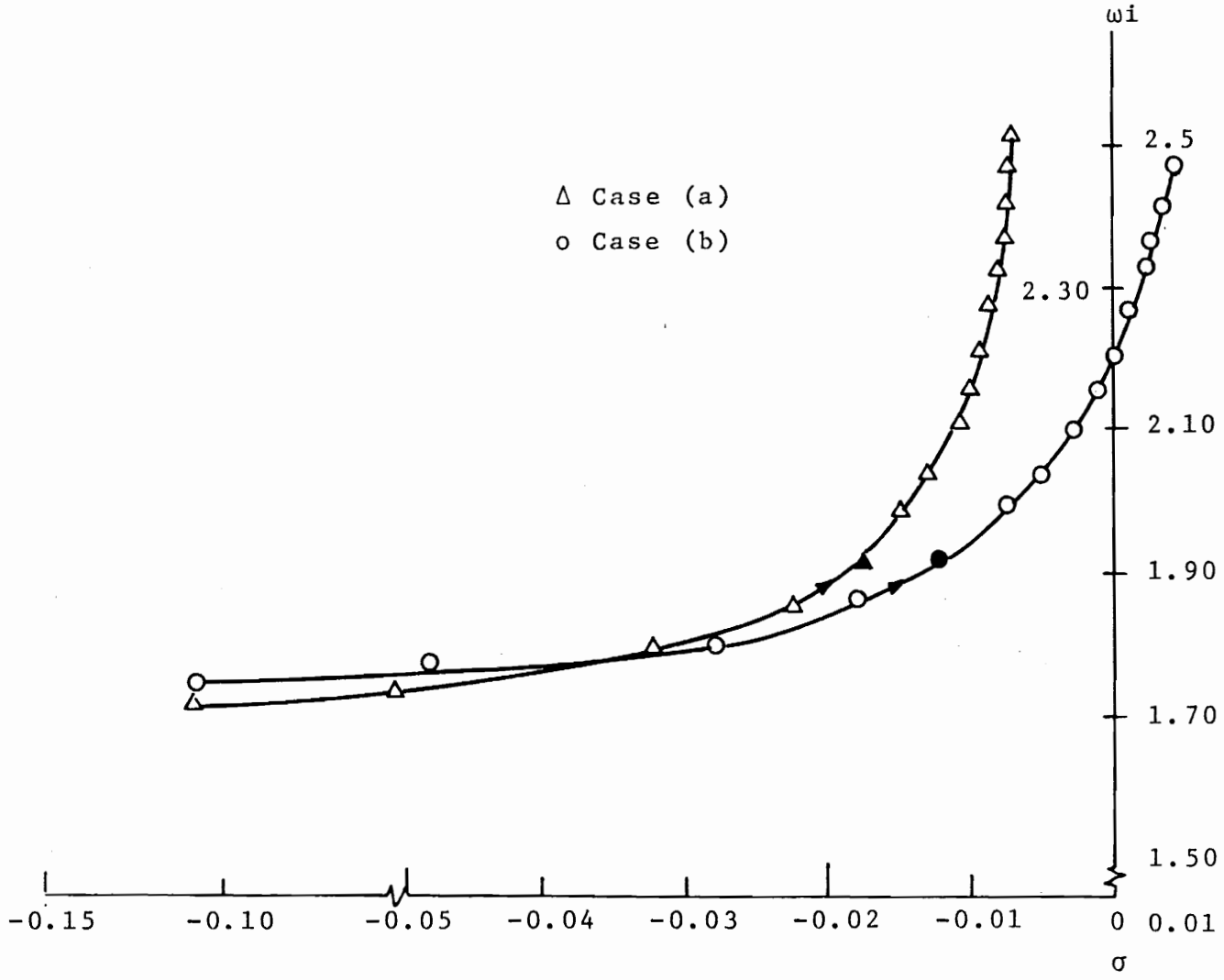

Figure 2.3 - PMM: Effect of $\hat{m}$ on Lateral Oscillatory Mode [$0.1 \leq \hat{m} \leq 1.5(0.1)$]

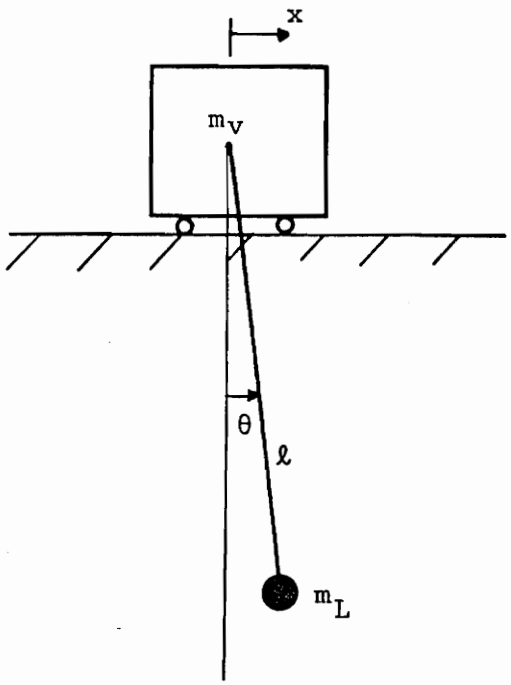

Figure 2.4 - Equivalent System of Vehicle and Load [Aerodynamic Drag is Neglected]

Table III - PMM Case(b): Effect of Parameters u_e, ℓ and C_D^L on System Oscillatory Modes

Parameter	Longitudinal Oscillatory Modes	Lateral Oscillatory Modes
u_e = 5 m/s	-0.00619 ±1.918i	-0.00303 ±1.918i
u_e = 30 m/s	-0.0363 ±1.939i	-0.0182 ±1.940i
ℓ = 4m	-0.0247 ±1.921i	-0.0121 ±1.922i
ℓ = 64m	-0.0245 ±0.477i	-0.0121 ±0.479i
C_{D_L} = 0.4	-0.00402 ±1.918i	-0.0113 ±1.918i
C_{D_L} = 1.0	-0.0247 ±1.921i	-0.0121 ±1.922i

little affected over the range of parameter values considered here.

2.4 System Stability in Steady Turn

In order to examine the stability of vehicle-load motion in a coordinated turn in the horizontal plane, the nonlinear equations 2.2 - 2.6 in the LHS are transformed to those in the flight path coordinates [also derived in CL 1] by using the transformation defined in Equation 2.8 consequently the vehicle motion is described by its velocity V, flight path angle γ and heading angle ψ, while the relative motion of the load with respect to the vehicle is described by θ_L and λ as considered previously. The transformed equations of motion are linearized about a steady turning flight condition specified by the equilibrium point $v = u^e$, $\gamma = \gamma^e = 0$, $\dot{\psi} = \dot{\psi}^e = c$, $\theta_L = \theta_L{}^e$, $r_L = r_L{}^e = c$. For convenience a new coordinate $\beta \triangleq \lambda - \psi$ is introduced in place of ψ. The corresponding steady state conditions, necessary for equilibrium, are

$$T_t{}^e = K_v u_e{}^2 - m_L \ell c^2 \cos\beta^e \sin\theta_L{}^e + K_L V_L{}^e (u^e - \ell c \sin\theta_L{}^e \sin\beta^e) \qquad (2.10a)$$

$$T_n{}^e = (m_v + m_L) g \qquad (2.10b)$$

$$T_o{}^e = (m_v + m_L) u^e c - m_L \ell c^2 \sin\beta^e \sin\theta_L{}^e$$

$$+ K_L V_L^e \ell c \sin\theta_L^e \cos\beta^e \qquad (2.10c)$$

$$m_L u^e c \cos\beta^e - K_L V_L^e (u^e \sin\beta^e - \ell c \sin\theta_L^e) = 0 \qquad (2.10d)$$

$$m_L u^e c \sin\beta^e \cos\theta_L^e - m_L \ell c^2 \cos\theta_L^e \sin\theta_L^e + m_L g \sin\theta_L^e + K_L V_L^e u^e \cos\beta^e \cos\theta_L^e = 0 \qquad (2.10e)$$

where

$$V_L^e = [u_e^2 + \ell^2 c^2 \sin^2\theta_L^e - 2u^e \ell c \sin\theta_L^e \sin\beta^e]^{\frac{1}{2}}$$

Clearly, for a given helicopter and load, and for a specified turn rate c and forward speed u^e, Equations 2.10 (a-c) are solved to determine the thrust force necessary for equilibrium, while the steady state values of θ and β are obtained by solving Equations 2.10 (d-e).

Unlike the case of straight flight, the resulting perturbation equations are found to be coupled in longitudinal and lateral dynamics of the vehicle and load. [No perturbations in the wind axes components of thrust are considered.] The linearized equations are rearranged in the standard form (2.11)

$$\dot{\bar{X}} = \underline{A}\bar{X}, \quad \bar{X}^T = [v \; \gamma \; \theta \; q \; \beta \; \lambda \; r] \qquad (2.11)$$

(elements of $\underline{A}$ are given in Appendix A) and the eigenvalues and corresponding eigenvectors of the system matrix, evaluated for a specified turning flight condition, are shown in Table IV. The oscillatory modes (S_1, S_2) are stable and are strongly coupled in both longitudinal and lateral dynamics of the vehicle and load. [The corresponding modes in straight flight are uncoupled but have about the same frequency of oscillation.] The phase relationships between the load displacements and velocities in these modes indicate cross coupling between pitching and azimuthal motion such that q_L is in phase with λ in mode S_1 while it is in opposite phase (phase difference of π) in mode S_2. Similar behavior is observed between r_L and θ_L. S_3 corresponds to convergence of vehicle lineal velocity. A weak divergence of angular displacements λ and ϕ is indicated by S_4. The zero eigenvalue corresponds to the rigid motion of the system in the plane of turning.

The effect of increasing $\hat{m}$ on the oscillatory modes are similar to that observed for the system in straight flight [Figure 2.5]. The critical value of $\hat{m}$, corresponding to undamped oscillation, is found to be lower in turning than in uniform translation. Increasing c (or load factor of the turn) or ℓ tends to increase the damping of lower frequency mode (LFM) while that of the higher frequency mode (HFM)

Table IV - PMM: Modes and Mode Shapes of the System in a Steady Turn [c = 0.5 r/s, C_D^L = 1.0]

EIGENVALUES AND EIGENVECTORS

S_1 = -0.0173 ±2.675i

v	0.868(0)
γ	0.040(94)
θ	0.308(3)
q	0.820(-87)
β	0.387(-87)
λ	0.413(-88)
r	1.000(-178)

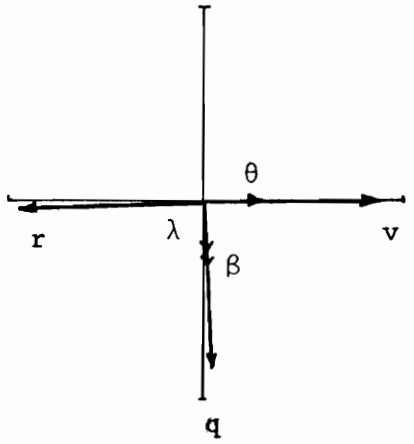

S_2 = -0.0197 ±1.998i

v	1.000(0)
γ	0.029(-97)
θ	0.299(173)
q	0.597(82)
β	0.444(-96)
λ	0.408(-97)
r	0.815(173)

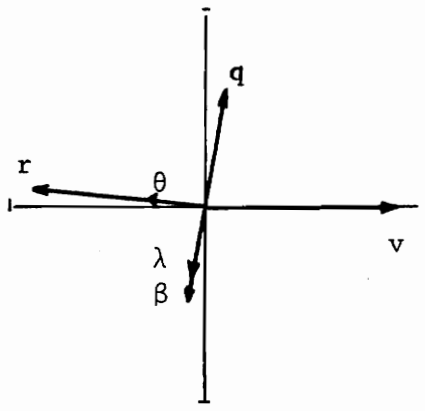

S_3 = -0.0503		S_4 = +0.00261		S_5 = 0.0	
v	1.000(0)	v	.109(180)	λ	1.0
γ	0(0)	γ	.586E-03(0)	β	0.
θ	.177E-02(0)	θ	.154E-03(0)		
q	.906E-04(0)	q	.475E-03(0)		
β	.423E-02(0)	β	.103E-02(0)		
λ	0.468(0)	λ	1.000(0)		
r	.023(18)	r	.259E-02(0)		

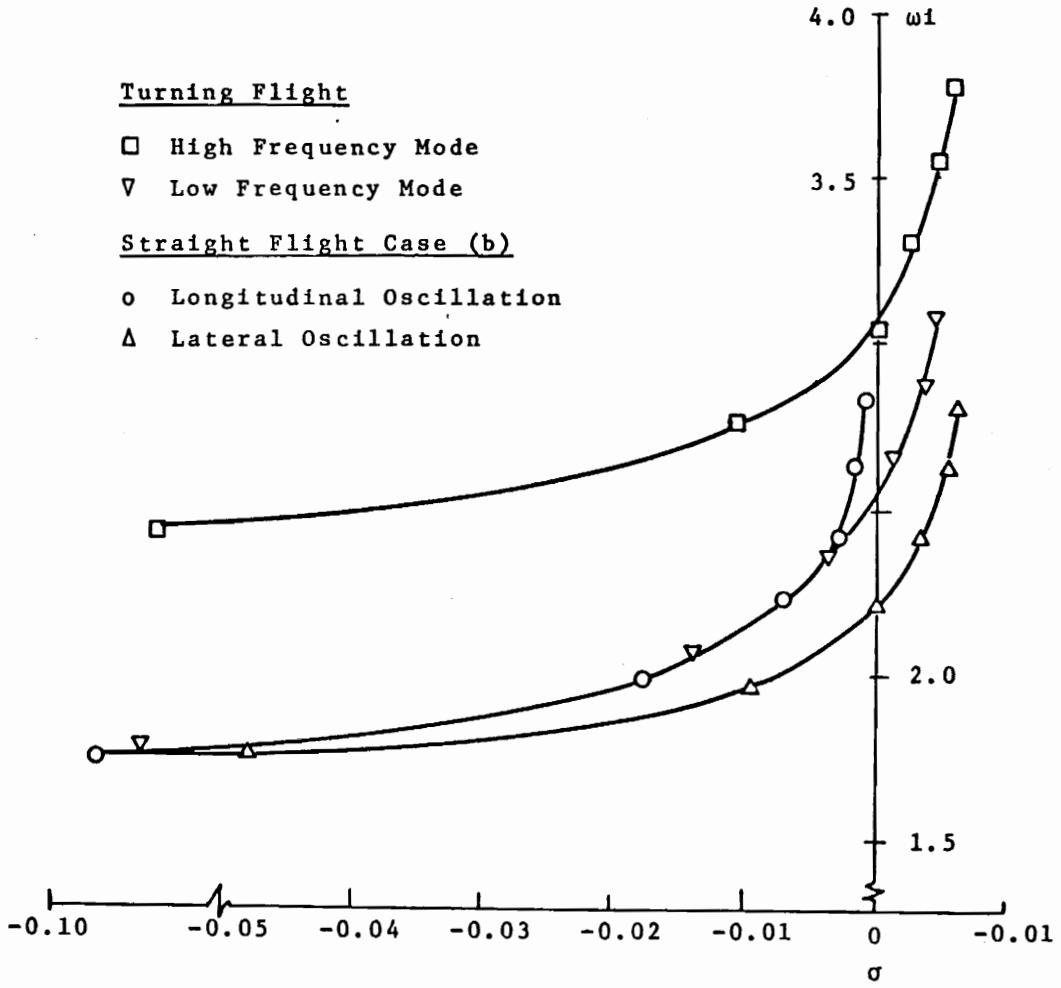

Figure 2.5 - PMM: Effect of $\hat{m}$ on Oscillatory Modes of the System in Straight and Steady Turning Flight Conditions [c = 0.5 r/s, u_e = 20 m/s, ℓ = 4m, C_D^L = 1.0, $0.2 \leq \hat{m} \leq 2.2(0.4)$]

decreases [Figure 2.6].

The above analysis indicates that the stability of the system in turning flight is more restricted in the parameter space as compared to that of the system in straight flight.

2.5 Summary

The general equations of motion of a helicopter carrying a suspended load have been derived assuming both the vehicle and load to be point masses connected by a rigid link. The stability of the system in uniform translation has been analyzed for specialized thrusting conditions; (a) constant thrust force fixed in LHS; (b) constant thrust force fixed in WAS. It is observed that in both cases (a) and (b) the perturbation equations are uncoupled in longitudinal and lateral motion. Typical modes of the system consist of oscillatory motion of the vehicle and load in both the longitudinal and lateral directions, and convergence of helicopter velocity components. The vehicle has a preferred heading in case (a) while in case (b) it does not.

The stability of the system in steady turn has also been examined. Typical modes of the system in turning flight consist of coupled longitudinal and lateral oscillatory motion, convergence of vehicle forward speed, a weak

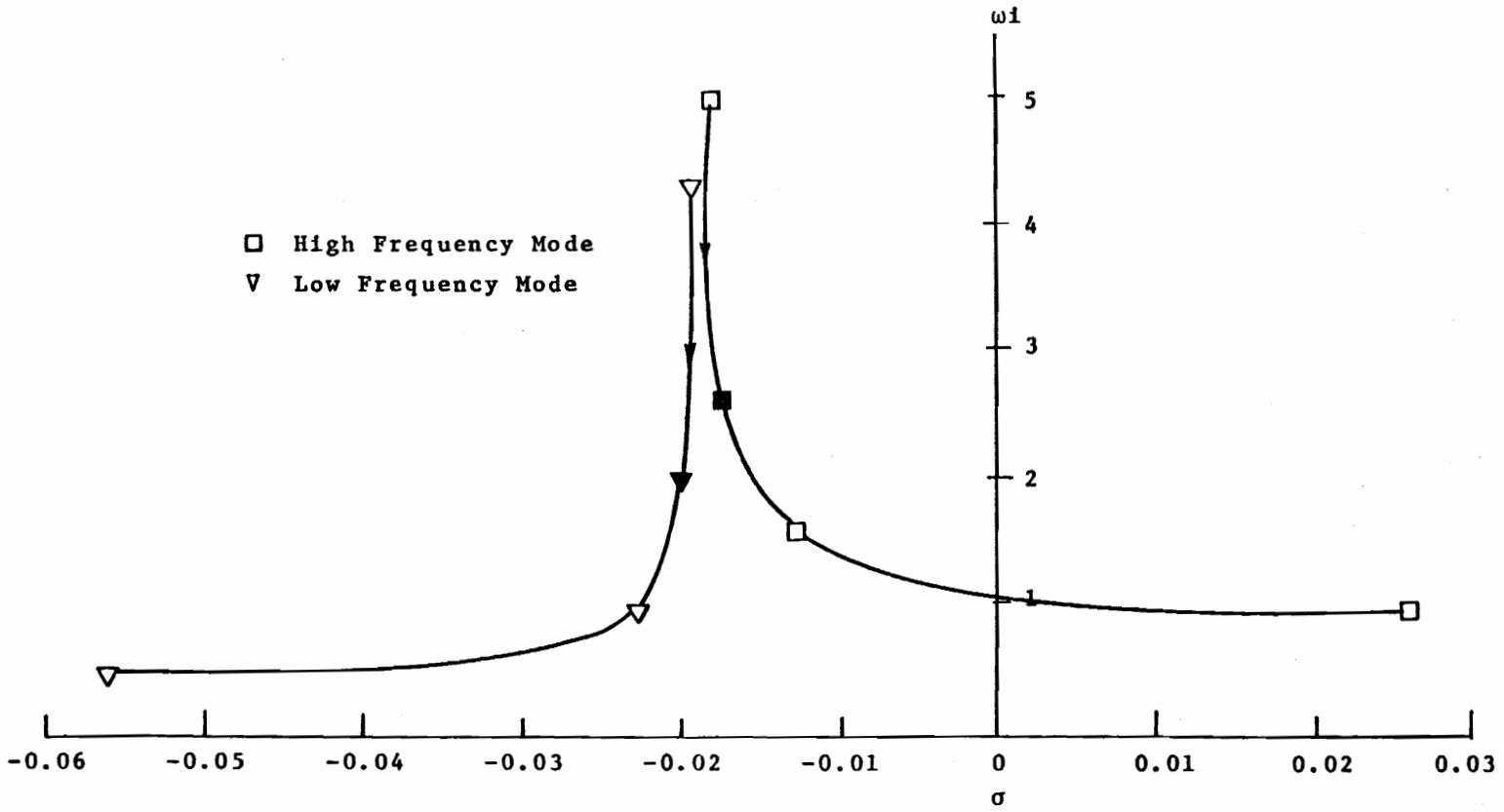

Figure 2.6 - PMM: Effect of ℓ on Oscillatory Modes of the System in a Steady Turn
[C = 0.5 r/s, C_D^L = 1.0, 1 ≤ ℓ ≤ 64(*4)]

divergence in the vehicle heading angle and load azimuthal displacement and rigid rotation of the system in the plane of turning. It is observed that the stability of the system in a steady turn is more restricted in the parameter space as compared to that of the system in straight flight.

CHAPTER III

SYSTEM MODELS WITH A DISC ROTOR

3.1 Introduction

In the system model discussed in Chapter II the vehicle thrust was assumed to be constant in magnitude and fixed in either LHS [case (a)] or WAS [case (b)]. In the present development the thrust is assumed to be generated by a rigid rotor disc that has pitch and roll degrees of freedom with respect to the LHS. As a first step, the helicopter is modeled as a point mass located at the center of the disc and the load is also assumed to be a point mass, as considered previously. The stability of the system, as predicted by this model, is analyzed and compared with corresponding results obtained earlier [Section 2.3, case (a)] where the thrust vector was fixed in LHS.

Subsequently, in order to consider a more realistic helicopter model, the vehicle is assumed to be a rigid body with conventional helicopter components like tail rotor and stabilizer. The main rotor, which is modeled as a rigid disc, is connected to the fuselage by a rigid shaft at the vehicle center of mass [$(cm)_V$]. The load is, again, assumed to be a point mass and is suspended from the fuselage from a point in its plane of symmetry.

The dynamical equations for this model of the system are derived by Lagrange's method. The stability of the system in uniform translation is analyzed to determine the effect of rigid body motion of the fuselage on the load induced modes as well as the effect of load dynamics on the conventional modes of the helicopter.

3.2 Rotor Forces in Hub Axes

Rotor Thrust from Momentum Theory

The rotor, modeled here as an actuator disc, is assumed to generate thrust by imparting additional momentum to the fluid in the plane of the disc. Using momentum theory the resultant rotor thrust is obtained and is expressed as components along the rotor hub axes. Although this is an idealized model, it predicts acceptable results [GE 1] in many calculations pertaining to rotor performance in forward flight. However, in the present analysis it is being used in determining the stability of the vehicle dynamics, the validity of which is examined by comparing with more realistic rotor models developed later. The rotor disc is assumed to have pitch and roll degrees of freedom with respect to the LHS. The following assumptions are made in using the momentum theory:

(a) The rotor consists of infinite number of blades,

and therefore, can be considered as a disc that uniformly accelerates the fluid passing through it.

(b) The induced velocity at the disc is uniform and is in the direction of downward normal on the disc.

(c) The resultant force on the rotor acts normal to the disc and is defined as thrust.

(d) Rotational energy in the slipstream is negligible.

(e) The fluid is inviscid.

Figure 3.1 shows the rotor disc in forward flight in a general orientation (θ_R, ϕ_R) with respect to the hub axes system (X_h, Y_h, Z_h) whose origin is at the center of the disc such that X_h and X_R are in the same vertical plane. The rotor coordinate system [fixed to the disc] is located with reference to the hub axes by the transformation

$$T_{R/H} = \begin{bmatrix} \cos\theta_R & 0 & -\sin\theta_R \\ \sin\phi_R \sin\theta_R & \cos\phi_R & -\sin\phi_R \cos\theta_R \\ \cos\phi_R \sin\theta_R & -\sin\phi_R & \cos\phi_R \cos\theta_R \end{bmatrix}$$

(3.1a)

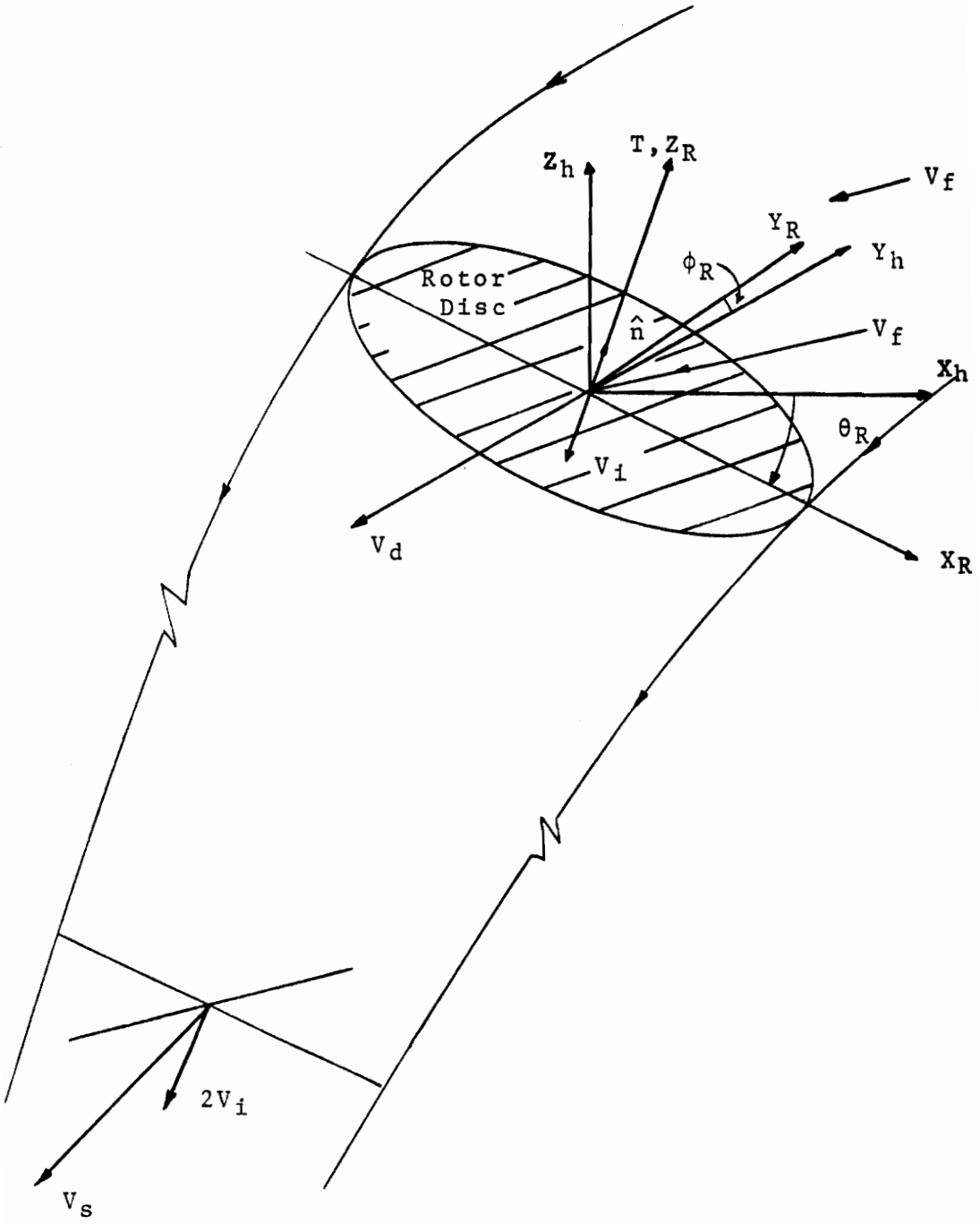

Figure 3.1 - Disc Rotor in Forward Flight

while the hub axes system is located with respect to the LHS, whose origin is at the center of the disc, by the transformation

$$T_{H/LHS} = \begin{bmatrix} 1 & 0 & 0 \\ 0 & -1 & 0 \\ 0 & 0 & -1 \end{bmatrix} \tag{3.1b}$$

According to momentum theory, the rate of change of linear momentum imparted to the fluid by the rotor disc is equal to the reactive force exerted on the rotor disc by the fluid.

Consider the change in linear momentum of the fluid in the direction normal to the disc ($\hat{n}$)

$$\Delta\overline{p}_n = \rho A_d V_d \cdot \hat{n} \, (\overline{V}_s - \overline{V}_f) \tag{3.2}$$

where

$$\overline{V}_d = \overline{V}_f + \overline{v}_i$$

Defining $\overline{V}_f$ and $\hat{n}$ as components in the hub axes system, the scalar product $\overline{V}_d \cdot \hat{n}$ is obtained as

$$\overline{V}_d \cdot \hat{n} = V_n = [V_x^f \cos\phi_R \sin\theta_R - V_y^f \sin\phi_R$$

$$+ V_z^f \cos\phi_R \cos\theta_R - v_i]$$

Introducing this scalar in Equation 3.2

$$\Delta\bar{p}_n = \rho A_d V_n \, (\bar{V}_s - \bar{V}_f) \tag{3.3}$$

Defining $\bar{T} = T\hat{n}$ as the reactive force exerted on the disc by the fluid, from momentum theory

$$T\hat{n} = \Delta\bar{p}_n \tag{3.4}$$

By simple momentum analysis of axial flow through a disc, it is observed that the induced velocity in the slipstream of the rotor disc is twice that at the disc (HO 1). General forward motion of the rotor can be considered as superposition of motions in the directions parallel to the hub axes. With this conception, the fluid velocity far down the slipstream is assumed as

$$\bar{V}_s = \bar{V}_f + 2\bar{v}_i \tag{3.5}$$

The validity of this assumption is verified by considering the work-energy relation; i.e., rate of work done by the fluid is equal to its rate of change of kinetic energy. Mathematically,

$$T\hat{n} \cdot (\bar{V}^f + \bar{v}_i) = \tfrac{1}{2} \rho A_d V_d \cdot \hat{n} \, (V_s^2 - V_f^2) \tag{3.6}$$

On substituting

$$\overline{V}_d = \overline{V}_f + \overline{v}_i$$

$$\overline{V}_s = \overline{V}_f + 2\overline{v}_i$$

in Equation 3.6 and simplifying, the identity in Equation 3.7 is obtained which indicates that the above assumption [Equation 3.5] is valid.

$$\rho A_d V_n \ (2\overline{v}_i \cdot \overline{V}_f + 2v_i^2) = \rho A_d V_n \ (\overline{V}_f \cdot 2\overline{v}_i + 2v_i^2) \qquad (3.7)$$

Consequently, from Equation 3.3 and 3.4, rotor thrust is given by

$$T = 2\rho A_d v_i \ [-V_x^f \cos\phi_R \sin\theta_R + V_y^f \sin\phi_R - V_z^f \cos\phi_R + v_i] \qquad (3.8)$$

Assuming zero wind conditions ($\overline{V}^h = \overline{V}^f$), the rotor thrust is expressed as components in the LHS as

$$\begin{Bmatrix} T_{x_v} \\ T_{y_v} \\ T_{z_v} \end{Bmatrix} = T \ [T_{LHS/H}] \ [T_{H/R}] = \begin{Bmatrix} T\cos\phi_R \sin\theta_R \\ T\sin\phi_R \\ -T\cos\phi_R \cos\theta_R \end{Bmatrix} \qquad (3.9)$$

where

$$T = 2\rho A_d v_i \left[-u \cos\phi_R \sin\theta_R - v \sin\phi_R + w \cos\phi_R \cos\theta_R + v_i\right]$$

Equivalent Profile Drag of the Rotor

The rotor disc is assumed to have profile drag equivalent to that of a real rotor with four blades. [Since the rotor model considered here is only conceptual, a real four-bladed rotor of the same diameter as the disc is used in evaluating the rotor performance. Geometric and aerodynamic data have been either assumed or estimated as indicated.] The profile drag of an elemental blade [Figure 3.2] is given approximately by

$$dD \simeq \tfrac{1}{2} \rho c \, C_{d_o} \, u_T^2 \, dr$$

$$dD \simeq \tfrac{1}{2} \rho c \, C_{d_o} \left[r\Omega + u \sin\psi + v \cos\psi\right]^2$$

where u and v are the components of hub velocity and ψ is the rotor azimuth angle, Ω is the angular velocity of the rotor, r is the radial distance of the blade element from the hub and C_{d_o} is the profile drag coefficient of the blade. This drag force is resolved into components along the vehicle axes as

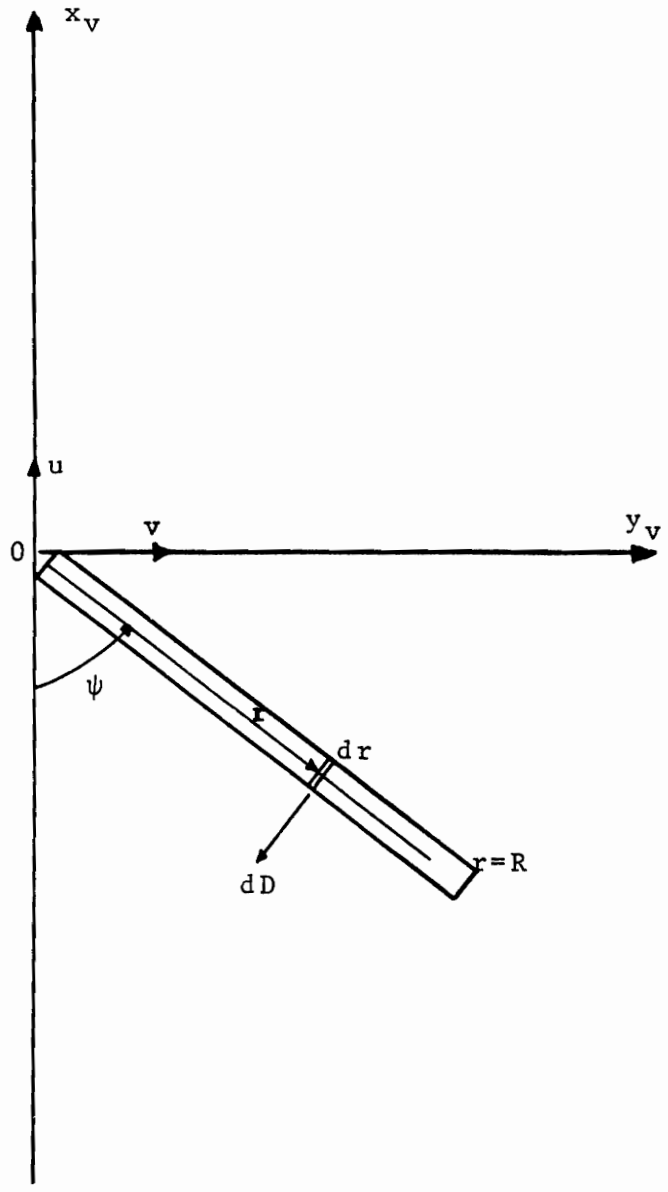

Figure 3.2 - Equivalent Rotor Profile Drag

$$dD_x = -dD \sin\psi$$

$$dD_y = -dD \cos\psi$$

The average value of the drag force due to all the b blades is determined by integrating over the entire blade and over one blade revolution as

$$D_x = -\frac{b}{2\pi} \int_0^{2\pi} \int_0^{R} \tfrac{1}{2} \rho c \, C_{d_o} \, [r\Omega + u \sin\psi + v \cos\psi]^2 \sin\psi \, dr d\psi$$

$$D_y = -\frac{b}{2\pi} \int_0^{2\pi} \int_0^{R} \tfrac{1}{2} \rho c \, C_{d_o} \, [r\Omega + u \sin\psi + v \cos\psi]^2 \cos\psi \, dr d\psi$$

The above integrals are evaluated to determine the average value of the drag force in terms of its components along LHS as

$$D_x = [-\tfrac{1}{4} \rho c b \, C_{d_o} \, \Omega R^2] \, u$$

$$D_y = [-\tfrac{1}{4} \rho c b \, C_{d_o} \, \Omega R^2] \, v \qquad (3.10)$$

3.3 Point Mass Vehicle with Disc Rotor (PVDR)

The point mass model of the system developed in the

previous chapter considered the helicopter to be a point mass with a constant thrust force. Presently this model of the helicopter is replaced by a rigid rotor disc that has a concentrated mass, equal to that of the helicopter, at its center and has pitch and roll degrees of freedom [Figure 3.3] with respect to the LHS. Note that this model of the system is similar to that in case (a) in Section 2.3, since in the present model the normal to the rotor disc, and hence, the direction of the rotor thrust, is fixed relative to the LHS.

The system dynamical equations for this model are identical to those developed earlier in Section 2.2 except for the nonpotential forces due to rotor thrust and drag. Equation 3.9 and 3.10 are substituted in Equations 2.2-2.6 and the resulting equations are linearized about the steady forward flight condition as discussed before. It is observed that for equilibrium

$$\tan\theta_R^{\,e} = \frac{(K_v + K_L)\, u_e^{\,2} + (D_x^{\,R})_e}{(m_v + m_L)\, g}$$

$$\tan\theta_L^{\,e} = \frac{K_L\, u_e^{\,2}}{m_L g}$$

and

$$\phi_R^{\,e} \equiv 0$$

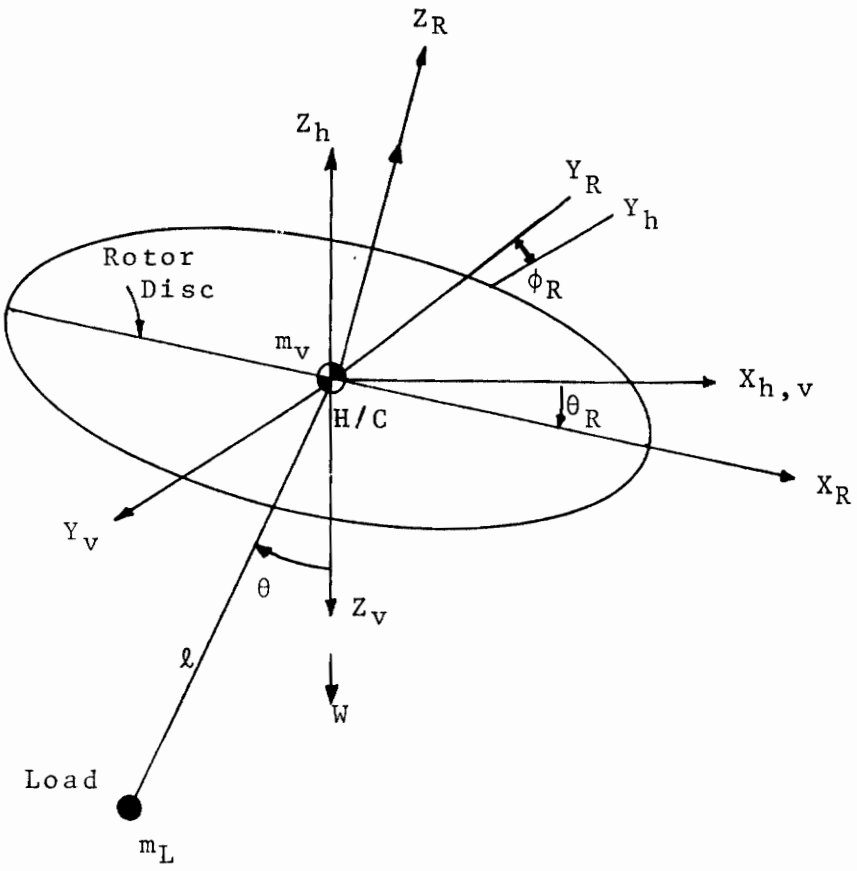

Figure 3.3 - Point Mass Model with Disc Rotor

The above trim conditions are self-explanatory.

The perturbation equations are found to be uncoupled in longitudinal and lateral motion. Tabe V shows the modes and mode shapes of the system for nominal values of the system parameters. The lateral and longitudinal oscillatory modes [S_1, S_2 respectively] are stable and have greater damping than that predicted previously for the system with a constant thrust force in LHS [Table I]. Also, the vehicle forward and lateral velocity convergence [S_3, S_4 respectively] indicate that the vehicle has a preferred heading, as expected. It is believed that lack of preferred heading, as seen in case (b) in Section 2.3, could be similarly demonstrated by using the present model with the normal to the disc fixed in WAS. The convergence of vehicle vertical velocity (S_5) is stronger than before [Table I] because of the rotor damping.

The effect of parameters $\hat{m}$, u_e and ℓ on the system modes are similar to that observed previously in Section 2.3. The modes and mode shapes predicted by this model are subsequently compared with that predicted by the rigid body helicopter model which is discussed in the following section.

3.4 Equations of Rigid Body Vehicle Motion

In order to consider a more realistic helicopter model,

Table V - PVDR: Modes and Mode Shapes [Nominal Parameter Values]

EIGENVALUES AND EIGENVECTORS

$S_1 = -0.0189 \pm 1.922i$

$v = 0.131(0)$

$\lambda = 0.520(91)$

$r_L = 1.000(0)$

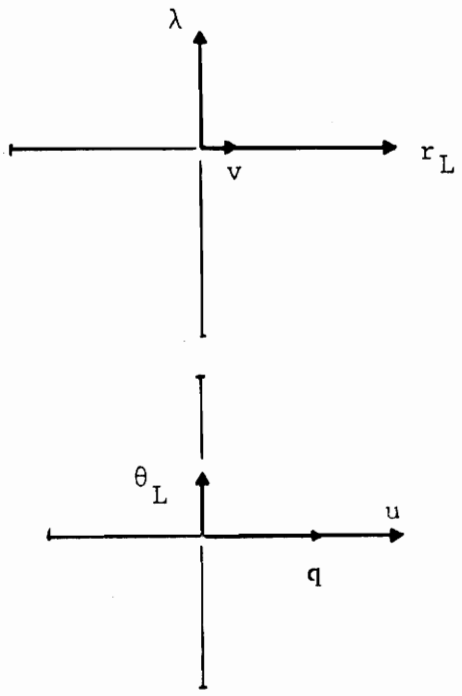

$S_2 = -0.0376 \pm 1.921i$

$u = 1.000(0)$

$w = 0.088(13)$

$\theta_L = 0.392(89)$

$q_L = 0.753(-2)$

$S_3 = -0.0525$

$u = 1.000(0)$

$w = 0.053(0)$

$\theta_L = 0.004(0)$

$S_4 = -0.0273$

$v = 1.000(0)$

$\lambda = 0.022(0)$

$S_5 = -1.196$

$w = 1.000(180)$

$u = 0.047(0)$

the vehicle is assumed to be a rigid body with conventional helicopter components like tail rotor and stabilizer. The rotor is assumed to be a rigid disc, as discussed in Section 3.2, and is connected to the fuselage by a rigid shaft whose axis passes through the vehicle center of mass. The load is assumed to be a point mass and is suspended from the fuselage in its plane of symmetry as shown in Figure 3.4. The vehicle, as a rigid body, has both translational and rotational degrees of freedom. These motions are described in terms of components along the body fixed principal axes. The lineal velocity components are $\dot{x}_v$, $\dot{y}_v$ and $\dot{z}_v$ while the angular velocity components are $\tilde{p}_v$, $\tilde{q}_v$ and $\tilde{r}_v$. The vehicle orientation is described by the usual Euler angles (ϕ_v, θ_v, ψ_v). The angular rates can be expressed in terms of these angles and their time derivatives (ET 2, page 126) as

$$\tilde{p}_v = \dot{\phi}_v - \dot{\psi}_v \sin\theta_v$$

$$\tilde{q}_v = \dot{\theta}_v \cos\phi_v + \dot{\psi}_v \cos\theta_v \sin\phi_v$$

$$\tilde{r}_v = -\dot{\theta}_v \sin\phi_v + \dot{\psi}_v \cos\theta_v \cos\phi_v$$

The load motions are described by angular coordinates λ and θ_L as defined earlier. The load suspension point is located in the plane of symmetry at horizontal and vertical

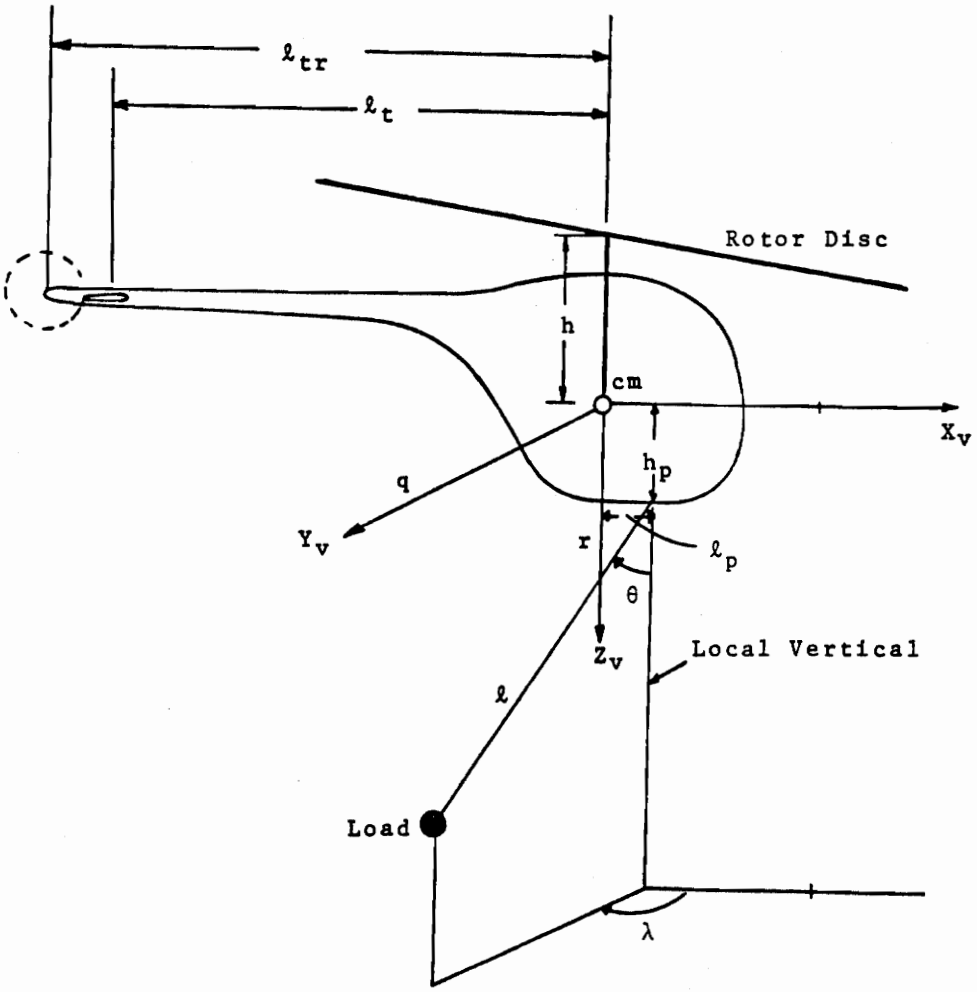

Figure 3.4 - Rigid Body Vehicle, Disc Rotor and Point Mass Load Model

distances, h_p and ℓ_p respectively, from the $(cm)_v$. The rotor shaft is assumed to be aligned with z-axis of the vehicle.

In order to derive Lagrange's equations of motion of the system, the Lagrangian L, is evaluated in terms of the system coordinates.

$$L = (KE)_s - (PE)_s \tag{3.11}$$

Total kinetic energy of the system is

$$\begin{aligned}(KE)_s &= (KE_{trans.} + KE_{rot.})_v + (KE)_L \\ &= \tfrac{1}{2} m_v (\dot{x}_v^2 + \dot{y}_v^2 + \dot{z}_v^2) + \tfrac{1}{2}(I_x \tilde{p}_v^2 \\ &\quad + I_y \tilde{q}_v^2 + I_z \tilde{r}_v^2) + \tfrac{1}{2} m_L [(V_L^x)^2 \\ &\quad + (V_L^y)^2 + (V_L^z)^2]\end{aligned}$$

V_L^x, V_L^y and V_L^z are components of the load velocity, $\overline{V}_L^v$, along the vehicle body axes and are given in the matrix form

$$\overline{V}_L^v = \overline{V}_p^v + [L]_{v/LHS}\, \overline{V}_{LP}^{LHS}$$

where

$$\overline{V}_L{}^v = \begin{Bmatrix} V_L{}^x \\ V_L{}^y \\ V_L{}^z \end{Bmatrix}$$

$$\overline{V}_p{}^v = \begin{Bmatrix} \dot{x}_v + h_p \tilde{q}_v \\ \dot{y}_v + \ell_p \tilde{r}_v - h_p \tilde{p}_v \\ \dot{z}_v - \ell_p \tilde{q}_v \end{Bmatrix}$$

$$\overline{V}_{Lp}{}^{LHS} = \begin{Bmatrix} \ell\dot{\theta}_L \cos\theta_L \cos\lambda - \ell\dot{\lambda} \sin\theta_L \sin\lambda \\ \ell\dot{\lambda} \sin\theta_L \cos\lambda + \ell\dot{\theta}_L \cos\theta_L \sin\lambda \\ -\ell\dot{\theta}_L \sin\theta_L \end{Bmatrix}$$

$$[L]_{v/LHS} = \begin{bmatrix} \cos\theta_v\cos\psi_v & \cos\theta_v\sin\psi_v & -\sin\theta_v \\ \sin\phi_v\sin\theta_v\cos\psi_v - \cos\phi_v\sin\phi_v & \sin\phi_v\sin\theta_v\sin\psi_v + \cos\phi_v\cos\psi_v & \sin\phi_v\cos\theta_v \\ \cos\phi_v\sin\theta_v\cos\psi_v + \sin\phi_v\sin\psi_v & \cos\phi_v\sin\theta_v\sin\psi_v - \sin\phi_v\cos\psi_v & \cos\phi_v\cos\theta_v \end{bmatrix}$$

In the above equation $\overline{V}_p{}^V$ is the velocity of the suspension point (P), expressed as components along the vehicle body axes, $\overline{V}_{LP}{}^{LHS}$ is the velocity of the load with respect to P, expressed as components along LHS and $[L]_{v/LHS}$ is the transformation matrix in terms of the Euler angles (ET 2, page 117).

The total potential energy of the system is given by

$$(PE)_s = -(m_v + m_L)\, g z_I - m_L g\, (-\ell_p \sin\theta_v + h_p \cos\theta_v \cos\phi_v + \ell \cos\theta_L)$$

z_I is an additional coordinate [not independent] introduced to evaluate the $(PE)_s$. z_I is related to the remaining coordinates by the velocity constraint in Equation 3.12.

$$\dot{z}_I + \dot{x}_v \sin\theta_v - \dot{y}_v \cos\theta_v \sin\phi_v - \dot{z}_v \cos\theta_v \cos\phi_v = 0 \qquad (3.12)$$

Lagrange's equations of motion in coordinates q_k that are related by a nonholonomic constraint are (ME 1, page 77).

$$\frac{d}{dt}\left(\frac{\partial L}{\partial \dot{q}_k}\right) - \frac{\partial L}{\partial q_k} = Q_{k_{np}} + \mu a_k,\ k = 1, 2, \ldots n \qquad (3.13)$$

subject to constraint

$$\sum_{k=1}^{n} a_k dq_k + a_0 dt = 0,$$

where μ is the Lagrange multiplier and a_k are functions of the coordinates q_k. In this case the coordinates are x_v, y_v, z_v, z_I, ϕ_v, θ_v, ψ_v, θ_L and λ. Using this formulation the following independent equations are obtained. [Note that the dependent coordinate z_I is eliminated using the constraint Equation 3.12.]

$$x_v : m_v\ddot{x}_v + m_L\dot{V}_L{}^x + (m_v + m_L)g \sin\theta_v = Q_{x_v} \quad (3.14)$$

$$y_v : m_v\ddot{y}_v + m_L\dot{V}_L{}^y - (m_v + m_L)g \cos\theta_v \sin\phi_v = Q_{y_v} \quad (3.15)$$

$$z_v : m_v\ddot{z}_v + m_L\dot{V}_L{}^z - (m_v + m_L)g \cos\theta_v \cos\phi_v = Q_{z_v} \quad (3.16)$$

$$\phi_v : I_x\dot{\tilde{p}}_v + (I_z - I_y)\,\tilde{q}_v\tilde{r}_v - m_L V_L \frac{\partial V_L}{\partial \phi_v} - m_L h_p \dot{V}_L{}^y + m_L g h_p \cos\theta_v \sin\phi_v = Q_{\phi_v} \quad (3.17)$$

$$\theta_v : I_y\,(\dot{\tilde{q}}_v \cos\phi_v - \tilde{p}_v\tilde{q}_v \sin\phi_v) + I_x\tilde{p}_v\dot{\psi}_v \cos\theta_v + I_z\,(-\dot{\tilde{r}}_v \sin\phi_v - \tilde{p}_v\tilde{r}_v \cos\phi_v) + m_L\,(\dot{V}_L{}^x h_p \cos\phi_v - \dot{V}_L{}^y \ell_p \sin\phi_v - \dot{V}_L{}^z \ell_p \cos\phi_v) + m_L\dot{\phi}_v\,(- V_L{}^x h_p \sin\phi_v - V_L{}^y \ell_p \cos\phi_v$$

$$+ V_L^{\,z}\, \ell_p \sin\phi_v) - m_L V_L \frac{\partial V_L}{\partial \theta_v} + m_L g\, (\ell_p \cos\theta_v$$

$$+ h_p \sin\theta_v \cos\phi_v) = Q_{\theta_v} \qquad (3.18)$$

$$\psi_v : I_z\, (\dot{\tilde{r}}_v \cos\theta_v \cos\phi_v - \tilde{r}_v \dot{\theta}_v \sin\theta_v \cos\phi_v$$

$$- \tilde{r}\, \dot{\phi}_v \cos\theta_v \sin\phi_v) + I_x\, (-\dot{\tilde{p}}_v \sin\theta_v - \tilde{p}_v \dot{\theta}_v \cos\theta_v)$$

$$+ I_y\, (\dot{\tilde{q}}_v \cos\theta_v \sin\phi_v - \tilde{q}_v \dot{\theta}_v \sin\theta_v \sin\phi_v$$

$$+ \tilde{q}_v \dot{\phi}_v \cos\theta_v \cos\phi_v) + m_L\, (\dot{V}_L^{\,x} h_p \cos\theta_v \sin\phi_v + \dot{V}_L^{\,y} h_p \sin\theta_v$$

$$+ \dot{V}_L^{\,y} \ell_p \cos\theta_v \cos\phi_v - \dot{V}_L^{\,z} \ell_p \cos\theta_v \sin\phi_v)$$

$$+ m_L \dot{\theta}_v\, (-V_L^{\,x} h_p \sin\theta_v \sin\phi_v - V_L^{\,y} \ell_p \sin\theta_v \cos\phi_v$$

$$+ V_L^{\,y} h_p \cos\theta_v + V_L^{\,z} \ell_p \sin\theta_v \sin\phi_v)$$

$$+ m_L \dot{\phi}_v\, (V_L^{\,x} h_p \cos\theta_v \cos\phi_v - V_L^{\,y} \ell_p \cos\theta_v \sin\phi_v$$

$$- V_L^{\,z} \ell_p \cos\theta_v \cos\phi_v) - m_L V_L \frac{\partial V_L}{\partial \psi_V} = Q_{\psi_v} \qquad (3.19)$$

$$\theta_L : m_L \dot{V}_L \frac{\partial V_L}{\partial \dot{\theta}_L} + m_L V_L \left[\frac{d}{dt} \left(\frac{\partial V_L}{\partial \dot{\theta}_L} \right) - \left(\frac{\partial V_L}{\partial \theta_L} \right) \right]$$

$$+ m_L g \ell \sin\theta_L = Q_{\theta_L} \qquad (3.20)$$

$$\lambda : m_L \dot{V}_L \frac{\partial V_L}{\partial \dot{\lambda}} + m_L V_L \left[\frac{d}{dt} \left(\frac{\partial V_L}{\partial \dot{\lambda}} \right) - \left(\frac{\partial V_L}{\partial \lambda} \right) \right] = Q_\lambda \qquad (3.21)$$

In the above equations Q_{x_v}, Q_{y_v} ... Q_λ are the nonpotential foces along each of the system coordinates. The contribution of the actual forces in the system to these generalized forces is evaluated next.

Nonpotential Forces in System Coordinates

Equation 3.14 - 3.21 describe the motion of and about the $(cm)_v$ together with the relative motion of the load. The nonpotential forces in these equations arise from the actual forces and moments that are considered in this model of the system. These physical forces are

(a) Aerodynamic drag of the vehicle and load

(b) Fuselage and stabilizer pitching moments

(c) Rotor thrust and damping moments about $(cm)_v$

(d) Tail rotor thrust and torque about the $(cm)_v$

The contribution of each of these forces and moments to the generalized forces of the system are determined from (ME 1, page 75).

$$Q_{k_j} = \bar{F}_j \frac{\partial \bar{R}_j}{\partial q_k}, \quad \begin{matrix} j = 1, 2, \ldots p \\ k = 1, 2, \ldots n \end{matrix}$$

where $\bar{F}_j$ are the physical forces in the system and $\bar{R}_j$ are the position vectors of the points at which these forces are applied.

Aerodynamic Drag of the Vehicle and Load

The drag on the fuselage is assumed to be acting at $(cm)_v$ and parallel to the vehicle velocity vector. Again, using square speed law ($D = KV^2$), it is evaluated in terms of a drag constant of the vehicle as

$$\overline{D}_v = -K_v V_v \overline{V}_v$$

The corresponding generalized forces due to this force are

$$\begin{aligned} D_x{}^v &= (-K_v V_v)\, u \\ D_y{}^v &= (-K_v V_v)\, v \\ D_z{}^v &= (-K_v V_v)\, w \end{aligned} \qquad (3.22)$$

[Note that the subscript "v" has been dropped in referring to vehicle body axes.]

Similarly the contribution of the drag force on the load, to the generalized forces are

$$\begin{aligned} D_x{}^L &= -K_L V_L V_L{}^x \\ D_y{}^L &= -K_L V_L V_L{}^y \\ D_z{}^L &= -K_L V_L V_L{}^z \end{aligned}$$

$$D_{\phi_v}{}^{L} = K_L V_L V_L{}^{y} h_p \tag{3.23}$$

$$D_{\theta_v}{}^{L} = -K_L V_L (h_p V_L{}^{x} - \ell_p V_L{}^{z})$$

$$D_{\psi_v}{}^{L} = -K_L V_L V_L{}^{y} \ell_p$$

$$D_{\theta_L}{}^{L} = -K_L V_L \ell \, (V_L{}^{x} \cos\theta_L \cos\lambda + V_L{}^{y} \cos\theta_L \sin\lambda - V_L{}^{z} \ell \sin\theta_L)$$

$$D_{\lambda}{}^{L} = -K_L V_L \ell \, (-V_L{}^{x} \sin\theta_L \sin\lambda + V_L{}^{y} \sin\theta_L \cos\lambda)$$

Equivalent profile drag of the disc rotor, evaluated in Section 3.2, also contributes to the generalized forces as

$$D_x{}^{R} = -(\tfrac{1}{4} \rho c b \, C_{d_o} \, \Omega R^2) \, u$$

$$D_y{}^{R} = -(\tfrac{1}{4} \rho c b \, C_{d_o} \, \Omega R^2) \, v$$

Fuselage Pitching Moment

Estimation of fuselage contribution to pitching moment of the vehicle is complicated by the rotor downwash. As an approximation (NI 1) the fuselage is assumed to be a slender body of revolution. The pitching moment of such a body is given approximately by Munk's relation,

$$M_{\theta_v}{}^{f} = 2 \, (\text{volume}) \, (K_1 - K_2) \, \bar{q} \alpha_f$$

where $(K_2 - K_1)$ is a correction factor based on fuselage fineness ratio [length/diameter] and $\bar{q}$ is dynamic pressure given by

$$\bar{q} \simeq \frac{\rho}{2} [u^2 + v^2 + (w - v_i)^2]$$

and α_f is the angle of attack of the fuselage given by

$$\alpha_f \simeq \alpha_R + \frac{(w - v_i)}{[u^2 + (w - v_i)^2]^{\frac{1}{2}}}$$

where α_R is the angle of attack of the rotor disc, assumed to be equal to the longitudinal tilt of the rotor corresponding to zero flight path angle of the vehicle. α_f is assumed to be small in this approximation.

Stabilizer Pitching Moment

Stabilizer contribution to pitching moment of the vehicle is estimated approximately, including rotor downwash effect, as the stabilizer lift, L_t, acting across the tail length (Figure 3.4), i.e.,

$$M_{\theta_v}{}^t = - S_t a_t \ell_t \bar{q}_t \alpha_t \qquad (3.25)$$

where

$$\alpha_t = \alpha_f + \theta_t$$

and

$$\bar{q}_t \simeq \frac{\rho}{2} [u^2 + (v - z_{tr} \tilde{p}_v)^2 + (w - \ell_t \tilde{q}_v - v_i)^2]$$

Rotor Thrust and Moment About $(cm)_v$

The thrust generated by the rotor disc was evaluated in Section 3.2 and is given in terms of its components along the LHS by Equation 3.9

$$\begin{Bmatrix} T_x \\ T_y \\ T_z \end{Bmatrix} = T \begin{Bmatrix} \cos\phi_R \sin\theta_R \\ \sin\phi_R \\ -\cos\phi_R \cos\theta_R \end{Bmatrix} \tag{3.9}$$

where

$$T = 2\rho A_D v_i \left[V_x^f \cos\phi_R \sin\theta_R - V_y^f \sin\phi_R + V_z^f \cos\phi_R \cos\theta_R - v_i \right]$$

Assuming zero wind conditions,

$$\overline{V}^f = \overline{V}^h = \overline{V}^{cm} + \overline{\omega}_v \times \overline{R}_h$$

where $\overline{\omega}_v \times \overline{R}_h$ is the velocity of the hub [center of the rotor disc] with respect to cm of the vehicle. The corresponding velocity components along the hub axes are

$$\begin{Bmatrix} V_x \\ V_y \\ V_z \end{Bmatrix} = \begin{Bmatrix} u - h\tilde{q}_v \\ -v - h\tilde{p}_v \\ -w \end{Bmatrix} \tag{3.26}$$

Equation 3.26 is introduced in Equation 3.9 and the resulting equation gives the rotor thrust as components along the vehicle body axes. The moment of the rotor thrust about the cm of the vehicle are correspondingly given by

$$M_{\theta_v}{}^R = -hT_x$$
$$M_{\phi_v}{}^R = hT_y \qquad (3.27)$$

Rotor Pitch and Roll Damping

The inertia of an articulated rotor blade produces a lag in the realignment of the rotor shaft and the rotor, following a tilt of the fuselage in pitch or roll. The rotor roll lag angle δ_R and the pitch lag angle δ_P that are produced by a constant pitch or roll velocity of the fuselage are determined from Equation (3.28). This relation will be derived subsequently in developing the articulated rotor model in Section 4.3.

$$\begin{bmatrix} -\frac{3}{2}\frac{\bar{e}}{1-\bar{e}}\Omega^2 & \frac{\gamma\Omega^2}{8}\left(1-\frac{1}{2}\mu_x{}^2\right) \\ -\frac{\gamma\Omega^2}{8}\left(1+\frac{1}{2}\mu_x{}^2\right) & -\frac{3}{2}\frac{\bar{e}}{1-\bar{e}}\Omega^2 \end{bmatrix} \begin{Bmatrix} \delta_R \\ \delta_P \end{Bmatrix}$$

$$= \begin{bmatrix} \frac{\gamma\Omega}{8} & -2\Omega\left(1+\frac{3}{2}\frac{\bar{e}}{1-\bar{e}}\right)+\frac{\gamma\Omega\lambda\bar{h}}{4} \\ 2\Omega\left(1+\frac{3}{2}\frac{\bar{e}}{1-\bar{e}}\right)-\frac{\gamma\Omega\lambda\bar{h}}{4} & \frac{\gamma\Omega}{8} \end{bmatrix} \begin{Bmatrix} p_v \\ q_v \end{Bmatrix} \qquad (3.28)$$

In the present model the rotor disc is assumed to respond as an articulated rotor for a given fuselage pitch or roll velocity. Consequently the total thrust generated by the disc can now be written as

$$\begin{Bmatrix} T_x \\ T_y \\ T_z \end{Bmatrix} = T \begin{Bmatrix} \cos(\phi_R + \delta_R) \sin(\theta_R + \delta_p) \\ \sin(\phi_R + \delta_R) \\ -\cos(\phi_R + \delta_R) \cos(\theta_R + \delta_p) \end{Bmatrix} \quad (3.29)$$

From Equations 3.28 and 3.29 the rotor damping moments in pitch and roll are obtained.

Tail Rotor Thrust and Torque

In conventional single rotor helicopters a tail rotor is used to apply torque to the main rotor shaft to overcome the resistive torque of the blades caused by aerodynamic drag. The tail rotor thrust required to produce this counter-torque is obtained from

$$T_{tr} = \frac{Q_E}{\ell_{tr}} = \frac{P}{\Omega \ell_{tr}}$$

where

- P - Power of the engine driving the main rotor shaft
- Ω - Main rotor angular velocity
- ℓ_{tr} - Perpendicular distance between tail rotor axle and main rotor shaft

Q_E - Engine torque

The tail rotor thrust coefficient is defined as

$$C_{T_{tr}} = \frac{T_{tr}}{\rho\ (\pi R_t^2)\ (\Omega_t R_t)^2}$$

It can be expressed in standard parametric form (SE 1, page 307) as

$$\left(\frac{2\ C_T}{a\sigma}\right)_{tr} = \frac{\theta_{tr}}{3}\ [1 + \tfrac{3}{2}\ \mu_{tr}^2] + \frac{\lambda_{tr}}{2}$$

where tail rotor inflow ratio λ_{tr} is obtained from

$$\alpha_{tr} = \frac{\lambda_{tr}}{\mu_{tr}} + \frac{C_T{}^{tr}}{2\mu_{tr}^2}$$

where

$$\mu_{tr} = \frac{V_{tr}}{\Omega_t R_t}$$

$$V_{tr} = [(u - z_{tr}\ \tilde{q})^2 + (v - \ell_{tr}\ \tilde{r} + z_{tr}\tilde{p} - v_i{}^{tr})^2 + (w + \ell_{tr}\tilde{q})^2]^{\frac{1}{2}}$$

θ_{tr} is the tail rotor collective pitch angle. Expressing tail rotor parameters as ratios of main rotor parameters and assuming level flight condition, the tail rotor thrust can be obtained as

$$T_{y_v}{}^{tr} = \frac{\bar{\eta}\ (m_v + m_L)\ g}{\left(\frac{2\ C_T}{a\sigma}\right)_R} \left[(1 + \tfrac{3}{2}\ \mu_{tr}{}^2)\ \frac{\theta_{tr}}{3} + \frac{\lambda_{tr}}{2}\right] \tag{3.30a}$$

where

$$\bar{\eta} \triangleq \frac{(b\ c\ \Omega^2\ R^3)_{tr}}{(b\ c\ \Omega^2\ R^3)_R}$$

Tail rotor torques about the $(cm)_v$ are given by

$$\begin{aligned} M_{\psi_v}{}^{tr} &= -\ T_{y_v}{}^{tr}\ \ell_{tr} \\ M_{\phi_v}{}^{tr} &= \quad T_{y_v}{}^{tr}\ z_{tr} \end{aligned} \tag{3.30b}$$

where z_{tr} is the height of the tail rotor axle above the $(cm)_v$.

From the preceding development, the total contribution of the actual forces in the system to the generalized forces are summarized below.

$$\begin{aligned} Q_x &= D_x{}^v + D_x{}^L + D_x{}^R + T_x{}^R \\ Q_y &= D_y{}^v + D_y{}^L + D_y{}^R + T_y{}^R + T_y{}^{tr} \\ Q_z &= D_z{}^v + D_z{}^L + T_z{}^R \\ Q_{\phi_v} &= D_{\phi_v}{}^L + M_{\phi_v}{}^R + M_{\phi_v}{}^{tr} + D_{\phi_v}{}^R \\ Q_{\theta_v} &= D_{\theta_v}{}^L + M_{\theta_v}{}^R + M_{\theta_v}{}^t + M_{\theta_v}{}^f + D_{\theta_v}{}^R \end{aligned} \tag{3.31}$$

$$Q_{\psi_v} = M_{\psi_v}{}^{tr} + D_{\psi_v}{}^{L}$$

$$Q_{\theta_L} = D_{\theta_L}{}^{L}$$

$$Q_{\lambda} = D_{\lambda}{}^{L}$$

Note that the above generalized forces have been derived with the intent of analyzing system stability in straight, level flight.

Introducing these nonpotential forces in Equation 3.31, in Equations 3.14-3.21, dynamical equations of the helicopter-load system are obtained. Comparing these equations of motion with those derived for the PMM of the system [Section 2.2] it is observed that the effect of rigid body motion of the fuselage and rotor damping, on the load dynamics depends on the location of the suspension point. It is found that suspending the load from the $(cm)_v$ results in minimal coupling between the fuselage and load dynamics.

3.5 Stability in Forward Flight

The system equations of motion (3.14-3.21) are coupled, nonlinear differential equations. In order to examine the vehicle-load stability in forward flight, it is convenient to linearize the general equations of motion about an equilibrium point. Consequently, the vehicle is assumed to be in steady level flight ($u = u^e$, $v^e = w^e =$

$\theta_v^e = 0$]. The load is assumed to be in the same vertical plane as the center of mass of the vehicle ($\lambda^e = \pi$). Substituting these equilibrium values of the variables in Equations 3.14-3.21, steady state equations are obtained and are solved to determine the following trim conditions.

$$\tan \theta_R^e = \frac{(K_v + K_L)\, u_e^2 + D^e_{rotor}}{(m_v + m_L)\, g} \tag{3.32}$$

$$\tan \phi_R^e = \frac{T_{tr}^e \cos \theta_R^e}{(m_v + m_L)\, g} \tag{3.33}$$

$$\tan \theta_L^e = \frac{K_L\, u_e^2}{m_L g} \tag{3.34}$$

$$\theta_t^e = \frac{1}{C_t\, \mu^2} \left[M_{\theta_v}{}^R + M_{\theta_v}{}^{fus} + C_t \left(\theta_R^e\, \mu^2 - \mu\lambda_i\right) + D_{\theta_v}{}^R\right]^e \tag{3.35}$$

where

$$C_t = S_t a_t \ell_t \left(\tfrac{1}{2}\rho\, u_e^2\right)$$

and

$$\mu^e \triangleq u_e / V_{tp}$$

V_{tp} is a reference tip speed based on a physical rotor that has the same performance as the rotor disc. Geometric and aerodynamic data used in the present analysis, and subsequently, are that of S-58 helicopter and are given in (SE 1, page 455) Table VI.

Table VI - Principal Dimensions and General Data of S-58 Helicopter

MAIN ROTOR	
Blade radius	8.53m
Number of blades	4
Chord	0.42m
Airfoil	NACA 0012
Hinge offset	0.43m
Normal RPM	222
TAIL ROTOR	
Blade radius	1.42m
Number of blades	4
Chord	0.18m
Tail rotor to main rotor gear ratio	6.0
Airfoil	NACA 0012
Tail length, ℓ_{tr}	8.53m
HORIZONTAL TAIL	
Area	$1.15 m^2$
Tail length, ℓ_t	10.1m
Airfoil	NACA 0009
TYPICAL MASS & DRAG CHARACTERISTICS	
Vehicle mass [reduced]	3000 kg
I_{xx}	7992 $kg-m^2$
I_{yy}	37285 $kg-m^2$
I_{zz}	31303 $kg-m^2$
Parasite area	3.39 m^2
Blade profile drag coefficient	0.01

The tail rotor collective pitch angle in trim is determined from the yawing moment equation as

$$\theta_{tr}^{e} = \frac{3}{(1 + \frac{3}{2}\mu_{tr}^{2})} \left[\frac{-T_{tr}^{e} (2C_T/a\sigma)_R}{\bar{V} (m_v + m_L) g} - \frac{\lambda_{tr}}{2} \right] \tag{3.36}$$

From the steady state rolling moment equation the vehicle bank angle required for equilibrium is given by

$$\phi_v^{e} = \sin^{-1} \left[\frac{T_{tr} z_{tr} - F_{y_v}^{R} h}{m_L g h_p} \right]_e \tag{3.37}$$

Typical trim values obtained for the nominal helicopter and load, for a specified flight condition are given below.

Nominal Parameter Values

m_v = 3000 Kg $\quad$ $\hat{m}$ = 0.5

ℓ = 4m $\quad$ ℓ_p = 0, h_p = 1.2m

C_D^L = 1.0 $\quad$ u^e = 20 m/s

Sea level flight (3.38)

Trim Values

θ_R^e = 3.2° $\quad$ ϕ_R^e = 0.5°

θ_L^e = 5.6° $\quad$ θ_t^e = -15° (+ve nose up)

θ_{tr}^e = 0.9° $\quad$ ϕ_v^e = 0.2°

T_R^e = 44197N $\quad$ T_{tr}^e = 361N (3.39)

In the interest of simplicity the vehicle bank angle in equilibrium, which is small, is assumed to be zero. Using these trim conditions [Equations 3.32-3.36] and linearizing the nonlinear equations of motion about the equilibrium point, the perturbation equations are obtained and put in the normal form

$$\dot{\bar{X}} = \underline{A}\,\bar{X} + \underline{B}\bar{U} \tag{3.40}$$

where

state vector $\bar{X}^T = [u\ w\ \theta_v\ q_v\ \theta_L\ q_L\ v\ \phi_v\ p_v\ r_v\ \lambda\ r_L]$

and

control vector $\bar{U}^T = [\theta_R\ \phi_R\ \theta_t\ \theta_{tr}]$

In Equation 3.40 variables $p_v \triangleq \dot{\phi}_v$, $q_v \triangleq \dot{\theta}_v$ and $r_v \triangleq \dot{\psi}_v$, have been formally introduced. $\underline{A}$ and $\underline{B}$ are given in Appendix A. Note that the perturbations in the variables are given by the same symbols as original variables. Unlike the case of PMM, the linearized equations are coupled in longitudinal and lateral motion of the helicopter and load. Stability of the system, as predicted by this Rigid body Vehicle Disc Rotor [RVDR] model, is determined by examining the eigenvalues of the system matrix. In order to understand the effects of load motion on that of the vehicle, the modes of helicopter alone, in the absence of load, are

obtained and are shown in Table VII. The aperiodic modes corresponding to forward speed convergence (S_3), rolling convergence (S_4) and vertical speed convergence (S_5) are similar to those observed in the case of PMM, but in the present case they include rotational motions of the helicopter in pitch, roll and yaw and are better identified as that of a real helicopter. S_6 correspond to the familiar, longitudinal oscillation of the helicopter and is found to be unstable. It includes lateral speed of the vehicle as well. The lateral oscillation of the helicopter (S_7), which is similar to a Dutch roll, is found to be stable. S_8 correspond to yawing convergence.

It is observed that the rotor dampings in pitch and roll introduce coupling in the longitudinal and lateral motion of the fuselage and hence that of the load. Indeed, by considering the case where the rotor disc is at the $(cm)_v$, this coupling was found to be minimal. Table VIII shows the modes observed in a case where the load is suspended from the $(cm)_v$ ($h_p = \ell_p = 0$). Comparing the load induced lateral and longitudinal oscillatory modes S_1 and S_2, respectively, with the corresponding modes observed in PVDR model [Table V], it is found that in the present case the S_2 mode contains azimuthal motion of the load. The frequencies and dampings of these modes, however, are in

Table VII - RVDR: Modes and Mode Shapes of Helicopter in the Absence of Load. Nominal Parameter Values

EIGENVALUES AND EIGENVECTORS	
$S_3 = -0.686$	$S_4 = -2.805$
$u = 1.000(180)$	$u = 0.103(180)$
$w = 0.151(180)$	$w = 0.469E-01(0)$
$\theta_v = 0.602E-01(180)$	$\theta_v = 0.796E-02(180)$
$q_v = 0.414E-01(0)$	$q_v = 0.223E-01(0)$
$v = 0.375(0)$	$v = 1.000(180)$
$\phi_v = 0.246E-01(180)$	$\phi_v = 0.166(0)$
$p_v = 0.169E-01(0)$	$p_v = 0.464(180)$
$r_v = 0.629E-01(0)$	$r_v = 0.411(0)$
$S_5 = -1.576$	$S_8 = -0.0557$
$u = 0.186(180)$	$u = 0.894E-02(180)$
$w = 1.000(0)$	$w = 0.116E-01(0)$
$\theta_v = 0.135E-01(180)$	$\theta_v = 0.187E-04(0)$
$q_v = 0.212E-01(0)$	$q_v = 0$
$v = 0.158E-01(180)$	$v = 1.000(0)$
$\phi_v = 0.238E-02(0)$	$\phi_v = 0.189E-02(180)$
$p_v = 0.375E-02(180)$	$p_v = 0.106E-03(0)$
$r_v = 0.117E-01(180)$	$r_v = 0.102(0)$

Table VII - [Cont'd]

EIGENVALUES AND EIGENVECTORS

$S_6 = 0.177 \pm 0.489i$

u	1.000(0)
w	0.697E-01(11)
θ_v	0.572E-01(115)
q_v	0.297E-01(44)
v	0.342(-27)
ϕ_v	0.192E-01(-93)
p_v	0.998E-02(-163)
r_v	0.289E-01(-17)

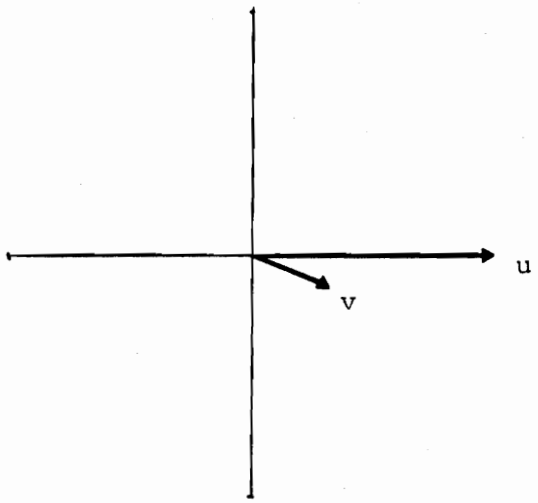

$S_7 = -0.279 \pm 0.659i$

u	0.102(-69)
w	0.168E-01(6)
θ_v	0.848E-02(-8)
q_v	0.607E-02(-12)
v	1.000(0)
ϕ_v	0.749E-01(-111)
p_v	0.537E-01(136)
r_v	0.101(26)

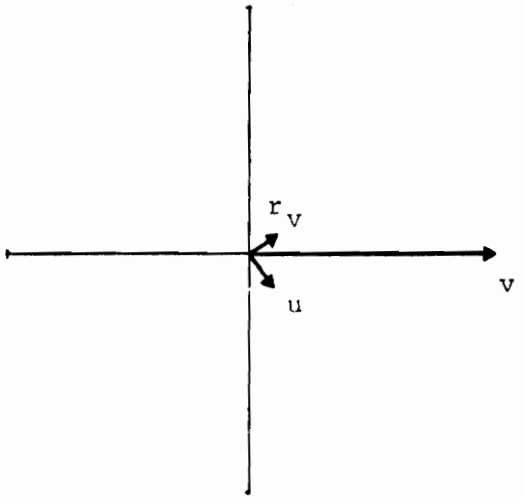

Table VIII - RVDR: Modes and Mode Shapes of Helicopter with Load Suspend from $(cm)_v$ [$h_p = 0$, $\ell_p = 0$]

EIGENVALUES AND EIGENVECTORS

$S_1 = -0.0149 \pm 1.961i$

$u = 0.793E\text{-}03(-61)$
$w = 0.499E\text{-}03(56)$
$\theta_v = 0.271E\text{-}03(-1)$
$q_v = 0.436E\text{-}03(-93)$
$\theta_L = 0.266E\text{-}03(32)$
$q_L = 0.517E\text{-}03(-59)$
$v = 0.141(0)$
$\phi_v = 0.276E\text{-}02(83)$
$p_v = 0.541E\text{-}02(-173)$
$r_v = 0.924E\text{-}02(45)$
$\lambda = 0.510(90)$
$r_L = 1.000(-1)$

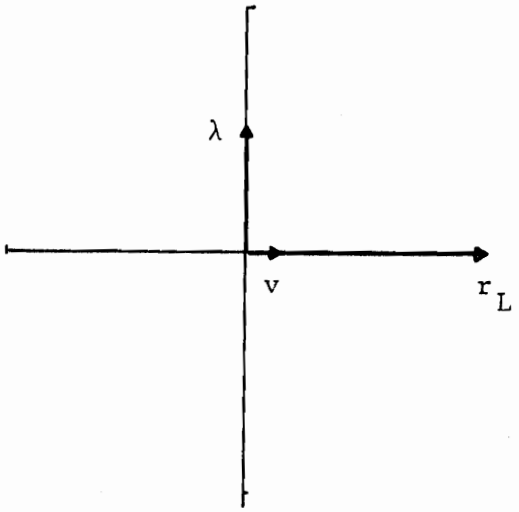

$S_2 = -0.0251 \pm 1.902i$

$u = 1.000(0)$
$w = 0.886E\text{-}01(15)$
$\theta_v = 0.511E\text{-}02(171)$
$q_v = 0.973E\text{-}02(80)$
$\theta_L = 0.395(88)$
$q_L = 0.752(-3)$
$v = 0.555E\text{-}01(-51)$
$\phi_v = 0.511E\text{-}03(52)$
$p_v = 0.973E\text{-}03(-39)$
$r_v = 0.395E\text{-}02(-9)$
$\lambda = 0.232(39)$
$r_L = 0.442(-51)$

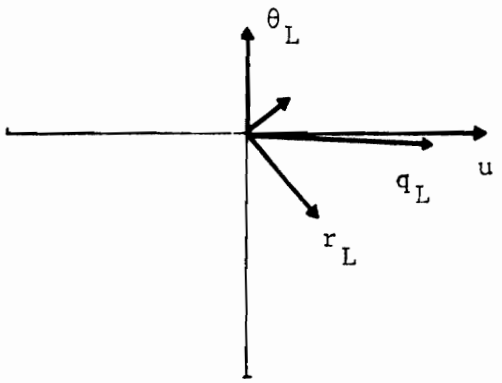

Table VIII - [Cont'd]

EIGENVALUES AND EIGENVECTORS	
$S_3 = -0.678$	$S_4 = -3.052$
$u = 1.000(180)$	$u = 0.652E-01(0)$
$w = 0.114(180)$	$w = 0.630E-02(180)$
$\theta_v = 0.596E-01(180)$	$\theta_v = 0.487E-02(0)$
$q_v = 0.404E-01(0)$	$q_v = 0.149E-01(180)$
$\theta_L = 0.520E-01(0)$	$\theta_L = 0.415E-02(180)$
$q_L = 0.352E-01(180)$	$q_L = 0.126E-01(0)$
$v = 0.867(0)$	$v = 0.498(0)$
$\phi_v = 0.548E-01(180)$	$\phi_v = 0.742E-01(180)$
$p_v = 0.371E-01(0)$	$p_v = 0.227(0)$
$\lambda = 0.481(180)$	$\lambda = 0.328(180)$
$r_L = 0.326(0)$	$r_L = 1.000(0)$
$r_v = 0.143(0)$	$r_v = 0.158(180)$
$S_5 = -1.216$	$S_8 = -0.0583$
$u = 0.257(180)$	$u = 0.773E-02(180)$
$w = 1.000(0)$	$w = 0.793E-02(0)$
$\theta_v = 0.198E-01(180)$	$\theta_v = 0.114E-04(180)$
$q_v = 0.241E-01(0)$	$q_v = 0.650E-06(180)$
$\theta_L = 0.115E-01(01)$	$\theta_L = 0.289E-04(180)$
$q_L = 0.139E-01(180)$	$q_L = 0.172E-06(180)$
$v = 0.741E-02(180)$	$v = 1.000(0)$
$\phi_v = 0.768E-03(0)$	$\phi_v = 0.342E-02(180)$
$p_v = 0.934E-03(180)$	$p_v = 0.199E-03(0)$
$\lambda = 0.567E-02(0)$	$\lambda = 0.102E-01(180)$
$r_L = 0.689E-02(180)$	$r_L = 0.594E-03(0)$
$r_v = 0.217E-02(180)$	$r_v = 0.102(0)$

Table VIII - [Cont'd]

EIGENVALUES AND EIGENVECTORS

$S_6 = 0.141 \pm 0.461i$

$u = 1.000(0)$
$w = 0.449E-01(16)$
$\theta_v = 0.527E-01(112)$
$q_v = 0.254E-01(39)$
$\theta_L = 0.577E-01(-58)$
$q_L = 0.278E-01(-131)$
$v = 0.395(-24)$
$\phi_v = 0.205E-01(-93)$
$p_v = 0.994E-02(-166)$
$\lambda = 0.219(-88)$
$r_L = 0.105(-161)$
$r_v = 0.342E-01(-14)$

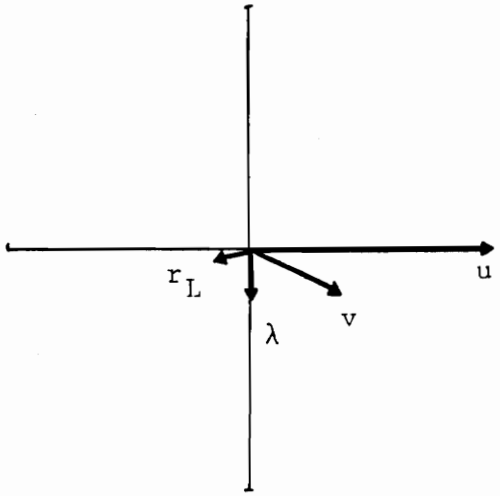

$S_7 = -0.437 \pm 0.537i$

$u = 0.175(-79)$
$w = 0.175E-01(-4)$
$\theta_v = 0.128E-01(-37)$
$q_v = 0.886E-02(-166)$
$\theta_L = 0.120E-01(148)$
$q_L = 0.833E-02(19)$
$v = 1.000(0)$
$\phi_v = 0.708E-01(-132)$
$p_v = 0.489E-01(109)$
$\lambda = 0.707(-136)$
$r_L = 0.489(95)$
$r_v = 0.119(25)$

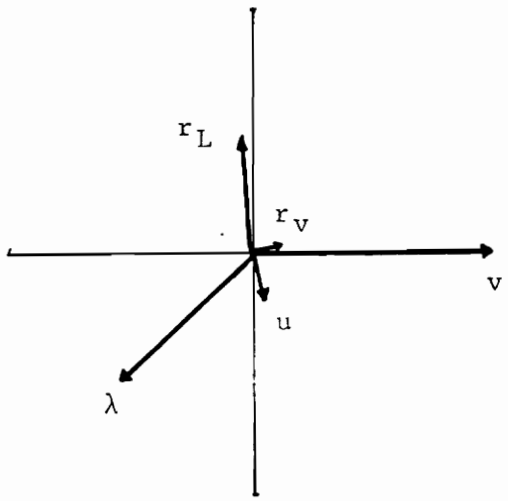

good agreement. The convergence modes of the helicopter [S_3, S_4, S_5 and S_8] are found to consist of load motions also. Comparing the helicopter oscillatory modes [S_6, S_7] with corresponding modes in the absence of the load [Table VII], it is observed that the damping of the lateral oscillatory mode is increased in the present case, primarily because of the sideforce damping provided by the load drag. This can also be interpreted from energy consideration by determining the phase difference between the perturbations in drag force of the load and velocity of the suspension point, corresponding to the perturbed motion in S_7 mode. If this phase difference is such that rate of work done is negative, which corresponds to a decrease in energy of the system, then the vehicle-load motion in this mode tends to be more stable, due to the increase in damping. Figure 3.5 shows the force-velocity phase diagram corresponding to mode S_7 and verifies the previous observation.

The modes of the helicopter load system in a case where the load is suspended from a point below the $(cm)_v$ (h_p = 1.2m, ℓ_p = 0) are shown in Table IX. Comparing modes S_1 and S_2 with corresponding modes observed previously with the suspension point at the $(cm)_v$ (Table VIII), it is found that in the present case the damping of the lateral mode (S_1) is greater while that of the longitudinal mode (S_2) is

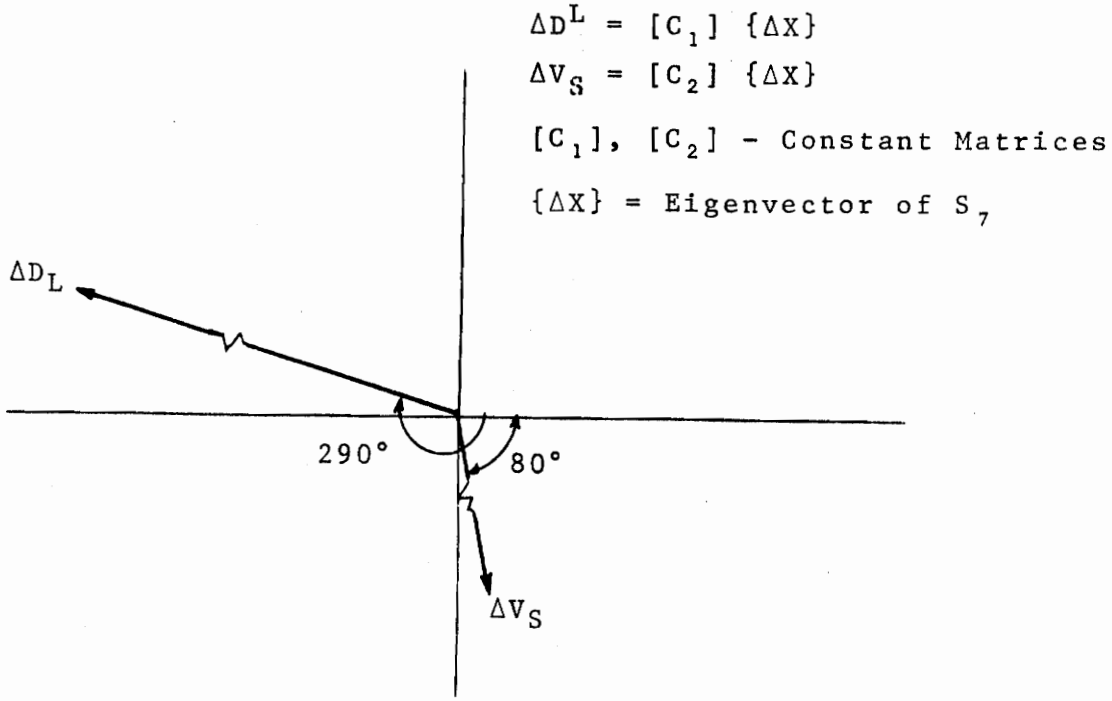

Figure 3.5 - Force-Velocity Phase Diagram Corresponding to the S_7 Mode [Table VIII]

Table IX - RVDR: Modes and Mode Shapes of Helicopter with Load Suspended from a Point Below $(cm)_v$ [h_p = 1.2m, ℓ_p = 0]

EIGENVALUES AND EIGENVECTORS

$S_1 = -0.318 \pm 2.744i$

$u = 0.607E\text{-}02(38)$
$w = 0.574E\text{-}03(124)$
$\theta_v = 0.160E\text{-}02(-22)$
$q_v = 0.446E\text{-}02(-118)$
$\theta_L = 0.300E\text{-}03(77)$
$q_L = 0.829E\text{-}03(-19)$
$v = 0.195(0)$
$\phi_v = 0.240E\text{-}01(-110)$
$p_v = 0.667E\text{-}01(153)$
$r_v = 0.630E\text{-}02(93)$
$\lambda = 0.361(94)$
$r_L = 1.000(-2)$

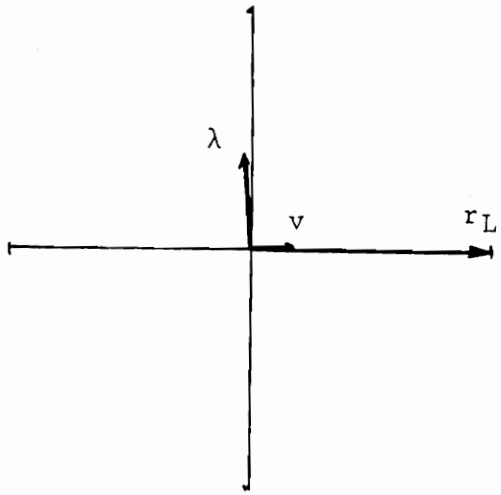

$S_2 = -0.0245 \pm 2.132i$

$u = 1.000(0)$
$w = 0.710E\text{-}01(-14)$
$\theta_v = 0.517E\text{-}01(104)$
$q_v = 0.109(-6)$
$\theta_L = 0.283(88)$
$q_L = 0.604(-6)$
$v = 0.891E\text{-}01(-98)$
$\phi_v = 0.122E\text{-}02(169)$
$p_v = 0.260E\text{-}02(78)$
$r_v = 0.570E\text{-}02(-52)$
$\lambda = 0.239(-8)$
$r_L = 0.511(-98)$

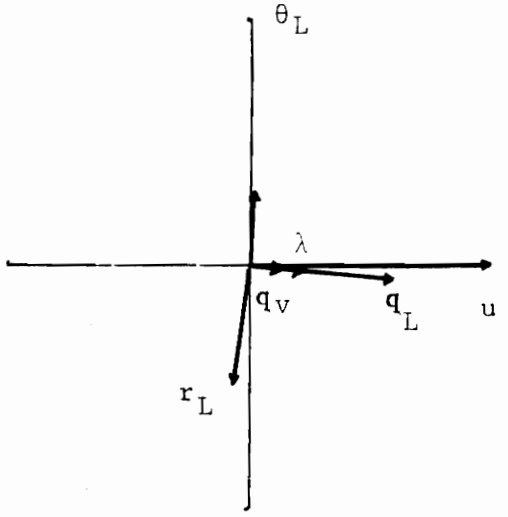

Table IX - [Cont'd]

EIGENVALUES AND EIGENVECTORS	
$S_3 = -0.716$	$S_4 = -2.793$
$u = 1.000(0)$	$u = 0.113(0)$
$w = 0.133(0)$	$w = 0.139E-01(180)$
$\theta_v = 0.613E-01(0)$	$\theta_v = 0.857E-02(0)$
$q_v = 0.438E-01(180)$	$q_v = 0.238E-01(180)$
$\theta_L = 0.515E-01(180)$	$\theta_v = 0.554E-02(180)$
$q_L = 0.368E-01(0)$	$q_L = 0.154E-01(0)$
$v = 0.454(180)$	$v = 0.928(0)$
$\phi_v = 0.289E-01(0)$	$\phi_v = 0.118(180)$
$p_v = 0.207E-01(180)$	$p_v = 0.328(0)$
$r_v = 0.779E-01(180)$	$r_v = 0.346(180)$
$\lambda = 0.246(0)$	$\lambda = 0.358(180)$
$r_L = 0.176(180)$	$r_L = 1.000(0)$
$S_5 = -1.219$	$S_8 = 0.0342$
$u = 0.301(180)$	$u = 0.712E-02(180)$
$w = 1.000(0)$	$w = 0.735E-02(0)$
$\theta_v = 0.233E-01(180)$	$\theta_v = 0.519E-04(0)$
$q_v = 0.284E-01(0)$	$q_v = 0.$
$\theta_L = 0.119E-01(0)$	$\theta_L = 0$
$q_L = 0.145E-01(180)$	$q_L = 0$
$v = 0.437E-02(0)$	$v = 1.000(0)$
$\phi_v = 0.423E-03(180)$	$\phi_v = 0.638E-02(0)$
$p_v = 0.515E-03(0)$	$p_v = 0.219E-03(0)$
$r_v = 0.171E-02(0)$	$r_v = 0.969E-01(0)$
$\lambda = 0.284E-02(180)$	$\lambda = 0.845E-01(0)$
$r_L = 0.347E-02(0)$	$r_L = 0.289E-02(0)$

Table IX - [Cont'd]

EIGENVALUES AND EIGENVECTORS

S_6 = 0.131 ±0.456i

u = 1.000(0)
w = 0.452E-01(17)
θ_v = 0.523E-01(112)
q_v = 0.248E-01(38)
θ_L = 0.581E-01(-58)
q_L = 0.275E-01(-132)
v = 0.346(-8)
ϕ_v = 0.180(-76)
p_v = 0.857E-02(-150)
r_v = 0.300E-01(3)
λ = 0.194(-72)
r_L = 0.919E-01(-146)

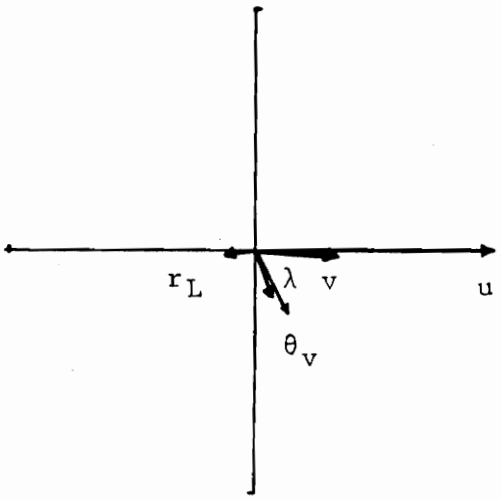

S_7 = -0.302 ±0.514i

u = 0.154(-80)
w = 0.144E-01(-7)
θ_v = 0.101E-01(-26)
q_v = 0.607E-02(-147)
θ_L = 0.970E-02(159)
q_L = 0.582E-02(39)
v = 1.000(0)
ϕ_v = 0.628E-01(-122)
p_v = 0.375E-01(117)
r_v = 0.109(21)
λ = 0.649(-125)
r_L = 0.386(114)

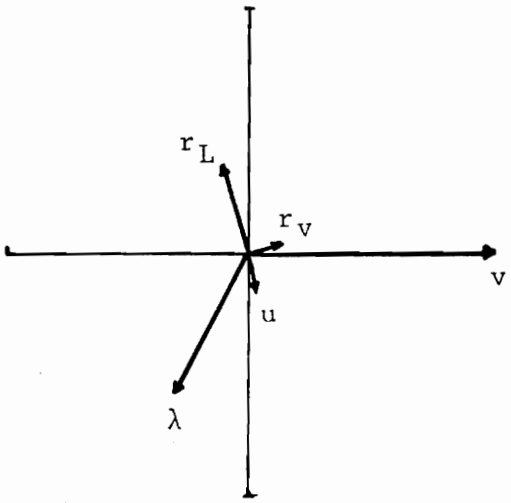

nearly same. This can be explained by noting that pitch and azimuthal motion of the load cause pitch and roll motion of the vehicle. Since the helicopter has greater damping in roll compared to damping in pitch, its effect on the lateral oscillatory mode is significantly greater. The increase in frequencies of these modes can be easily understood by considering a simpler model [see Figure 3.6] of the system as a rigidbody with a simple pendulum suspended from it. This system has two oscillatory modes [for $h_p = 0$, one mode is a rigid rotation of the system] one of which is of higher frequency and corresponds to the oscillation of the suspended mass, similar to S_1 or S_2. The other mode which has relatively lower frequency, corresponds to the oscillation of the rigidbody, similar to S_6 or S_7. For nominal values of the parameters, it is observed that with increasing h_p, the increase in frequency of the lateral oscillatory mode S_1 is greater than that of S_2 mode. This is because the helicopter has greater inertia in pitch than in roll. Similarly the decrease in frequencies of the helicopter oscillatory modes S_6 and S_7 with increasing h_p, can be explained by this simple model. The damping of the helicopter lateral oscillatory mode is found to be lower in the present case, because, the sideforce damping provided by the load drag decreases due to the increased effect of vehicle roll motion for $h_p > 0$. The aperiodic

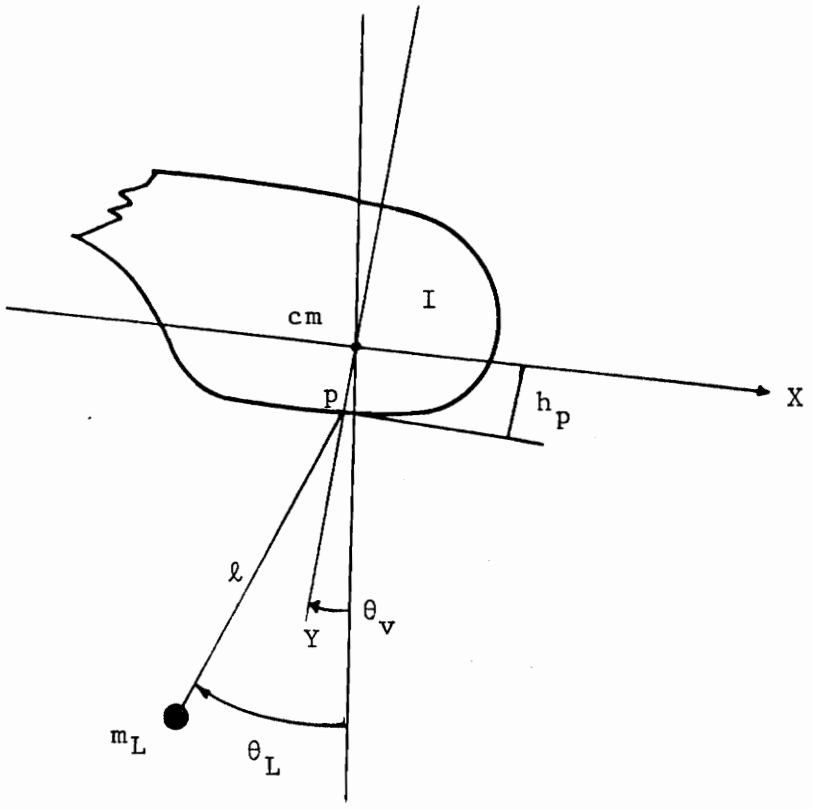

Figure 3.6 - Rigid Body with a Slung Mass

yawing motion (S_8) is observed to be weakly divergent in this case. These results are summarized in Table X.

It is observed that aft ($\ell_p < 0$) or forward ($\ell_p > 0$) location of the suspension point (P) with respect to the $(cm)_v$, has significant effect on the helicopter lateral and directional motions. Moving P from behind the $(cm)_v$ towards it and ahead, results in a less stable (damping decreases) lateral oscillation (S_7) at higher frequency [see Table X]. The variation in frequency occurs primarily due to the drag force on the load, which produces a stabilizing [weather-cock stability] yawing moment for $\ell_p < 0$ while it produces a destabilizing yawing moment for $\ell_p > 0$. It is found that the aperiodic yawing motion (S_8) tends to be favorably damped as P moves forward. This happens because the side force damping provided by the load drag, increases due to the increased effect of vehicle yawing velocity as P moves forward. It is observed that the degree of coupling between the vehicle and load motion in the oscillatory modes of the system depends considerably on the values of the parameters $\hat{m}$ and ℓ. The effect of varying $\hat{m}$ on the load induced oscillatory modes (S_1, S_2) are shown in Figure 3.7, for a case where the load is suspended by a short cable of length 4m. Unlike the case of PMM [Figure 2.3], the lateral oscillation

Table X - RVDR: Effect of Suspension Point Location on System Modes S_1, S_2, S_6 and S_8

ℓ_p (m)	h_p (m)	Load Induced Lat. Oscil. (S_1)	Load Induced Lngtd. Oscil. (S_2)	Helicopter Lat. Oscil. (S_7)	Helicopter Yawing (S_8)
0	0	-0.0149 ±1.961i	-0.0251 ±1.902i	-0.437 ±0.537i	-0.0583
0	2	-0.468 ±3.336i	-0.0348 ±2.314i	-0.256 ±0.479i	0.0685
0	4	-0.747 ±4.956i	-0.0835 ±2.863i	-0.200 ±0.408i	0.117
0	6	-0.975 ±6.609i	-0.148 ±3.482i	-0.176 ±0.361i	0.139
-3	1.2	-0.345 ±2.962i	-0.0269 ±2.127i	-0.595 ±0.115i	0.100
-1	1.2	-0.314 ±2.786i	-0.0239 ±2.147i	-0.346 ±0.377i	0.0682
+1	1.2	-0.331 ±2.735i	-0.0266 ±2.098i	-0.283 ±0.653i	0.007
+3	1.2	-0.402 ±2.862i	-0.0311 ±2.017i	-0.301 ±0.917i	-0.020

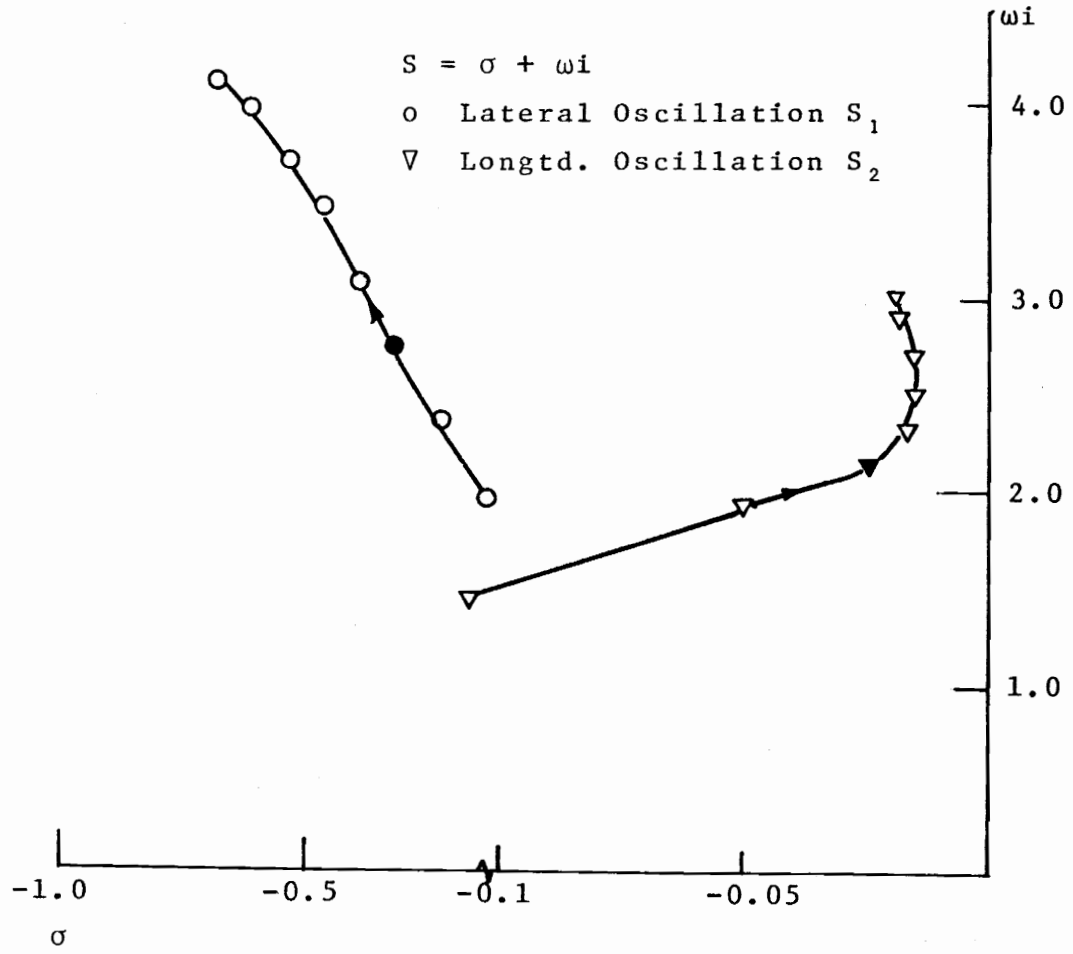

Figure 3.7 - RVDR: Effect of $\hat{m}$ on Load Induced Oscillatory Modes S_1 and S_2 $[0.1 \leq \hat{m} \leq 1.5(0.2)]$

(S_1) tends to be more heavily damped at higher $\hat{m}$. This can be explained by noting that increasing $\hat{m}$ [increasing load mass] tends to induce greater vehicle roll motion, which is well damped by the rotor damping moments. It is observed that for large values of ℓ the load motion has greater effect on helicopter oscillatory modes, particularly at higher $\hat{m}$. Also the load induced modes consist of greater vehicle motion in this case. It is found that for large values of ℓ, the load induced longitudinal oscillation of the system (S_2) tends to become stable with increasing $\hat{m}$ [Figure 3.8] while the helicopter oscillatory modes (S_6 and S_7) tend to become unstable [Figure 3.9].

Increasing the length of suspension cable is found to decrease the frequencies of all the oscillatory modes (S_1, S_2, S_6 and S_7). This can also be observed with the simple model [Figure 3.6] considered previously. For longer ℓ, modes S_1 and S_6 tend to become more stable while S_2 and S_7 tend to become unstable [Figure 3.10-3.11]. In this case modes S_1 and S_2 are primarly load induced oscillations of the helicopter in the lateral and longitudinal directions respectively. The increase in damping of S_1 and decrease in damping of S_2, observed here, follows from the fact that the vehicle has greater damping in roll than in pitch.

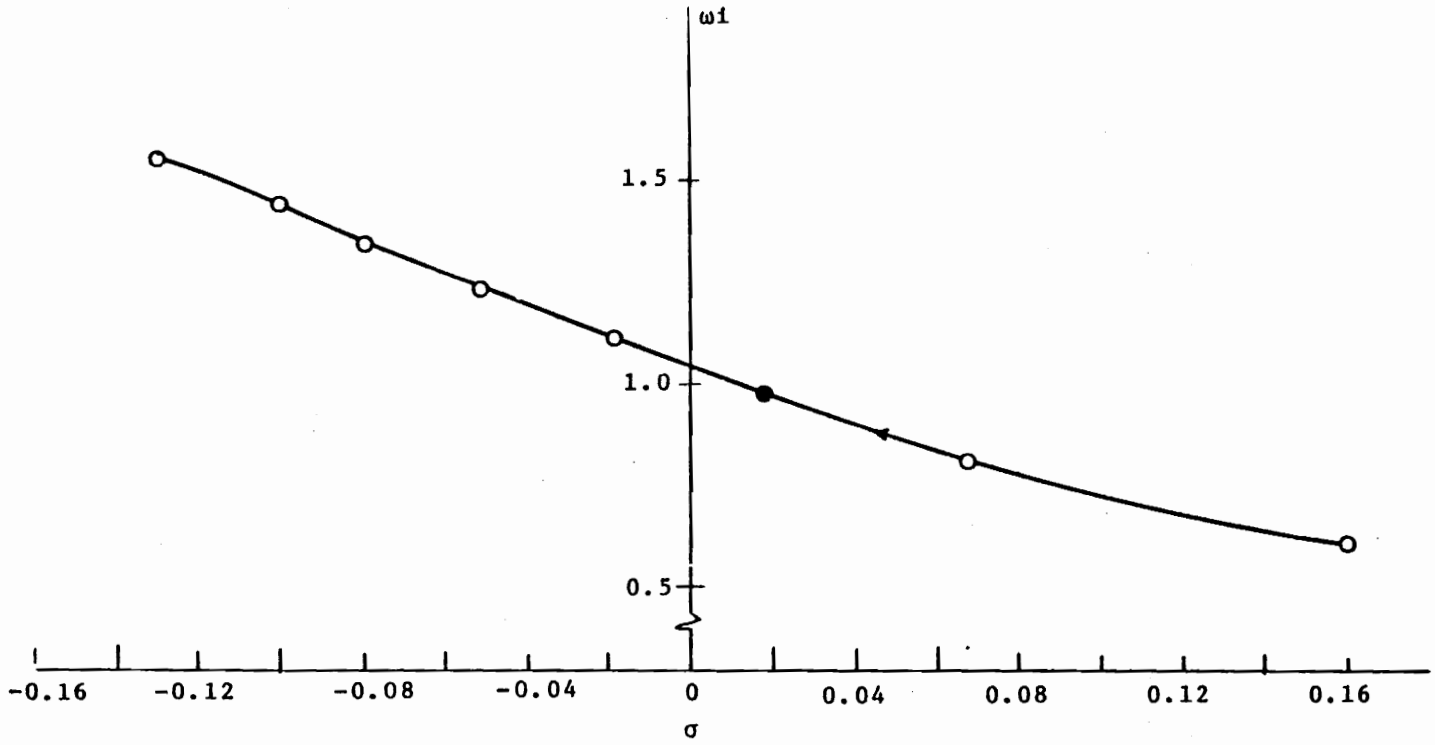

Figure 3.8 - RVDR: Effect of $\hat{m}$ on Load Induced Longitudinal Oscillatory Mode S_2
$[0.1 \leq \hat{m} \leq 1.5(0.2),\ \ell = 64m]$

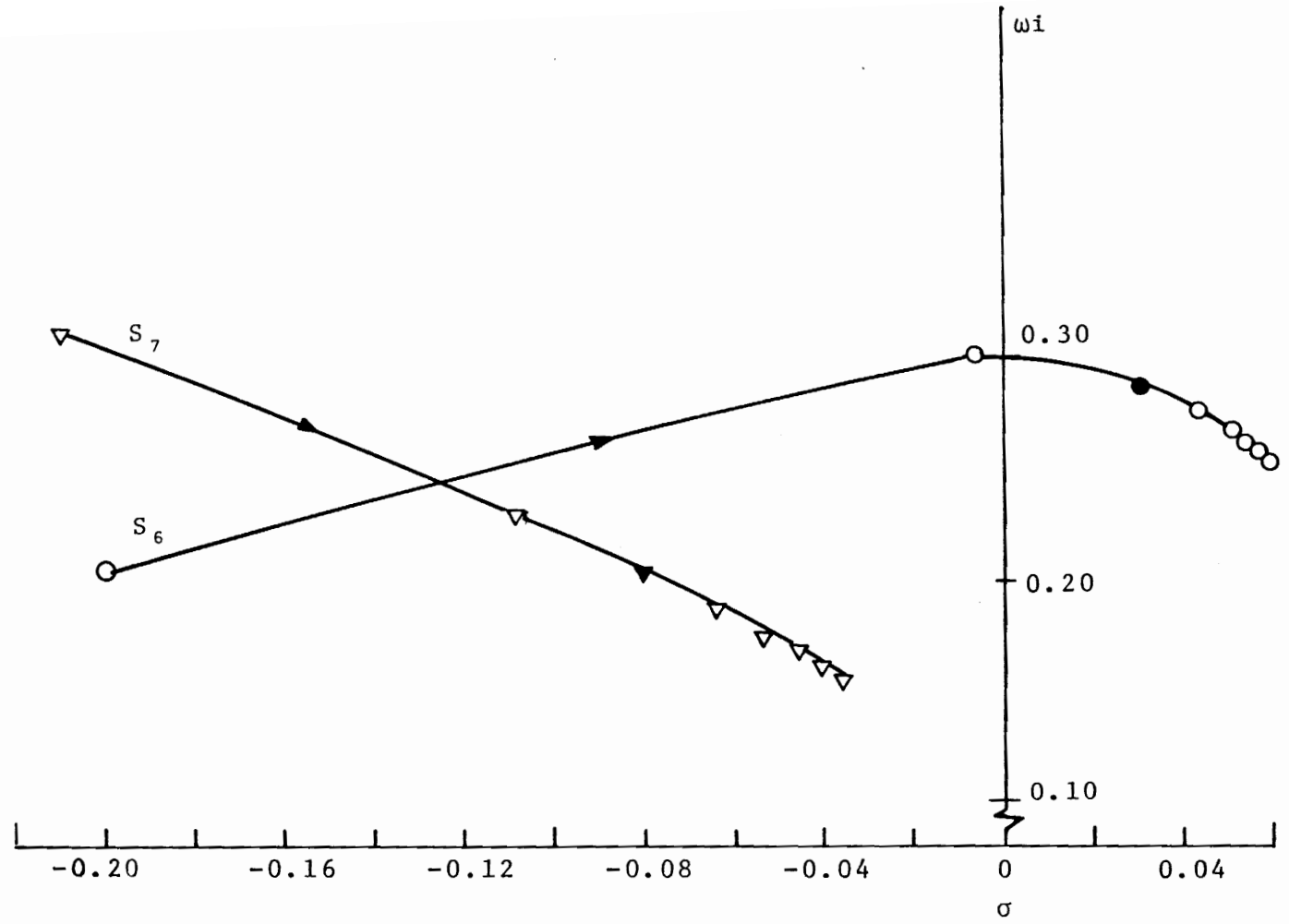

Figure 3.9 - RVDR: Effect of $\hat{m}$ on Helicopter Oscillatory Modes S_6 and S_7 [$0.1 \leq \hat{m} \leq 1.5(0.2)$, ℓ = 64m]

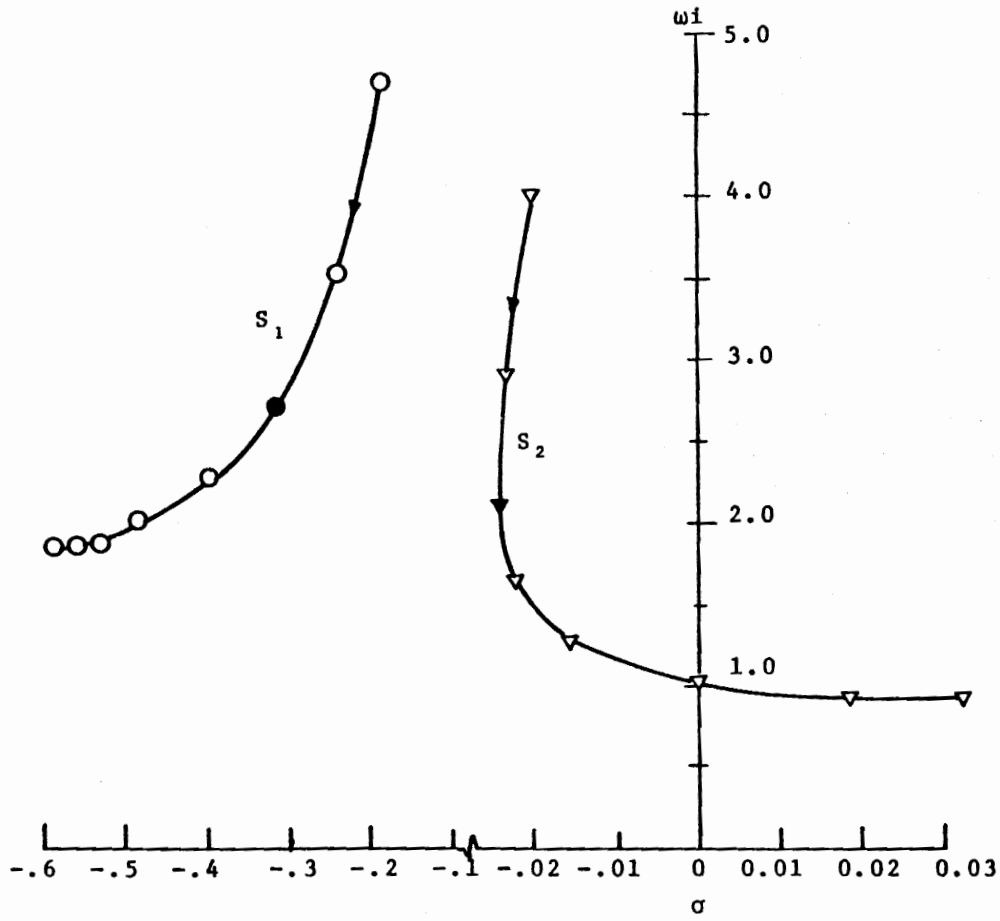

Figure 3.10 - RVDR: Effect of ℓ on Load Induced Oscillatory Modes S_1 and S_2 [$1 \leq \ell \leq 128(*2)$]

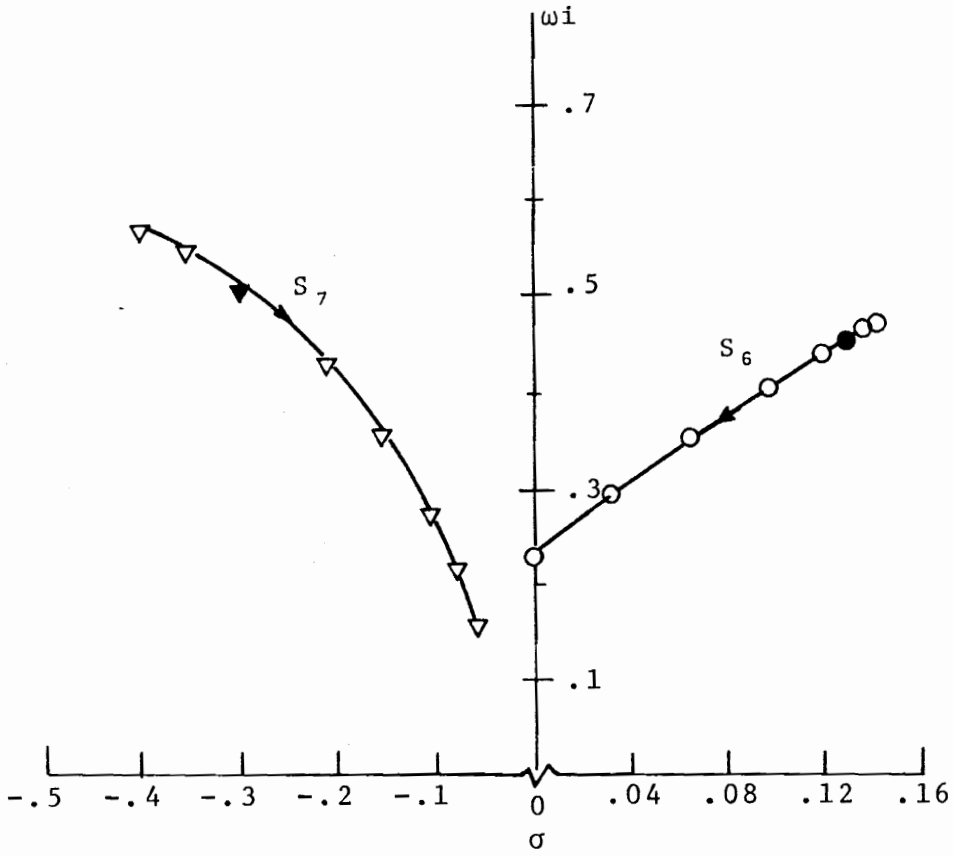

Figure 3.11 - RVDR: Effect of ℓ on Helicopter Oscillatory Modes S_6 and S_7 [$1 \leq \ell \leq 128(*2)$]

Figure 3.12 shows the effect of varying forward speed on the longitudinal oscillatory modes S_2 and S_6. It is observed that the load induced oscillation of the helicopter becomes unstable at higher speeds while the inherent oscillation of the helicopter (S_6) tends to become stable. In the absence of the load, however, S_6 tends to become unstable at higher speeds as discussed in (SE 1).

3.6 Summary

The thrust on the vehicle has been assumed to be generated by a rigid rotor disc that has pitch and roll degrees of freedom with respect to LHS. The helicopter has been modeled as a point mass located at the center of the disc and the load is also assumed to be a point mass, suspended from it. Stability of the system in forward flight, as predicted by this model, has been analyzed. It is observed that the modes predicted by this model are similar to those predicted by point mass model with fixed thrust vector in the LHS [Section 2.3, case (a)].

Subsequently, the vehicle is assumed to be a rigid body with conventional helicopter components. The rotor is modeled as a rigid disc that is connected to the fuselage by a rigid shaft at the $(cm)_v$. The load has been assumed

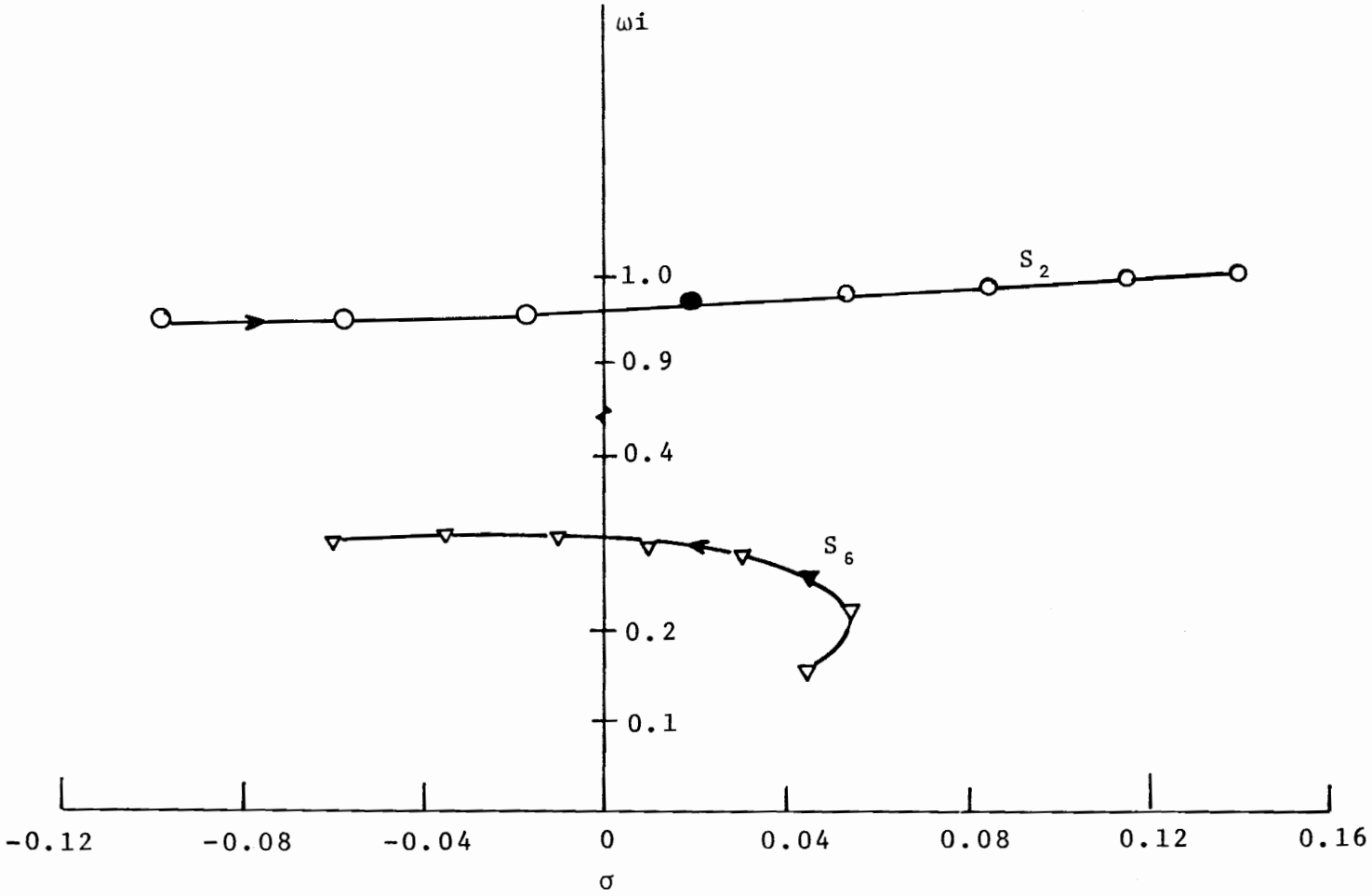

Figure 3.12 - RVDR: Effect of u_e on Longitudinal Oscillatory Modes S_2 and S_6 [$5 \leq u_e \leq 40(5)$, $\ell = 64m$]

to be a point mass and is suspended from the fuselage in it's plane of symmetry. Lagrange's equations of motion for this model of the system have been derived and stability of the system in forward flight has been analyzed. Typical modes of the system consist of load induced longitudinal and lateral oscillation of the system, inherent helicopter longitudinal and lateral oscillations, and convergence of helicopter forward speed, vertical speed, rolling and yawing velocities.

The effects of system parameters ℓ_p, h_p, $\hat{m}$, ℓ and u_e on the system modes have been examined. It is observed that the location of the load suspension point and length of the suspension cable are important parameters that determine the degree of coupling between the load motion and rigidbody motion of the vehicle. It has been found that suspending the load from a point below the $(cm)_v$ ($h_p > 0$) results in greater damping of the load induced oscillations of the system, than observed in the case where the load is suspended from the $(cm)_v$. The effect of load motion on the inherent modes of the helicopter is found to be more significant with increasing suspension length.

CHAPTER IV

ROTOR DYNAMICS INCLUDING HUB MOTION

4.1 Introduction

The rotor disc model developed in the last chapter is only conceptual and did not explicitly consider the dynamics of the rotor and its effects on the fuselage motion. In order to determine these effects, the rotor is modeled here as a real, articulated rotor with four blades, each hinged at a point offset from the center of the rotor hub. In this chapter the equations of motion of the rotor blades, including specified hub motions, are obtained in terms of coordinates that are defined with respect to a nonrotating reference frame. Rotor forces and their moments about $(cm)_v$ are also derived. In Chapter V these results are applied to the fuselage and load system to form a complete set of equations for the rotor-fuselage-load system.

4.2 Blade Equations of Motion

Figure 4.1 shows the coordinate system used in describing the blade motion. The rotor blade is assumed to be rigid and is attached to the hub at a hinge offset distance e, as shown. Coordinates β, ζ and θ describe the blade flapping, lagging and pitching motion, respectively. The equations of motion of a single blade are obtained by equating the net external moment about the flapping hinge

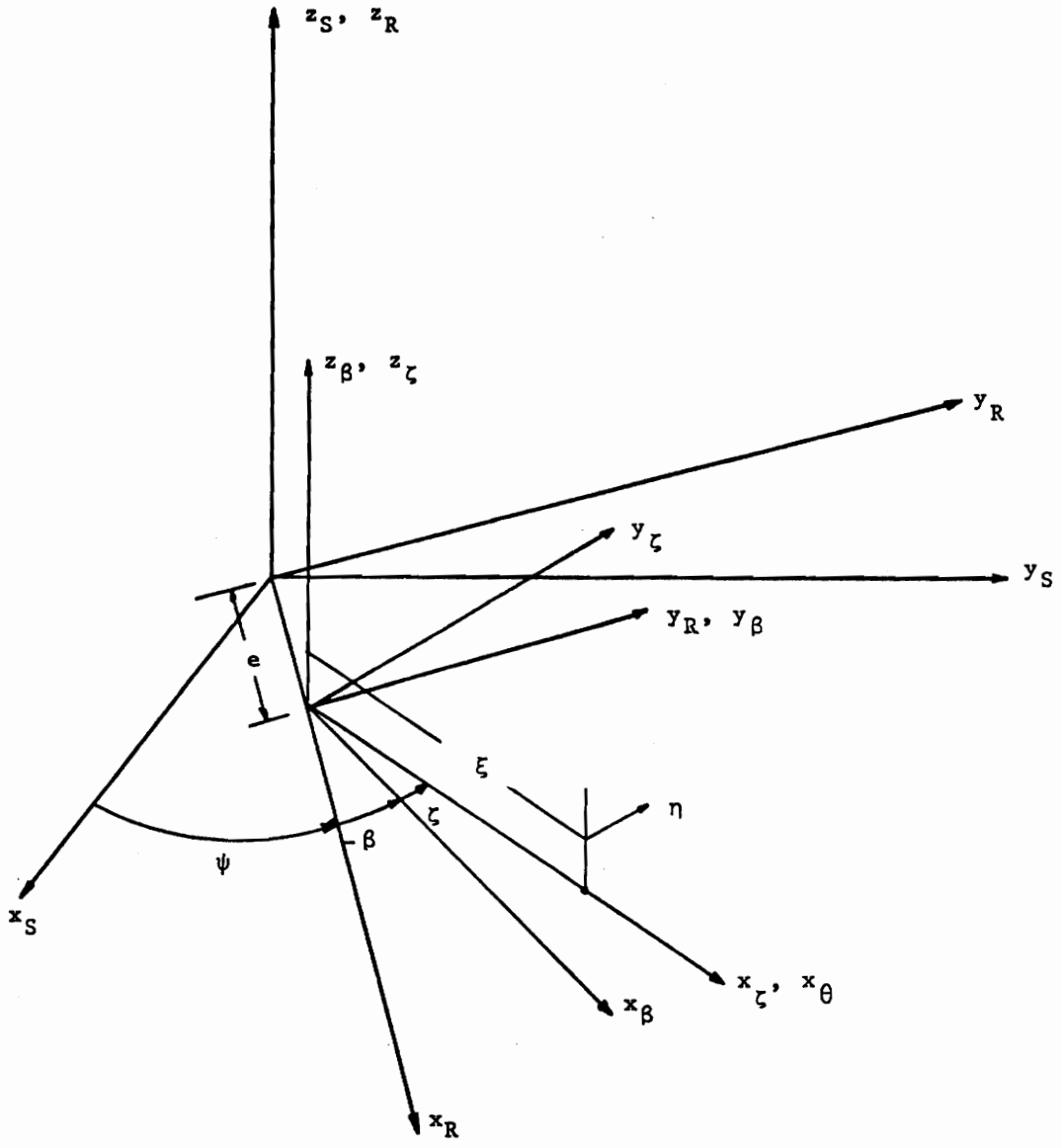

Figure 4.1 - Rotor Blade Axes System

to the time rate of change of angular momentum about the hinge, plus the moments due to the acceleration of the hinge. These equations have been derived in reference HA1 and are used in the present work in the form

$$\frac{M_{y_\beta}}{I_{yy}} = \ddot{\beta} + (\Omega^2+2\Omega\dot{\zeta})\,\beta - (\ddot{\theta}_v+2\Omega\dot{\phi}_v)\cos\psi + (\ddot{\phi}_v-2\Omega\dot{\theta}_v)\sin\psi + \tfrac{3}{2}\frac{\overline{e}_\beta}{1-\overline{e}_\beta}\,[\Omega^2\beta-(\ddot{\theta}_v+2\Omega\dot{\phi}_v)\cos\psi + (-\ddot{\phi}_v+2\Omega\dot{\theta}_v)\sin\psi] \tag{4.1}$$

$$\frac{M_{Z_\zeta}}{I_{ZZ}} = \ddot{\zeta} - 2\Omega\beta\dot{\beta} + \tfrac{3}{2}\frac{\overline{e}_\zeta}{1-\overline{e}_\zeta}\,\Omega^2\zeta + \tfrac{3}{2}\frac{\overline{e}_\zeta}{1-\overline{e}_\zeta}\,[-\ddot{\theta}_v\sin\psi+\ddot{\phi}_v\cos\psi] + \tfrac{3}{2}\frac{1}{1-\overline{e}_\zeta}\,[\dot{u}\sin\psi+\dot{v}\cos\psi] \tag{4.2}$$

It is assumed that the feathering uncoupled natural frequency is above twice per revolution. Consequently only flap-lag dynamics are of significance, and hence the blade pitching dynamics is not considered in this study. Further, the design and flight condition of the vehicle are assumed to be such that the rotor blade trim angles β_0, ζ_0 correspond to a stable operating point. Essentially, the blade flapping and lead-lag motion are assumed to be asymptotically

stable. In this vein, the term representing blade flapping acceleration due to lagging velocity in Equation 4.1 is neglected. For the present analysis, only the flapping Equation (4.1) is of significance, as the rotor inplane motions are not considered. The external flapping moment acting at the hinge, are due to the airloads and flapping hinge stiffness, and are evaluated next.

Aerodynamic Forces and Moments

Aerodynamics of a rotating wing in forward flight is highly complicated and predictions may involve extensive numerical computations. In order to obtain an approximate mathematical model that is tractable, the following assumptions are made. These have been found to yield acceptable results in stability and control analyses.

- Aerodynamic forces are assumed to be quasi-steady. Stall, compressibility and unsteady effects are neglected.

- Radial flow along the blade has no contribution to blade aerodynamic loads.

- The induced velocity at the rotor is assumed to be directed along the rotor shaft and has the distribution given by

$$v_i = v_i^H \ (1+k_v r\cos\psi)$$

where k_v is Glauert's factor (H01)

- The hinge offset is negligible in evaluating the aerodynamic forces of the blade.
- The blade airfoil section has a constant lift curve slope.

The blade element geometry is schematically shown in Figure 4.2. The velocity components of a blade element at a radial distance r from the axis of rotation and at azimuth angle ψ are (HA1)

$$U_p(r,\psi) = r\dot{\beta} - (r\dot{\phi}_v+\theta u+\beta v)\sin\psi - (r\dot{\theta}_v-\beta u+\theta v)\cos\psi - w + v_i \qquad (4.3)$$

$$U_T(r,\psi) = r\Omega+r\dot{\beta}\theta + (v+h\dot{\phi}_v)\cos\psi - (u-h\dot{\theta}_v)\sin\psi-\theta w$$

From quasi-steady aerodynamics, the lift on an airfoil of span, dr, is given by

$$dL(r,\psi) = \tfrac{1}{2}\rho ac\alpha(r,\psi)U^2(r,\psi)\,dr \qquad (4.5)$$

where

$$U^2 = U_p^2+U_T^2+U_R^2 \cong U_p^2+U_T^2$$

The moment of the elemental lift about the flapping hinge is

$$dM(r,\psi) = \tfrac{1}{2}\rho ac\alpha(r,\psi)[U_p^2(r,\psi)+U_T^2(r,\psi)]\,rdr \qquad (4.6)$$

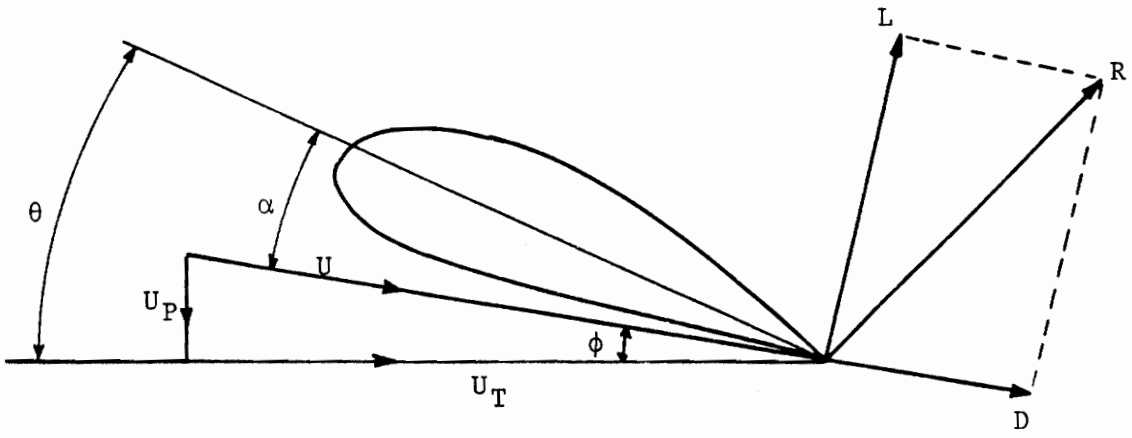

Figure 4.2 - Velocity Components of a Blade Element

From Figure 4.2

$$\alpha \cong \theta - \frac{U_P}{U_T} \tag{4.7}$$

Using strip theory the total aerodynamic moment about the flapping hinge is

$$M(\psi) = \tfrac{1}{2}\,\rho a c \int_0^{\beta R} [U_p{}^2+U_T{}^2]\left[\theta - \frac{U_P}{U_T}\right] r\cdot dr \tag{4.8}$$

The geometric pitch angle θ is assumed to vary with ψ according to

$$\theta = \theta_0+\theta_c \cos\psi + \theta_s \sin\psi \tag{4.9}$$

where

$\theta_0 \triangleq$ rotor collective pitch angle

$\theta_s, \theta_c \triangleq$ rotor longitudinal and lateral cyclic pitch angles, respectively.

Substituting Equations 4.3, 4.4 and 4.9 in 4.8 and retaining only first order terms in $\dot{\phi}_v$, $\dot{\theta}_v$, the aerodynamic moment is expressed in the form

$$M(\psi) = (C_\beta)\beta+(C_{\dot\beta})\dot\beta+(C_{\dot\phi_v})\dot\phi_v+(C_{\dot\theta_v})\dot\theta_v+C_0 + C_{\theta_0}\theta_0+C_{\theta_s}\theta_s+C_{\theta_c}\theta_c. \tag{4.10}$$

where the coefficients C_β, $C_{\dot\beta}$ .. C_{θ_c} are given in Table XI.

Table XI - Aerodynamic Coefficients

$$C_{\beta} = \frac{\gamma\Omega^2}{8}\left[\tfrac{4}{3}\mu_x B^3\cos\psi + \mu_x^2 B^2 \sin 2\psi - \tfrac{4}{3} B^3 \mu_y \sin\psi - 2B^2 \mu_x \mu_y \sin^2\psi + 2B^2 \mu_x \mu_y \cos^2\psi\right]$$

$$C_{\dot{\beta}} = \frac{\gamma\Omega}{8}\left[B^4 + \tfrac{4}{3}\mu_x B^3 \sin\psi + \tfrac{4}{3} B^3 \mu_y \cos\psi\right]$$

$$C_{\dot{\phi}_v} = \frac{\gamma\Omega}{8}\left\{-B^4 \sin\psi - \tfrac{2}{3}\mu_x B^3 (1 - \cos 2\psi) + \lambda\bar{h}\left[2B^2\cos\psi + \tfrac{2}{3} B^3 K_v (1 + \cos 2\psi)\right]\right\}$$

$$C_{\dot{\theta}_v} = \frac{\gamma\Omega}{8}\left[-B^4\cos\psi - \tfrac{2}{3}\mu_x B^3 \sin 2\psi - \lambda\bar{h}\left(2B^2 \sin\psi + \tfrac{2}{3} B^3 K_v \sin\psi\right)\right]$$

$$C_{0} = \frac{\gamma\Omega^2}{8}\left[-\tfrac{4}{3} B^3\lambda - 2\mu_x B^2\lambda \sin\psi - B^4\lambda K_v \cos\psi - \tfrac{2}{3}\mu_x B^3\lambda K_v \sin 2\psi + \tfrac{4}{3} B^3 \mu_Z + 2B^2 \mu_x \mu_y \sin\psi - 2B^2\lambda \mu_y \cos\psi - \tfrac{4}{3}\lambda K_v B^3 \mu_y \cos^2\psi\right]$$

$$C_{\dot{\theta}_0} = \frac{\gamma\Omega^2}{8}\left[B^4 + 2\mu_x^2 B^2 (1 - \cos 2\psi) + 4\mu_x B^3 \sin\psi + 4B^3\mu_y \cos\psi + 4B^2\mu_x\mu_y \sin 2\psi + 2\lambda B^2\mu_Z + \tfrac{4}{3}\lambda K_v B^3 \mu_Z \cos\psi\right]$$

$$C_{\theta_s} = C_{\theta_0} \sin\psi$$

$$C_{\theta_c} = C_{\theta_0} \cos\psi$$

The moment due to the flapping hinge restraint is

$$M_{sp} = K_{\beta}\beta \tag{4.11}$$

Introducing Equations 4.10 and 4.11 in 4.1 and rearranging, the blade flapping equation of motion is given by

$$\ddot{\beta} + (C_{\beta})\beta + \left[C_{\beta} + \left\{ 1 + \tfrac{3}{2}\frac{\bar{e}}{1-\bar{e}} + \frac{K_{\beta}}{I_{yy}\Omega^2} \right\} \right]\beta$$

$$- \left(1 + \tfrac{3}{2}\frac{\bar{e}}{1-\bar{e}} \right)(\ddot{\theta}_v + 2\Omega\dot{\phi}_v)\cos\psi$$

$$- \left(1 + \tfrac{3}{2}\frac{\bar{e}}{1-\bar{e}} \right)(-\ddot{\phi}_v + 2\Omega\dot{\theta}_v)\sin\psi$$

$$+ (C_{\dot{\theta}_v})\dot{\theta}_v + (C_{\dot{\phi}_v})\dot{\phi}_v = C_0 + C_{\theta_s}\theta_s + C_{\theta_c}\theta_c \tag{4.12}$$

Coordinate Transformation

Equation 4.12 describes the flapping motion of a single blade in terms of its flapping angle β which has been defined with respect to a rotating reference frame. It is convenient to consider the blade motion in terms of coordinates that are defined with respect to a nonrotating reference frame, in which the blade motions are better understood. Accordingly, the blade flapping angle is approximated by its constant and first harmonic content as

$$\beta(t) = \beta_0(t) - \theta_R(t)\cos\Omega t - \phi_R(t)\sin\Omega t \tag{4.13}$$

where

β_0 is the average coning angle of all the blades

and θ_R, ϕ_R are defined as pitch and roll angles of the rotor and are determined by averaging over one revolution of a blade. Usually, the motion of a four bladed-rotor is described in terms of coning, rotor pitching and rolling and differential flapping (flapping of blades 1, 3 in one direction and 2, 4 in the other direction). In this study the differential flapping of the blades is not considered as its influence on the other degress of freedom are only through higher harmonics, in forward motion of the rotor (BI1). It is observed that for the rotor aerodynamic model considered here, the pitch and roll angles of the rotor can be interpreted physically as the angles made by the average rotor thrust vector with respect to the shaft axis. This has been verified by rotor performance calculations done subsequently in Chapter V. Before introducing the approximate flapping angle [Equation 4.13] in the flapping Equation (4.12) it is important to note that this equation is nonlinear in the fuselage variables. In order to analyze the stability and control of the rotor-fuselage system in forward flight, it is convenient that the rotor dynamical equations be linear in fuselage variables as well. Consequently the following scheme that combines the flapping angle approximation and perturbation about an equilibrium point, corresponding to uniform translation of the helicopter, is used.

4.3 Rotor Equations of Motion in Forward Flight

Since it is intended to study the stability of the rotor-fuselage system in uniform translation, the blade equation in 4.12 is simultaneously approximated in terms of the flapping angle and linearized about the equilibrium point specified by

$$u = u^e,\ v^e = w^e \equiv 0,\ \phi_v{}^e = \theta_v{}^e \equiv 0 \tag{4.14}$$

and

$$\beta^e = \beta_0{}^e - \theta_R{}^e \cos\psi - \phi_R{}^e \sin\psi \tag{4.15}$$

$$\theta^e = \theta_0{}^e + \theta_c{}^e \cos\psi + \theta_s{}^e \sin\psi \tag{4.16}$$

From 4.15 it follows that

$$\dot{\beta}^e = \theta_R{}^e\Omega \sin\psi - \phi_R{}^e\Omega \cos\psi$$

and $$\ddot{\beta}^e = \theta_R{}^e\Omega^2\cos\psi + \phi_R{}^e\Omega^2\sin\psi$$

Substituting the above steady state conditions in Equation 4.12, it is observed that introducing the approximate $\beta(\psi)$ involves multiplication of the coefficients in Equation 4.12, which contain $\sin\psi$, $\cos\psi$, $\sin2\psi$, $\cos2\psi$, by $\sin\psi$ and $\cos\psi$. The resulting cross products are converted to constant terms and higher harmonic (2ψ, 4ψ) terms. As an approximation, second and higher harmonic terms are neglected, which results in the following steady state equations (4.17) that relate rotor position angles (β_0, ϕ_R, θ_R) and rotor

control angles (θ_0, θ_s, θ_c)

$$\underline{A} \begin{Bmatrix} \beta_0 \\ \phi_R \\ \theta_R \end{Bmatrix}_e = \underline{B} \begin{Bmatrix} \theta_0 \\ \theta_s \\ \theta_c \end{Bmatrix}_e + \{\underline{C}\} \qquad (4.17)$$

$$\underline{A} = \begin{bmatrix} 1+\frac{3}{2}\frac{\bar{e}}{1-\bar{e}} + \frac{K\beta}{I_{yy}\Omega^2} & 0 & 0 \\ 0 & -\frac{3}{2}\frac{\bar{e}}{1-\bar{e}} - \frac{K\beta}{I_{yy}\Omega^2} & \frac{\gamma}{8}(1-\mu^2/2) \\ \gamma\mu/6 & -\frac{\gamma}{8}(1+\mu^2/2) & -\frac{3}{2}\frac{\bar{e}}{1-\bar{e}} - \frac{K\beta}{I_{yy}\Omega^2} \end{bmatrix}_e$$

$$\underline{B} = \begin{bmatrix} \frac{\gamma}{8}(1+2\mu^2) & \frac{\gamma}{4}\mu & 0 \\ \frac{\gamma}{2}\mu & \frac{\gamma}{8}(1+3\mu^2) & 0 \\ 0 & 0 & \frac{\gamma}{8}(1+\mu^2) \end{bmatrix}_e$$

$$\{\underline{C}\} = \begin{Bmatrix} -\frac{\gamma}{6}\lambda \\ -\frac{\gamma}{4}\mu\lambda \\ -\frac{\gamma}{8}\lambda k_v \end{Bmatrix}_e$$

In order to linearize the flapping Equation 4.12 about the equilibrium point specified above, small perturbations in rotor flapping is assumed in the form

$$\beta = \beta_0(t) - \theta_R(t)\cos\Omega t - \phi_R(t)\sin\Omega t$$

where the perturbations have been denoted by the same symbols as original variables. The corresponding perturbations in the flapping velocity and acceleration are given by

$$\dot{\beta} = \dot{\beta}_0 + (-\dot{\theta}_R - \phi_R\Omega)\cos\psi + (-\dot{\phi}_R + \theta_R\Omega)\sin\psi$$

and

$$\ddot{\beta} = \ddot{\beta}_0 + (-\ddot{\theta}_R + \theta_R\Omega^2 - 2\Omega\dot{\phi}_R)\cos\psi + (2\Omega\dot{\theta}_R - \ddot{\phi}_R + \phi_R\Omega^2)\sin\psi$$

Substituting these perturbations in Equation 4.12 and performing operations indicated earlier in deriving the steady state equations, the following linearized equations are obtained (note that second and higher harmonics have, again, been neglected).

$$\begin{aligned}
&\ddot{\beta}_0 + \left(\frac{\gamma\Omega}{8}\right)\dot{\beta}_0 + (\hat{\Omega}^2)\,\beta_0 + \left(-\frac{\gamma\Omega}{12}\mu^e\right)\dot{\phi}_R \\
&\quad + \frac{\gamma\Omega}{12}(\lambda k_v\bar{h} - \mu^e)\,\dot{\phi}_v + \frac{\gamma\Omega^2}{8}(-4\mu^e\theta_0{}^e - 2\theta_s{}^e)\,\mu_x \\
&\quad + \frac{\gamma\Omega^2}{8}(\tfrac{2}{3}\lambda k_v - 2\theta_c{}^e)\,\mu_y + \frac{\gamma\Omega^2}{8}(-\tfrac{4}{3} - 2\lambda\theta_0{}^e - \tfrac{2}{3}\lambda k_v\theta_c{}^e)\,\mu_z \\
&= \frac{\gamma\Omega^2}{8}(1+2\mu_e{}^2)\,\theta_0 + \left(\frac{\gamma\Omega^2}{4}\mu_e{}^2\right)\theta_s \qquad (4.18)
\end{aligned}$$

$$\ddot{\phi}_R + \left(\frac{\gamma\Omega}{8}\right)\dot{\phi}_R + (\hat{\Omega}^2-\Omega^2)\phi_R + (-2\Omega)\dot{\theta}_R + \frac{\gamma\Omega^2}{8}(\tfrac{1}{2}\mu_e{}^2-1)\theta_R$$
$$+ \left(-\frac{\gamma\Omega}{6}\mu_e\right)\dot{\beta}_0 + \left(1 + \tfrac{3}{2}\frac{\bar{e}}{1-\bar{e}}\right)\ddot{\phi}_v + \left(\frac{\gamma\Omega}{8}\right)\dot{\phi}_v$$
$$+ \left[\frac{\gamma\Omega}{4}\lambda\bar{h} - 2\mu\left(1 + \tfrac{3}{2}\frac{\bar{e}}{1-\bar{e}}\right)\right]\dot{\theta}_v + \frac{\gamma\Omega^2}{8}(\mu_e\theta_R{}^e - 2\lambda$$
$$+ 4\theta_0{}^e + 6\mu_e\theta_s{}^e)\mu_x + \frac{\gamma\Omega^2}{8}(\tfrac{4}{3}\beta_0{}^e - \mu_e\phi_R{}^e + 2\mu_e\theta_c{}^e)\mu_y$$
$$+ \frac{\gamma\Omega^2}{8}(2\mu_e + 2\lambda\theta_s{}^e)\mu_Z = \left(-\frac{\gamma\Omega^2}{4}\mu_e\right)\theta_0 - \frac{\gamma\Omega^2}{8}(1+3\mu_e{}^2)\theta_s \qquad (4.19)$$

$$\ddot{\theta}_R + \left(\frac{\gamma\Omega}{8}\right)\dot{\theta}_R + (\hat{\Omega}^2-\Omega^2)\theta_R + (2\Omega)\dot{\phi}_R$$
$$+ \frac{\gamma\Omega^2}{8}(1 + \tfrac{1}{2}\mu_e{}^2)\phi_R + \left(-\frac{\gamma\Omega^2}{6}\mu_e\right)\beta_0$$
$$+ \left[2\Omega\left(1 + \tfrac{3}{2}\frac{\bar{e}}{1-\bar{e}}\right) - \frac{\gamma\Omega}{4}\lambda\bar{h}\right]\dot{\phi}_v + \left(1 + \tfrac{3}{2}\frac{\bar{e}}{1-\bar{e}}\right)\ddot{\theta}_v$$
$$+ \frac{\gamma\Omega}{8}\dot{\theta}_v + \frac{\gamma\Omega^2}{8}(-\tfrac{4}{3}\beta_0{}^e + \mu_e\phi_R{}^e + 2\mu_e\theta_c{}^e)\mu_x$$
$$+ \frac{\gamma\Omega^2}{8}(\mu_e\theta_R - 2\lambda + 4\theta_0 + 2\mu_e\theta_s{}^e)\mu_y + \frac{\gamma\Omega^2}{8}(\tfrac{4}{3}\lambda k_v\theta_0{}^e$$
$$+ 2\lambda\theta_c{}^e)\mu_Z = -\frac{\gamma\Omega^2}{8}(1 + \mu_e{}^2)\theta_c \qquad (4.20)$$

where $\hat{\Omega}^2 = 1 + \frac{3}{2}\frac{\bar{e}}{1-\bar{e}} + \frac{K_\beta}{I_{yy}\Omega^2}$

$\bar{e} = e/R$

$\bar{h} = h/R$

$\mu_x = u/\Omega R$, $\mu_y = v/\Omega R$, $\mu_Z = w/\Omega R$

Equations 4.18-20 are more general than those derived in reference (BI1), where the rotor hub motion was not considered. In developing the RVDR model in Chapter III, the disc rotor damping in pitch and roll were evaluated from Equations 4.19-20 by neglecting the effect of rotor angular velocities and accelerations on the fuselage motion. In the next chapter the above Equations (4.18-20) are combined with those of the fuselage-load system to obtain perturbation equations for the complete rotor-fuselage-load system in steady forward flight.

4.4 Rotor Forces on Fuselage

In deriving the equations of motion of the helicopter-load system described by the RVDR model (Section 3.4) the rotor forces were treated as external forces acting at the hub. Similarly, the forces generated by the articulated rotor are necessary for developing the dynamical equations of the helicopter that has an articulated rotor. Consequently, the rotor forces are now evaluated as components along the vehicle axes.

The rotor forces considered in the present analysis are essentially the aerodynamic lift and drag forces generated by the rotor blades. Figure 4.3 shows a blade element and the lift and drag generated by it. These forces are resolved in directions parallel to the vehicle body axes, as

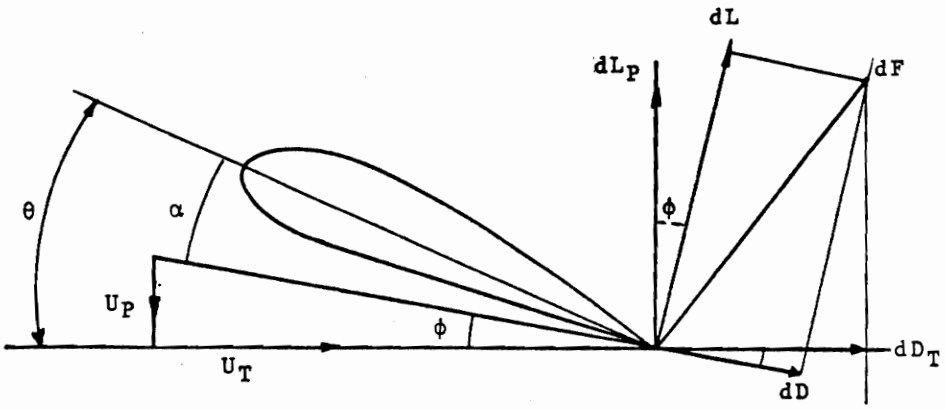

Figure 4.3 - Blade Element Force Components

shown in Figure 4.4. Using strip theory, the total rotor force components due to the entire blade, as well as all the blades, are evaluated. From Figure 4.3,

$$\phi = \tan^{-1} \frac{U_p}{U_T} \cong \frac{U_p}{U_T} \tag{4.21}$$

and

$$\left.\begin{aligned} dL_p &= dL \cos\phi - dD \sin\phi \\ dL_T &= dL \sin\phi + dD \cos\phi \end{aligned}\right\} \tag{4.22}$$

Resolving the blade element forces along the vehicle axes system,

$$\left.\begin{aligned} dF_{x_v} &\cong \beta dL_p \sin\psi - dD_T \cos\psi \\ dF_{y_v} &\cong -\beta dL_p \cos\psi - dD_T \sin\psi \\ dF_{z_v} &\cong -dL_p \end{aligned}\right\} \tag{4.23}$$

Here β denotes the flapping angle and is not a perturbation. From airfoil theory,

$$\begin{aligned} dL &= \tfrac{1}{2} \rho V^2 C_L S \cong \tfrac{1}{2} \rho (U_p^2 + U_T^2) a\alpha c \, dr \\ dD &= \tfrac{1}{2} \rho V^2 C_d S \cong \tfrac{1}{2} \rho (U_p^2 + U_T^2) C_{do} c \, dr \end{aligned} \tag{4.24}$$

where $$\alpha = \theta - \phi \cong \left(\theta - \frac{U_p}{U_T} \right)$$

C_{do} is the profile drag coefficient of the blade section, U_p, U_T are blade velocity components given by Equations 4.3

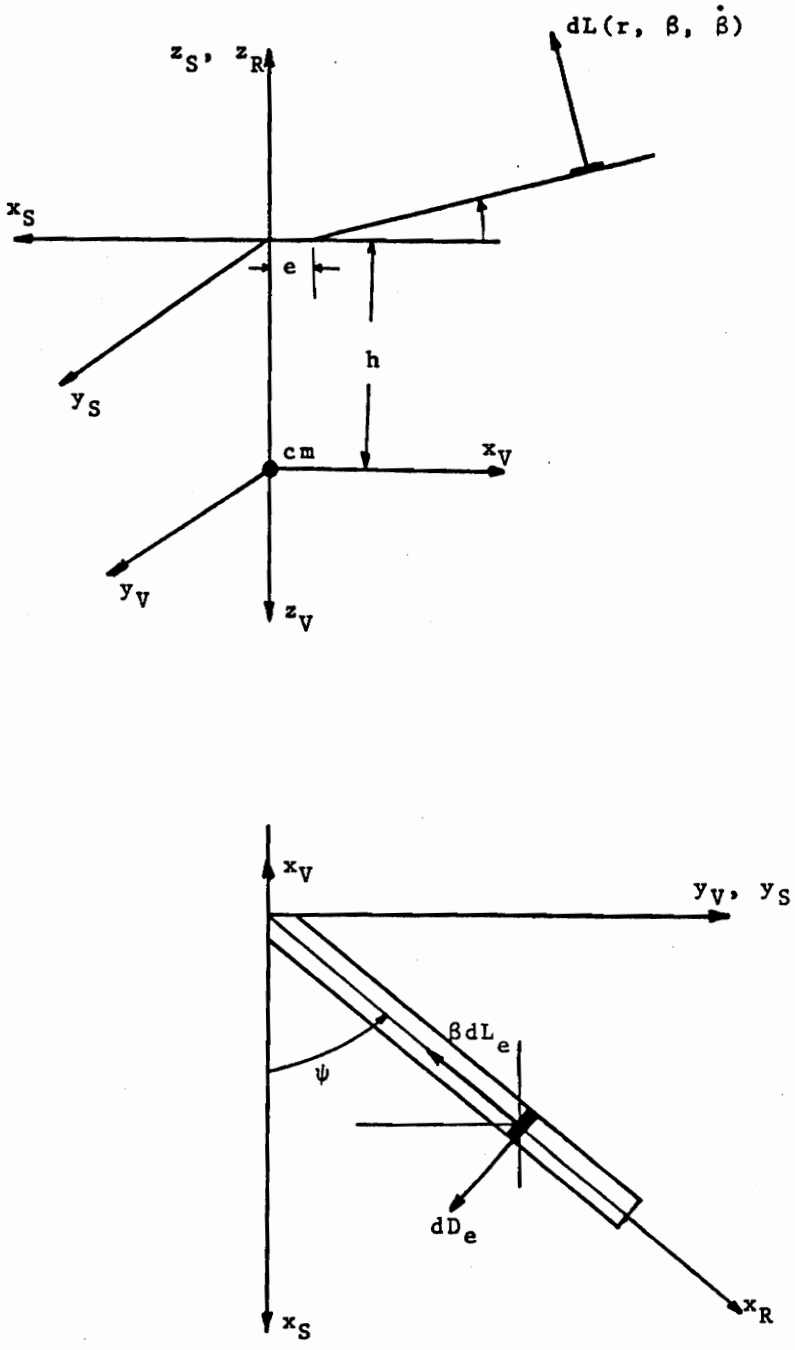

Figure 4.4 - Rotor Force Components in Vehicle Axes System

and 4.4 respectively. Introducing Equations 4.3, 4.4 and 4.24 in 4.23 and integrating over the entire blade length and averaging over one revolution of the blade, the rotor force components in vehicle axes system are given by

$$F_{x_v} \cong \frac{1}{4\pi} \rho b c \int_0^{2\pi} \int_0^{BR} \left[a \left(\theta - \frac{U_p}{U_T} \right) (U_p^2 + U_T^2) \left(\beta \cos\psi - \frac{U_p}{U_T} \sin\psi \right) - C_{d_0} (U_p^2 + U_T^2) \sin\psi \right] dr \, d\psi \tag{4.25}$$

$$F_{y_v} \cong \frac{1}{4\pi} \rho b c \int_0^{2\pi} \int_0^{BR} \left[a \left(\theta - \frac{U_p}{U_T} \right) (U_p^2 + U_T^2) \left(-\beta \sin\psi - \frac{U_p}{U_T} \cos\psi \right) - C_{d_0} (U_p^2 + U_T^2) \cos\psi \right] dr \, d\psi \tag{4.26}$$

$$F_{Z_v} \cong \frac{1}{4\pi} \rho b c \int_0^{2\pi} \int_0^{BR} \left[-a (\theta - U_p U_T) (U_p^2 + U_T^2) \right] dr \, d\psi \tag{4.27}$$

In evaluating the above integrals the following approximations are made, which have been found to yield satisfactory results.

- The blade flapping angle is adequately described by its constant and first harmonic content [Equation 4.13].
- Vehicle velocity components v, w are small compared to component u so that squares and products of the former are negligible while with that of the latter are retained.
- Only first order terms in fuselage pitch and roll velocities are considered.
- Tip loss factor, B = 1
- Reverse flow effects are negligible since the advance ratios considered are small ($\mu < 0.5$).
- Only squares and products of all rotor angles are retained, since their values are significant in determining the rotor force components.

Evaluating the integrals in 4.25-4.27, the rotor forces in vehicle axes are,

$$F_{x_v} = a\tilde{b} \left[- \frac{(u - h\dot{\theta}_v)}{\Omega R} \left(\frac{C_{d_o}}{2} + \frac{\theta_0 \lambda}{2} + \frac{\beta_0^2}{4} \right) \right.$$

$$\frac{(v + h\dot{\phi}_v)}{\Omega R} \left[\tfrac{3}{2} \beta_0 (\theta_0 - \lambda) \right] + \theta_R \frac{\lambda}{4}$$

$$\left. + \frac{\dot{\phi}_v}{\Omega} \left(\frac{\theta_0}{6} - \frac{\lambda}{2} \right) + \frac{\dot{\theta}_v \beta_0}{6\Omega} \right.$$

$$+ \frac{\theta_c \beta_0}{6} - \frac{\theta_s \lambda}{4} + \phi_R \frac{\beta_0}{6} + \frac{\dot{\phi}_R}{\Omega}\left(\frac{\theta_0}{6} - \frac{\lambda}{2}\right) + \frac{\dot{\theta}_R}{\Omega}\frac{\beta_0}{6}\Bigg]$$

$$+ \theta_R F_{Z_v} \qquad (4.28)$$

$$F_{y_v} = a\tilde{b}\Bigg[-\frac{(u-h\dot{\theta}_v)}{\Omega R}\ \frac{3}{4}\beta_0\left(\frac{\theta_0}{2} - \lambda\right) - \frac{(v+h\dot{\phi}_v)}{\Omega R}\left(\frac{C_{d_o}}{2}\right.$$

$$\left. + \frac{\theta_0 \lambda}{2} + \frac{\beta_0^2}{4}\right) + \frac{\dot{\theta}_v}{\Omega}\left(\frac{\theta_0}{6} - \frac{\lambda}{2}\right)\ \frac{\dot{\phi}_v \beta_0}{6\Omega} - \phi_R \frac{\lambda}{4} - \dot{\phi}_R \frac{\beta_0}{6}$$

$$+ \theta_R \frac{\beta_0}{6} + \frac{\dot{\theta}_R}{\Omega}\left(\frac{\theta_0}{6} - \frac{\lambda}{2}\right) - \theta_s \frac{\beta_0}{6} - \theta_c \frac{\lambda}{4}\Bigg] - \phi_R F_{Z_v}$$

(4.29)

$$F_{z_v} = -a\tilde{b}\ \Bigg[\theta_0\left(\frac{1}{3} + \frac{u^2}{2\Omega^2 R^2}\right) + \frac{u\theta_c}{2\Omega R} - \frac{v\theta_c}{2\Omega R} + \frac{\dot{\phi}_v \theta_v \bar{h}}{2\Omega}$$

$$- \dot{\theta}_v\left(\theta_0 \frac{u\bar{h}}{\Omega R} + \frac{\theta_c \bar{h}}{2}\right)\Bigg] + \tilde{c}\Bigg[\frac{\theta_0}{6}\left(\theta_R - \frac{\dot{\phi}_R}{\Omega}\right)^2$$

$$+ \frac{\theta_0}{6}\left(\frac{\dot{\theta}_R}{\Omega} + \phi_R\right)^2 + \frac{\dot{\beta}_0}{3\Omega} + \frac{u}{4\Omega R}\left(\theta_R - \frac{\dot{\phi}_R}{\Omega}\right) - \frac{u^2}{2\Omega^2 R^2}\ \theta_0$$

$$- \frac{u}{4\Omega R}\theta_s - \frac{u}{4\Omega R}\theta_R + \frac{\lambda}{4}\ \Bigg\{2 + \theta_s\left(\theta_R - \frac{\dot{\phi}_R}{\Omega}\right)$$

$$- \theta_c\left(\frac{\dot{\theta}_R}{\Omega} + \phi_R\right) + \frac{2\dot{\beta}_0}{\Omega}\theta_0\Bigg\} - \frac{\lambda}{6} k_v \theta_0\left(\frac{\dot{\theta}_R}{\Omega} + \phi_R\right)$$

$$+ \frac{v}{\Omega R}\left(\frac{\theta_c}{4} - \frac{\lambda k_v}{4}\right) - \frac{w}{\Omega R}\left(\frac{1}{2} + \lambda\theta_0\right) + \frac{\dot{\phi}_v}{\Omega}\left(-\phi_R \frac{\bar{h}}{4} - \frac{u}{4\Omega R}\right.$$

$$\left. - \frac{\bar{h}\beta_0 u}{4\Omega R} + \frac{\lambda}{4} k_v \bar{h}\right) + \frac{\dot{\theta}_v}{\Omega}\left(-\theta_R \frac{\bar{h}}{4} + \frac{\theta_0 u}{2\Omega R}\bar{h}\right)\Bigg] \qquad (4.30)$$

where $\tilde{b} = \frac{1}{2}\rho b c \Omega^2 R^3$

$\tilde{c} = \tilde{b}\ (a + C_{d_o})$

The corresponding moments about the $(cm)_v$ are

$$M^R_{\theta_v} = - F_{x_v} h \tag{4.31}$$

$$M^R_{\theta_v} = F_{y_v} h \tag{4.32}$$

Equation 4.28-4.32 are used in the next chapter in obtaining the equations of motion of the helicopter which has an articulated rotor. These equations are also used to obtain the corresponding perturbations in rotor forces and moments, about a vehicle equilibrium flight condition. Figure 4.5 illustrates the response of rotor force component F_x, for a step input in longitudinal cyclic pitch angle and vehicle pitch rate.

4.5 Summary

General equations of motion of a single rotor blade have been specialized to consider only the out of plane motion of the blades, which is described by the blade flapping equation. Using an approximate flapping angle, given by its constant and first harmonic content, the flapping equation is linearized about an equilibrium point corresponding to steady forward flight of the helicopter. The resultint perturbation equations describe the dynamics of the rotor in terms of average values of rotor coning, pitching and rolling angles and include the effects of fuselage motion.

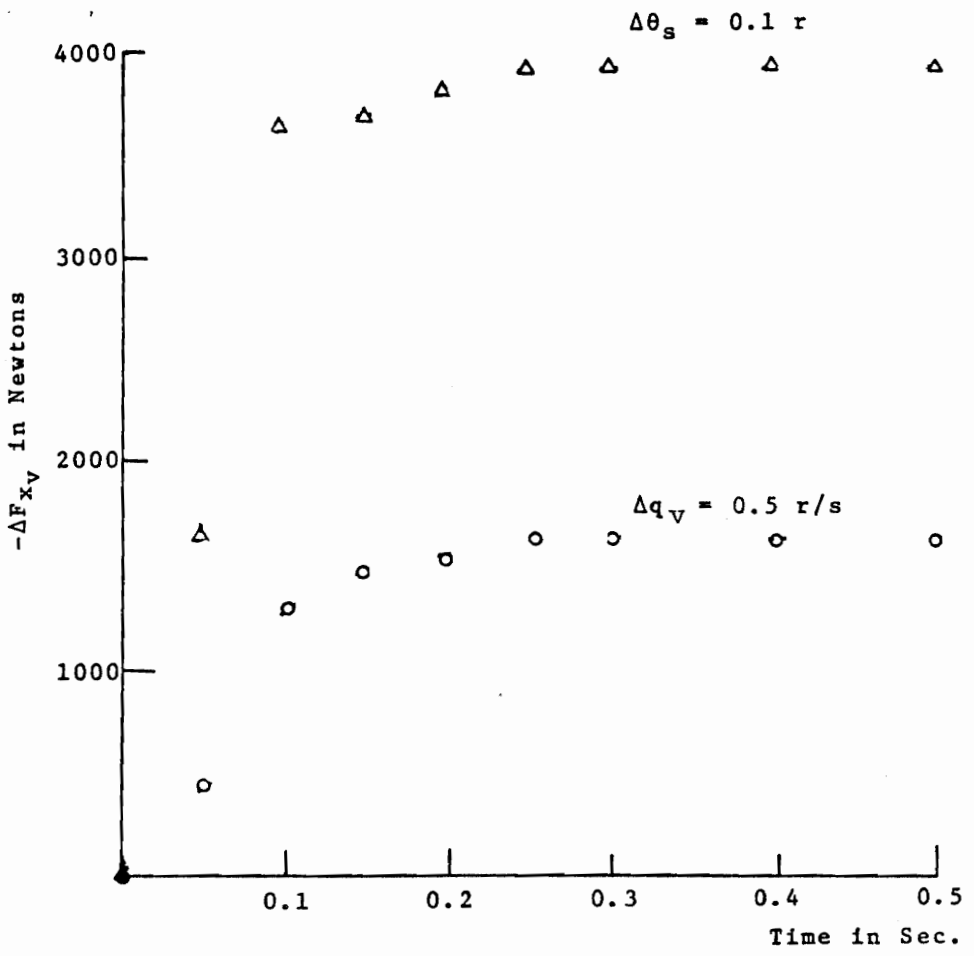

Figure 4.5 - Response of Rotor Force Component F_{x_v} to Step Inputs in Longitudinal Cyclic Pitch Angle and Vehicle Pitch Velocity

The average aerodynamic forces generated by an articulated rotor are evaluated and expressed as components along the vehicle axes. The corresponding moments about the center of mass of the vehicle are also determined.

CHAPTER V

SYSTEM MODEL WITH RIGID-BODY FUSELAGE ARTICULATED ROTOR AND POINT MASS LOAD (RVAR)

5.1 Introduction

In order to consider the dynamical effects of an articulated rotor on the stability of fuselage and load motion in forward flight, the perturbation equations of the rotor, aptly developed in Section 4.3, are combined with those of the fuselage-load system, developed in Section 3.4. The resulting equations that represent the rotor-fuselage-load system are used to examine the stability of the system in forward flight for a specified design and flight conditions. An approximate model of the rotor (H04) is then obtained by assuming the changes in rotor velocities and accelerations to be instantaneous such that they have negligible effect on the forces generated by the rotor. Using this quasi-static rotor model, a lower order dynamic model of the system is obtained. Stability of the vehicle-load configuration, as predicted by this model, is determined and compared with corresponding results obtained by using the model with complete rotor dynamics. The effects of varying the values of some of the principal parameters of the configuration on the stability of the system are determined and compared

with similar results predicted by the RVDR model.

5.2 Dynamical Equations of the System with an Articulated Rotor

In Section 3.4 the equations of motion of the helicopter-load system were derived by modeling the helicopter as a rigid body with a disc rotor and the load as a point mass. Presently it is intended to replace the disc rotor by an articulated rotor which has four rigid blades hinged at an offset. The forces generated by this rotor have already been evaluated in Section 4.4. Consequently in Equations 3.14-21 the non-potential forces due to disc rotor thrust [Equation 3.9] and their moments about the $(cm)_v$ [Equation 3.27] are replaced by corresponding articulated rotor thrust [Equations 4.28-30] components and their moments about the $(cm)_v$ [Equations 4.31-32]. The resulting nonlinear dynamical equations describe the motion of the vehicle-load system in terms of the rotor, fuselage and load variables. In order to analyze the motion of the complete system it is required that the equations of motion of the rotor be considered along with those of the fuselage and load, as will be done subsequently.

5.3 Stability in Forward Flight

In order to examine the stability of the helicopter-load system in forward flight, it is convenient to linearize

the nonlinear equations of motion about the equilibrium point corresponding to uniform translation, as done in Section 3.5. The steady state equations corresponding to Equations 3.14-16 are

$$
\begin{aligned}
0 = Q_x^e &= (D_x{}^v)^e + (D_x{}^L)^e + (F_x{}^R)^e \\
0 = Q_y^e &= (F_y{}^R)^e + (T_y{}^{tr})^e \\
-(m_v + m_L)g = Q_Z^e &= (F_Z{}^e)_R
\end{aligned}
\tag{5.1}
$$

where $(F_x{}^R)^e$, $(F_y{}^R)^e$ and $(F_Z{}^R)^e$ are steady state values of the rotor force components along vehicle body axes. These are functions of rotor position angles $\beta_0{}^e$, $\phi_R{}^e$, $\theta_R{}^e$ and control pitch angles θ_0 $\theta_s{}^e$ and $\theta_c{}^e$. $T_{tr}{}^e$, which is used to counter the main rotor torque, is determined for a specified operation of the engine. In order to determine the control pitch angles necessary for trim, Equation 4.17 is used to express the rotor position angle in terms of rotor control pitch angles in Equation 5.1 and the resulting equations are solved numerically by Newton-Ralphson iteration procedure. For the nominal design and forward flight condition [Equation 3.38] the trim values are

$$
\begin{aligned}
\beta_0{}^e &= 3.371^\circ & \theta_0{}^e &= 2.242^\circ \\
\phi_R{}^e &= -0.458^\circ & \theta_c{}^e &= 0.559^\circ \\
\theta_R{}^e &= -3.497^\circ & \theta_s{}^e &= -4.449^\circ
\end{aligned}
$$

[The rotor pitch and roll angles in trim, evaluated here, are in good agreement with corresponding values obtained for the disc rotor; the differences in sign occur because of opposite sense of rotation.] The corresponding equilibrium values of stabilizer setting angle θ_t, tail rotor collective pitch angle θ_{tr}^e and vehicle bank angle ϕ_v^e are obtained as before [Equations 3.35-37].

The combined linearized equations of the fuselage-load system are arranged in the matrix form

$$[SA] \begin{Bmatrix} \dot{\bar{X}}_V \\ \dot{\bar{X}}_L \end{Bmatrix} = [SB]\, \bar{X}_R + [SC]\, \dot{\bar{X}}_R + [SD] \begin{Bmatrix} \bar{X}_V \\ \bar{X}_L \end{Bmatrix} + [SE]\, \bar{U} \qquad (5.2)$$

where

$$\bar{X}_V^T = [u\ v\ w\ \theta_v\ q_v\ \phi_v\ p_v\ r_v]$$

$$\bar{X}_L^T = [\theta_L\ q_L\ \lambda\ r_L]$$

$$\bar{X}_R^T = [\beta_0\ \phi_R\ \theta_R]$$

$$\bar{U}^T = [\theta_0\ \theta_s\ \theta_c\ \theta_t\ \theta_{tr}]$$

Note that the perturbations are given by the same symbols as the original variables. Matrices [SA], [SB], ... [SE] are given in Appendix A.

In Equation 5.2 the fuselage-load motions are coupled with that of the rotor, and hence, additional equations, corresponding to dynamics of the rotor, are required for analyzing the stability of the system. Indeed, such a set of equations corresponding to perturbed motion of the rotor in forward flight have already been derived in Section 4.3 [Equations 4.18-20] and they are presented here in matrix form

$$\{\ddot{\bar{X}}_R\} = [MB]\ \bar{X}_R + [MC]\ \dot{\bar{X}}_R + [MD]\ \bar{X}_V + [ME]\ \dot{\bar{X}}_V + [MF]\ \bar{U} \qquad (5.3)$$

(Matrices [MB], ... [MF] are given in Appendix A). The linearized equations of the complete rotor-fuselage-load system are obtained by combining Equations 5.2 and 5.3, as

$$\underline{A}\dot{\bar{X}} = \underline{B}\bar{X} + \underline{C}\bar{U} \qquad (5.4)$$

where

$$\bar{X}^T = [\bar{X}_R\ \dot{\bar{X}}_R\ \bar{X}_V\ \bar{X}_L]$$

(Matrices $\underline{A}$, $\underline{B}$ and $\underline{C}$ are given in Appendix A.)

For the nominal design and flight conditions of the helicopter-load configuration the eigenvalues and corresponding eigenvectors of the system matrix $\underline{A}^{-1}\ \underline{B}$ in Equation 5.4 are evaluated and are given in Table (XII). Comparing these

Table XII - RVAR: Modes and Mode Shapes of Helicopter with a Load Suspended from a Point Below the $(cm)_v$ [h_p = 1.2m, ℓ_p = 0]

EIGENVALUES AND EIGENVECTORS

$S_1 = -0.414 \pm 2.726i$

$p_R = 0.014(-124)$
$v = 0.200(0)$
$\phi_v = 0.025(-116)$
$p_v = 0.069(146)$
$\lambda = 0.363(97)$
$r_L = 1.000(2)$

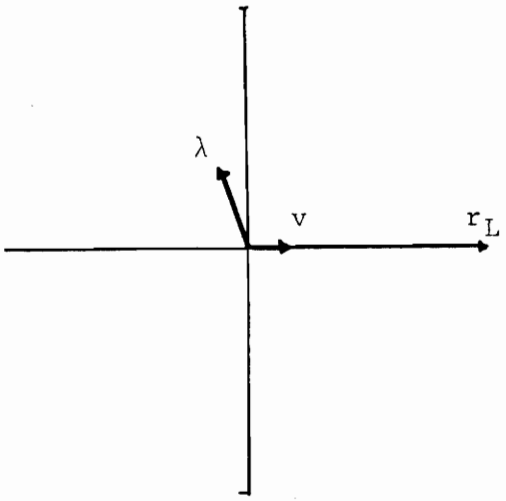

$S_2 = -0.0247 \pm 2.053i$

$q_R = 0.016(87)$
$u = 1.000(0)$
$v = 0.048(-93)$
$w = 0.082(5)$
$\theta_v = 0.0541(83)$
$q_v = 0.110(8)$
$\theta_L = 0.289(88)$
$q_L = 0.589(2)$
$\lambda = 0.140(-8)$
$r_L = 0.289(-83)$

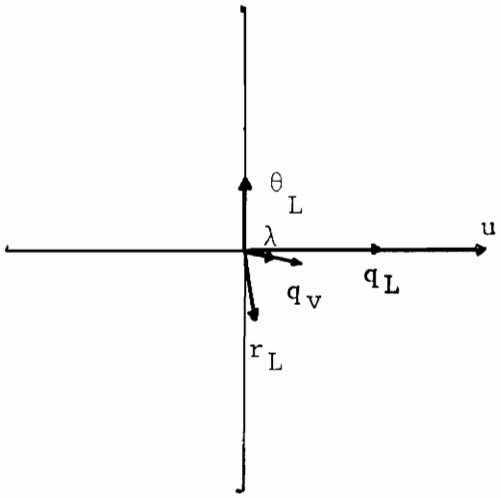

Table XII - [Cont'd]

EIGENVALUES AND EIGENVECTORS	
$S_3 = -0.774$	$S_4 = -3.109$
$u = 1.000(180)$	$\phi_R = 0.035(180)$
$v = 0.977(0)$	$\theta_R = 0.028(0)$
$w = 0.316(180)$	$p_R = 0.108(0)$
$\phi_V = 0.067(180)$	$q_R = 0.088(180)$
$p_V = 0.067(0)$	$u = 0.229(0)$
$\theta_V = 0.065(180)$	$v = 1.000(0)$
$q_V = 0.051(0)$	$w = 0.081(0)$
$r_V = 0.176(0)$	$\phi_V = 0.132(180)$
$\theta_L = 0.059(0)$	$p_V = 0.411(0)$
$q_L = 0.046(0)$	$\theta_V = 0.017(0)$
$\lambda = 0.544(180)$	$q_V = 0.052(180)$
$r_L = 0.430(0)$	$r_V = 0.292(180)$
	$q_L = 0.035(0)$
	$\lambda = 0.319(180)$
	$r_L = 1.000(0)$
	$S_8 = -0.485$
	$u = 0.189(180)$
$S_5 = -1.320$	$v = 1.000(0)$
$\dot{\beta}_0 = 0.011(0)$	$w = 0.037(180)$
$u = 0.256(0)$	$\phi_V = 0.045(180)$
$w = 1.000(0)$	$p_V = 0.022(0)$
$\theta_V = 0.021(0)$	$r_V = 0.143(0)$
$q_V = 0.027(180)$	$\lambda = 0.403(180)$
$q_L = 0.012(0)$	$r_L = 0.195(0)$

Table XII - [cont'd]

EIGENVALUES AND EIGENVECTORS

S_6 = 0.135 ±0.509i

u = 1.000(0)
v = 0.165(16)
w = 0.086(20)
θ_V = 0.059(111)
q_V = 0.031(35)
r_V = 0.014(28)
θ_L = 0.073(-59)
q_L = 0.038(-134)
λ = 0.105(-49)
r_L = 0.055(-124)

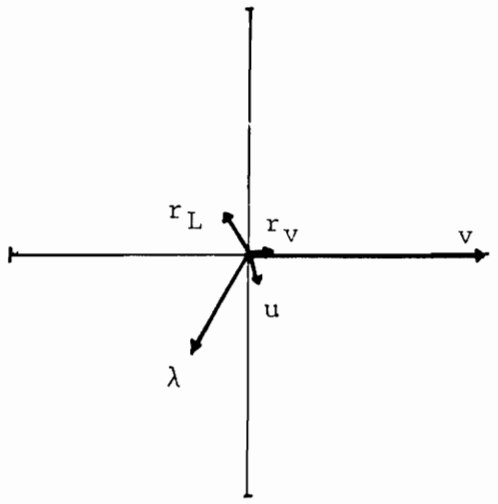

S_7 = -0.188 ±0.376i

u = 0.123(-69)
v = 1.000(0)
w = 0.017(-56)
ϕ_V = 0.043(-114)
p_V = 0.018(129)
r_V = 0.105(14)
λ = 0.439(-114)
r_L = 0.184(129)

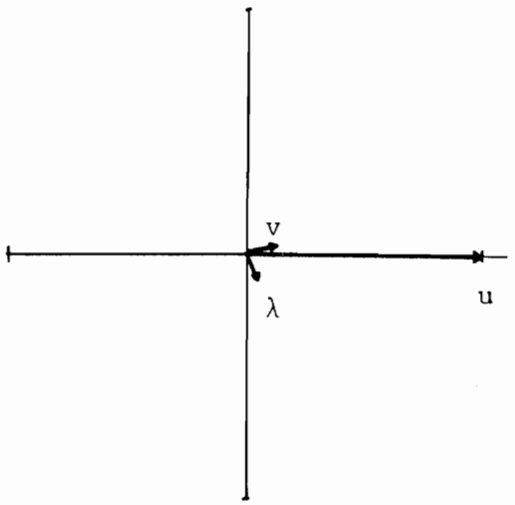

Table XII - [Cont'd]

EIGENVALUES AND EIGENVECTORS

$S_9 = -14.513 \pm 42.392i$

$\phi_R = 0.022(-161)$
$\theta_R = 0.022(109)$
$\dot{\beta}_0 = 0.060(-200)$
$p_R = 0.994(90)$
$q_R = 1.000(0)$
$w = 0.012(-28)$

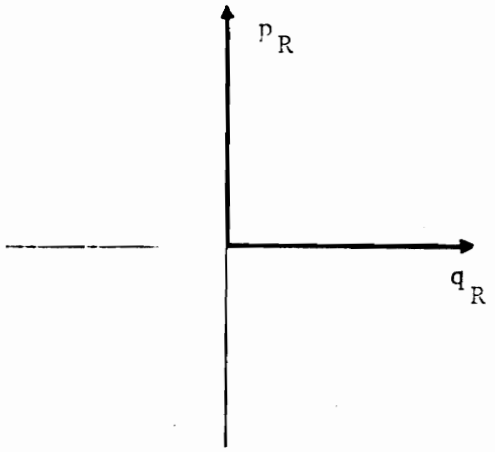

$S_{10} = -13.149 \pm 4.826i$

$\phi_R = 0.072(160)$
$\theta_R = 0.072(60)$
$\dot{\beta}_0 = 0.104(196)$
$p_R = 1.000(0)$
$q_R = 1.000(-100)$
$u = 0.102(45)$
$v = 0.119(-40)$
$w = 0.095(-13)$
$\phi_v = 0.011(125)$
$p_v = 0.148(-35)$
$q_v = 0.031(-132)$
$q_L = 0.017(37)$
$\lambda = 0.012(-37)$
$r_L = 0.012(153)$

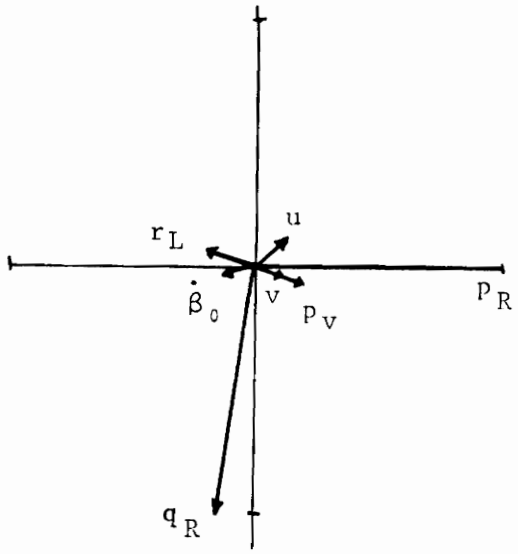

Table XII - [Cont'd]

EIGENVALUES AND EIGENVECTORS

$S_{11} = -14.483 \pm 18.297i$

$\beta_0 = 0.042(129)$
$\dot{\beta}_0 = 1.000(0)$
$p_R = 0.105(132)$
$q_R = 0.105(110)$
$u = 0.011(-67)$
$w = 0.302(126)$

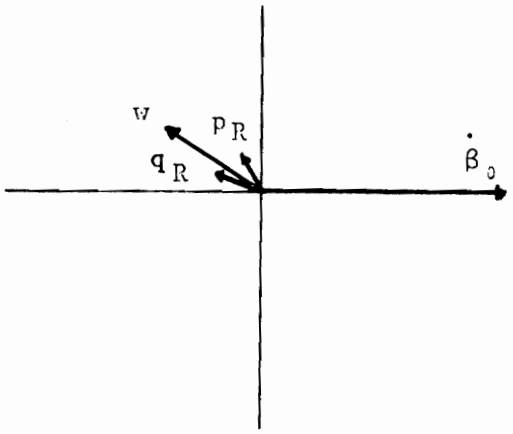

modes and modeshapes with similar results (Table IX), predicted previously by the RVDR model, it is observed that the load induced longitudinal and lateral oscillatory modes, S_1 and S_2 respectively, as well as the helicopter longitudinal and lateral oscillatory modes, S_6 and S_7 respectively, are in good agreement. The forward speed convergence mode (S_3) consists of greater vehicle lateral velocity in the present case. Also the vehicle motion in yaw (S_8) is found to be favorably damped in this case. Modes S_9 and S_{10} correspond to heavily damped, coupled pitch and roll oscillations of the rotor. By analogy to a gyroscope, the higher frequency mode (S_9) is usually referred to as nutation while the lower frequency mode (S_{10}) is referred to as precession. It is observed that the description of rotor motion in terms of its average pitch and roll angles has resulted in the nutation mode frequency being Ω higher than that of a single blade flapping which is described in terms of its flapping angle (β). Similarly, the precession mode frequency is found to be Ω lower than the single blade flapping frequency and this mode consists of fuselage roll velocity and load azimuthal velocity. Mode S_{11} corresponds to oscillatory motion of the rotor in coning and it consists of vertical velocity of the vehicle.

Over the range of values of the principal parameters of the configuration that is considered in this study, it is

observed that rotor induced oscillatory modes (S_9, S_{10} and S_{11}) are stable and heavily damped. Further, the dynamics of the rotor is found to have negligible effect on the other modes of the system. Consequently it is believed that the rotor induced modes are not critical in determining the stability of the vehicle-load system. In pursuing the interests of this work an approximate articulated rotor model that omits the dynamics of the rotor is discussed next.

5.4 Quasi-static Rotor Model [RVARQ]

A simpler model of the rotor is obtained by assuming the rotor to be quasi-static (H04), which means, it can be tilted instantaneously so that changes in rotor forces and moments due to changes in rotor velocities ($\dot{\beta}_0$, p_R, q_R) and accelerations ($\ddot{\beta}_0$, $\dot{p}_R$, $\dot{q}_R$) are negligible. This assumption is reasonable since the frequencies of the rotor motions are found to be considerably higher than those of the fuselage and load. Consequently, in Equation 5.3, neglecting the perturbations in rotor velocities and accelerations, Equation 5.5 is obtained which includes only rotor displacements.

$$\{\bar{X}_R\} = [-MB]^{-1}\,[MD]\,\{\bar{X}_V\} + [-MB]^{-1}\,[ME]\,\{\dot{\bar{X}}_V\} + [-MB]^{-1}\,[MF]\,\{\bar{U}\} \qquad (5.5)$$

Substituting Equation 5.5 in 5.2 and again neglecting

perturbations in rotor velocities, the rotor states are eliminated from the system representation. Note, however, that the effect of rotor statics has been implicitly retained by this procedure. The reduced equations become:

$$[A]\ \{\dot{\bar{X}}\} = [B]\ \{\bar{X}\} + [C]\ \{U\} \qquad (5.6)$$

where $\{\bar{X}\}^T = [\bar{X}_V\ \bar{X}_L]$

Matrices A, B and C in Equation 5.6 are given in Appendix A. It is observed that the order of this model of the system is same as that of the RVDR model (twelfth).

In order to examine the system stability in forward flight, as predicted by this lower order model, the eigenvalues and corresponding eigenvectors of the system matrix in Equation 5.6 were computed and are compared (Table XIII) with corresponding results obtained previously by considering the complete dynamics of the rotor. It is observed that motions of the fuselage and load as predicted by the dynamic rotor model are well approximated by the quasi-static rotor model. The corresponding modeshapes are also found to be in good agreement. Consequently, in the subsequent analysis only the quasi-static model of the articulated rotor will be considered. Comparing the corresponding modes predicted by the RVDR model with those of RVARQ model, it is observed

Table XIII - RVAR: Comparison of System Modes Predicted by Dynamic, Quasi-Static and Disc Rotor Models [Nominal Parameter Values]

Mode	Dynamic Rotor	Quasi-Static Rotor	Disc Rotor
1	-0.414 ±2.726i	-0.370 ±2.683i	-0.318 ±2.744i
2	-0.0247 ±2.053i	-0.0242 ±2.051i	-0.0245 ±2.132i
3	-0.774	-0.810	-0.716
4	-3.108	-2.986	-2.793
5	-1.320	-1.247	-1.219
6	0.135 ±0.509i	0.135 ±0.506i	0.131 ±0.456i
7	-0.188 ±0.376i	-0.182 ±0.381i	-0.302 ±0.514i
8	-0.485	-0.434	0.034
9	-14.513 ±42.392i	-	-
10	-13.150 ±4.826i	-	-
11	-14.482 ±18.297i	-	-

that the former model predicts a weak divergence in yaw (S_8). This difference is perhaps due to the greater damping of vehicle yawing motion induced by the load, as observed in the present case.

A number of parameters associated with an articulated rotor have been introduced in the present model, but the effects of their variation on the system stability will not be examined here. However, the effects of varying some of the fuselage-load parameters, that were used before, on the stability of this configuration are determined and compared with similar results obtained in the case of RVDR model. Table XIV shows the effect of suspension point location on the load induced oscillatory modes S_1, S_2 and helicopter lateral oscillatory mode S_7. The variations in frequencies and dampings of these modes are similar to those observed before (Table X). The effects of varying $\hat{m}$ on the load induced oscillatory modes [Figures 5.1 and 5.2] and helicopter longitudinal oscillatory mode [Figure 5.3] are also similar to that predicted by the RVDR model. Figures 5.4 and 5.5 show the effect of varying ℓ on the load induced modes (S_1, S_2) and helicopter oscillatory modes (S_6, S_7) respectively. The effect of varying forward speed on the longitudinal oscillatory modes of the system are shown in Figure 5.6. From these results it is observed that the stability characteristics of

Table XIV - RVAR: Effect of Suspension Point Location on System Modes S_1, S_2, S_6 and S_8 (Nominal Parameter Values)

ℓ_p (m)	h_p (m)	Load Induced Lat. Osc. (S_1)	Load Induced Lngtd. Osc. (S_2)	Helicopter Lat. Osc. (S_7)	Helicopter Yawing (S_8)
0	0	-0.0144 ±1.963i	-0.0189 ±1.818i	-0.189 ±0.397i	NA
0	2	-0.564 ±3.266i	-0.0388 ±2.231i	-0.167 ±0.370i	-0.286
0	4	-0.917 ±4.905i	-0.0987 ±2.766i	-0.137 ±0.329i	-0.119
0	6	-1.167 ±6.582i	-0.173 ±3.364i	-0.126 ±0.296i	-0.044
-3	1.2	-0.404 ±2.923i	-0.0322 ±2.046i	-0.0406 ±0.259i	NA
-1	1.2	-0.370 ±2.731i	-0.0267 ±2.0641i	-0.0329 ±0.312i	NA
+1	1.2	-0.380 ±2.672i	-0.0226 ±2.019i	-0.280 ±0.550i	NA
+3	1.2	-0.439 ±2.771i	-0.0231 ±1.938i	-0.354 ±0.862i	NA

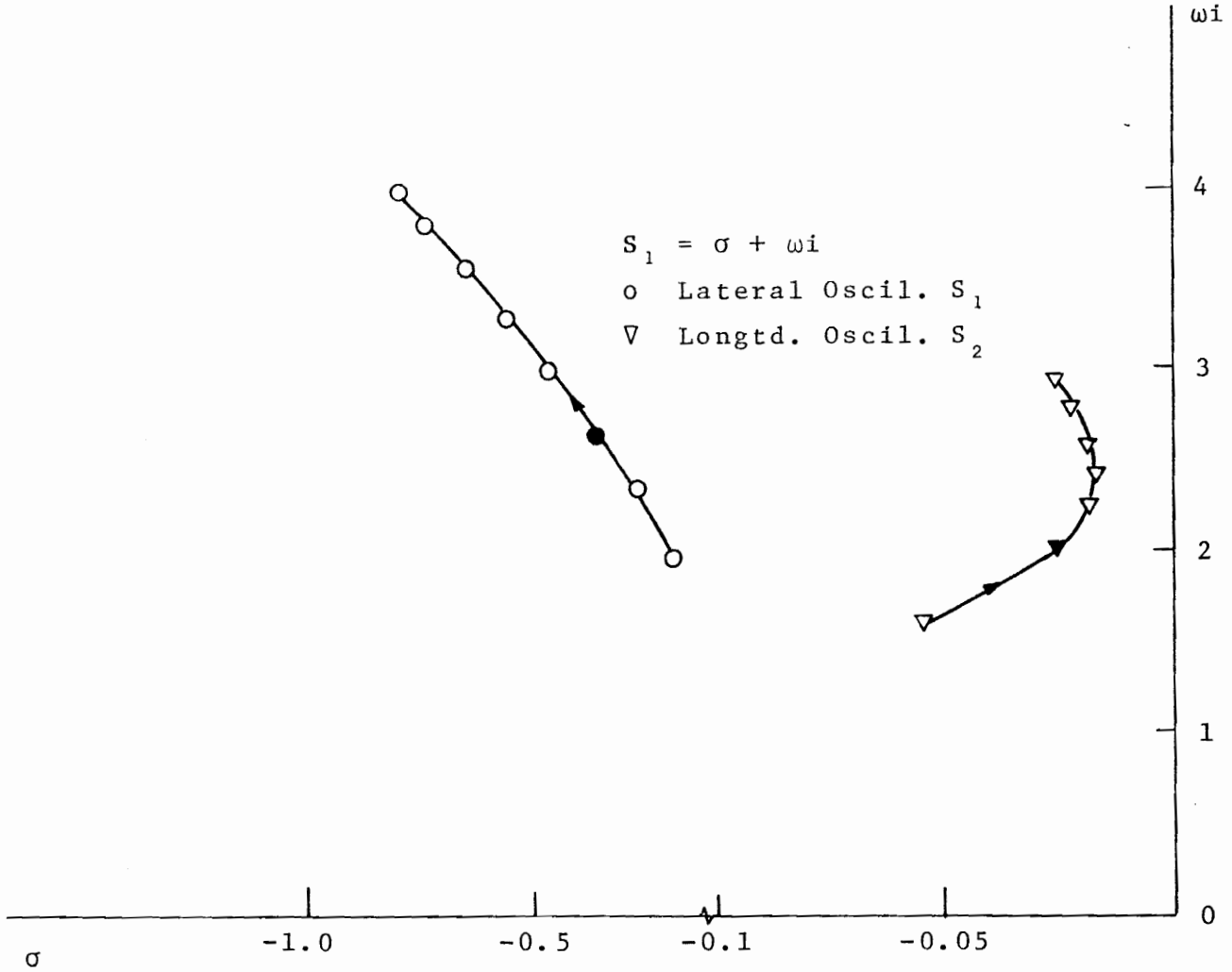

Figure 5.1 - RVARQ: Effect of $\hat{m}$ on Load Induced Oscillatory Modes S_1 and S_2 $[0.1 \leq \hat{m} \leq 1.5(0.2)]$

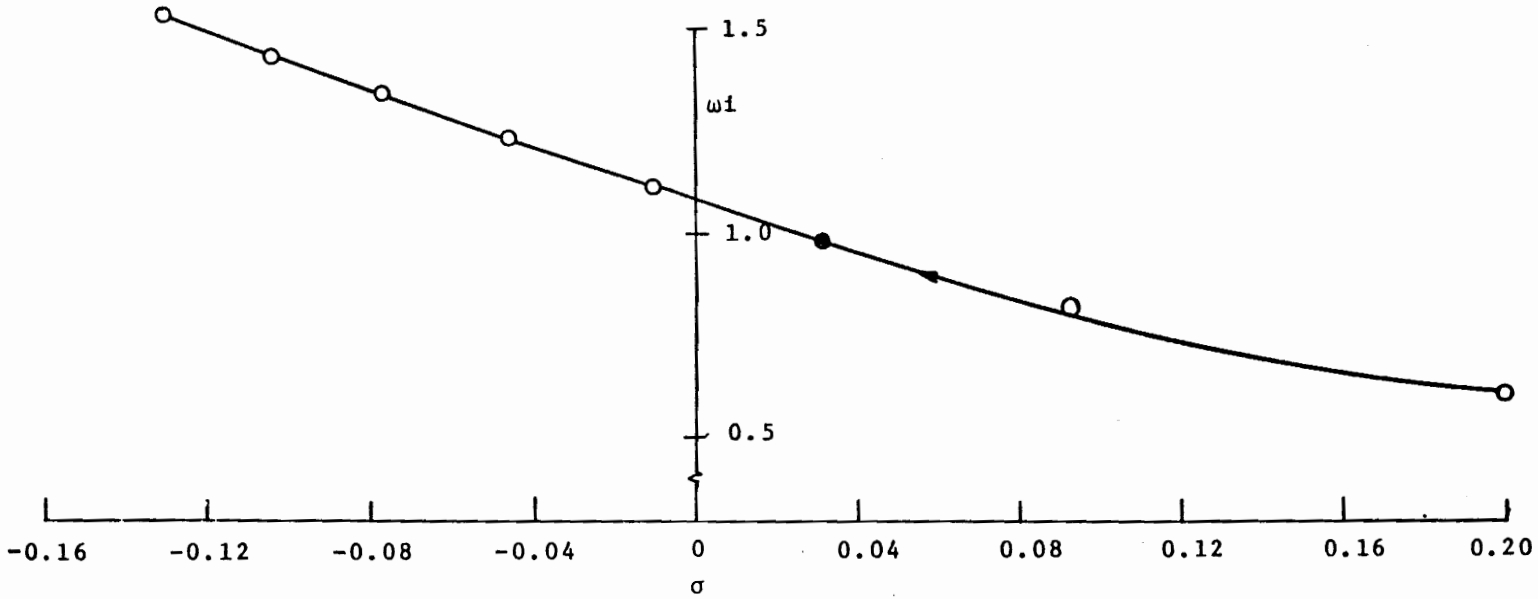

Figure 5.2 - RVARQ: Effect of $\hat{m}$ on Load Induced Longitudinal Oscillation (S_2)
$[0.1 \leq \hat{m} \leq 1.5(0.2),\ \ell = 64m]$

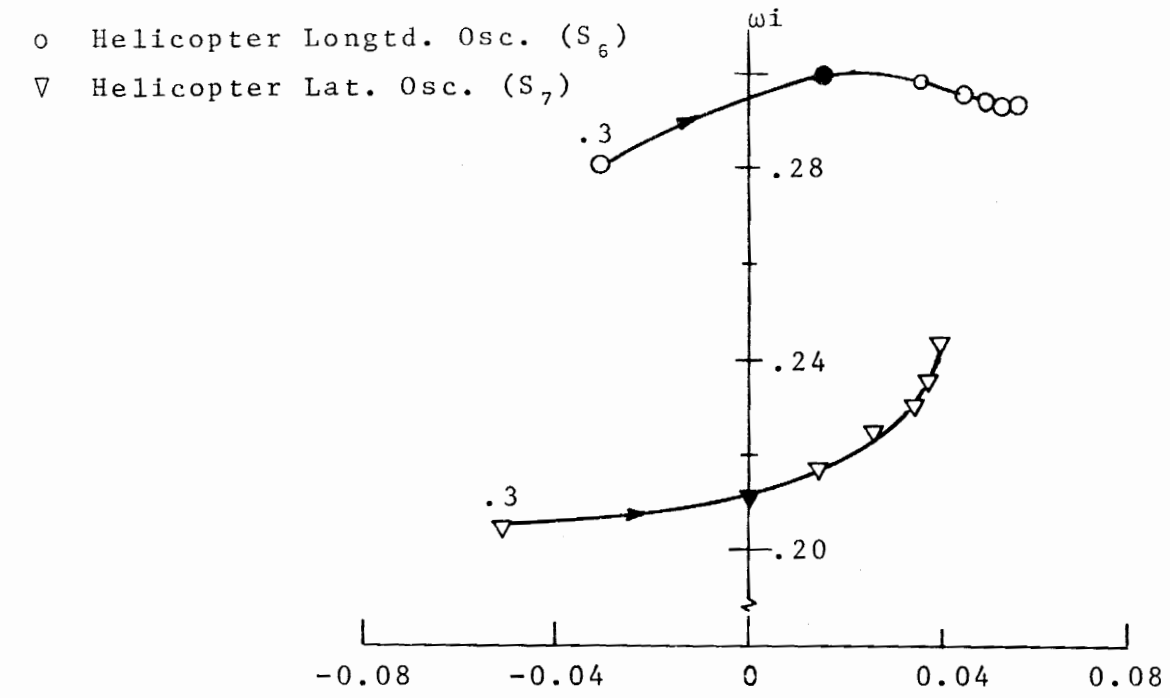

Figure 5.3 - RVARQ: Effect of $\hat{m}$ on Helicopter Oscillatory Modes S_6 and S_7 [$0.3 \leq \hat{m} \leq 1.5(0.2)$, ℓ = 64m]

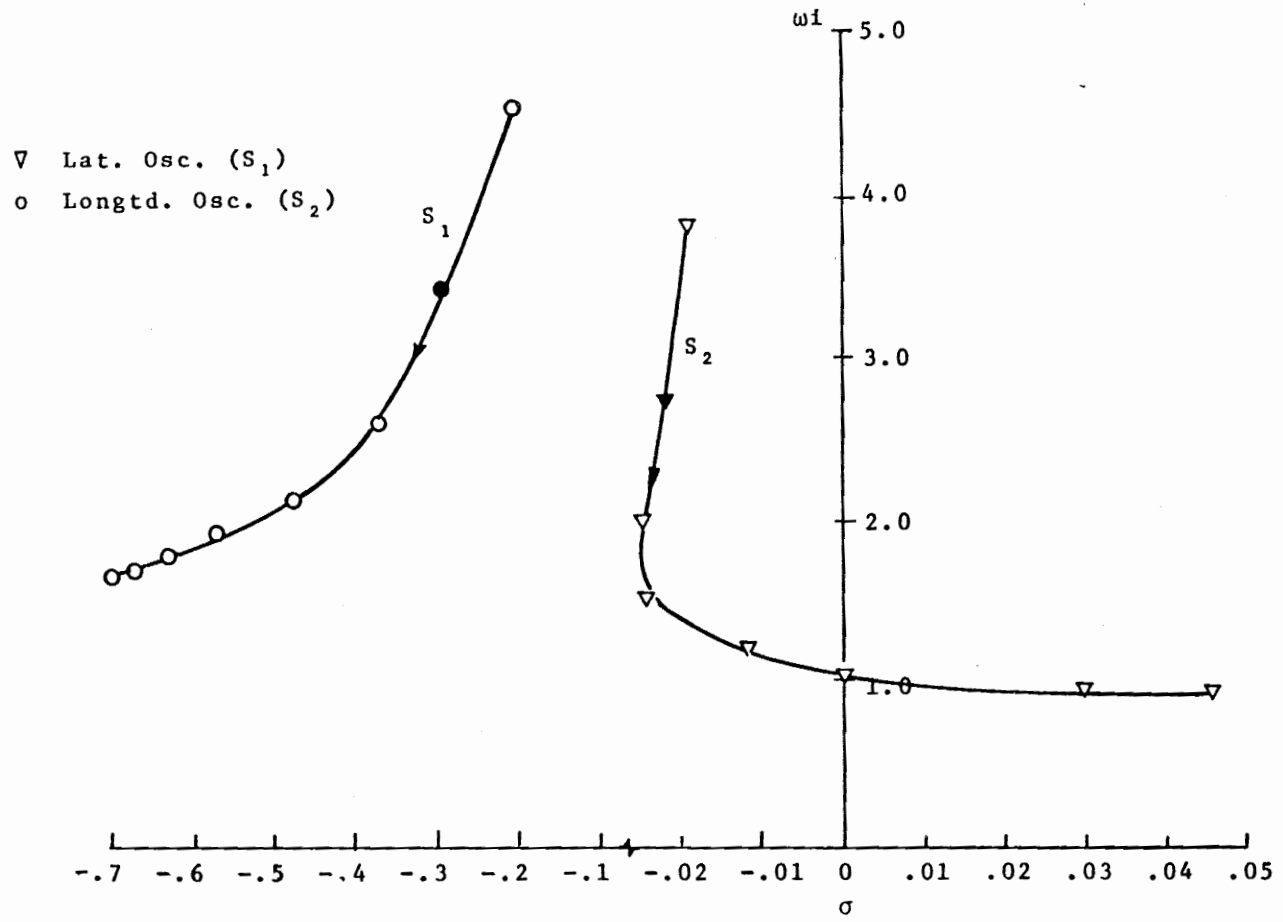

Figure 5.4 - RVARQ: Effect of ℓ on Load Induced Oscillatory Modes S_1 and S_2 [$1 \leq \ell \leq 128(*2)$]

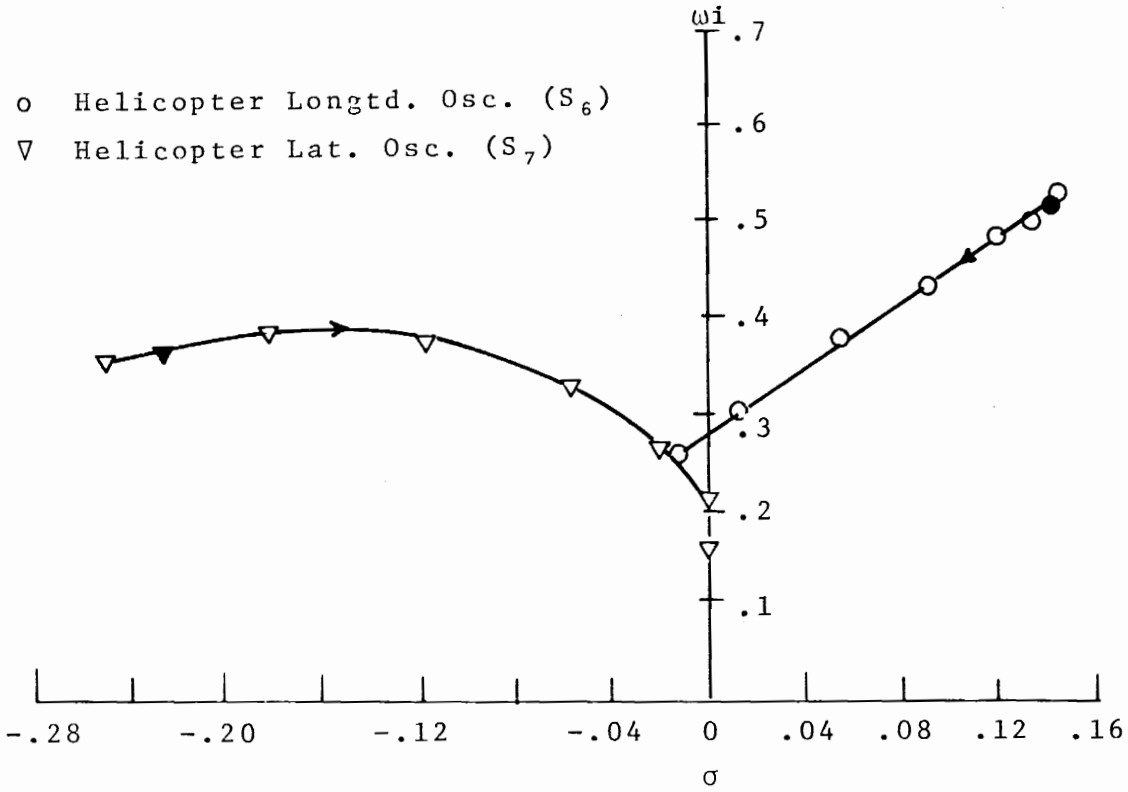

Figure 5.5 - RVARQ: Effect of ℓ on Helicopter Oscillatory Modes S_6 and S_7 [$1 \leq \ell \leq 128(*2)$]

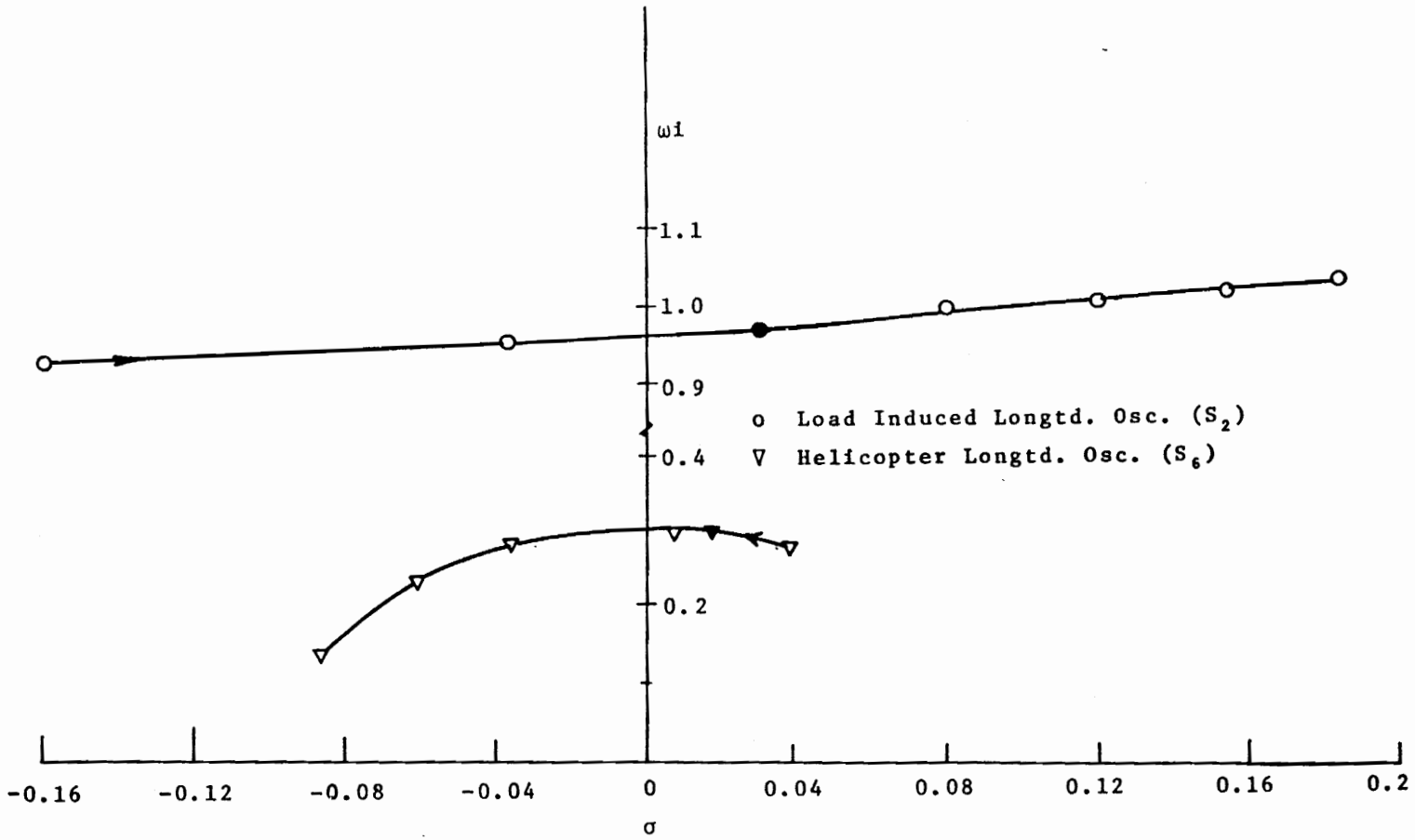

Figure 5.6 - RVARQ: Effect of u_e on Longitudinal Oscillatory Modes S_2 and S_6
[$10 \leq u_e \leq 40(5)$, $\ell = 64$m]

the vehicle-load configuration as predicted by the present model, are similar to those predicted by the RVDR model.

5.5 Summary

The linearized equations of motion of the articulated rotor-fuselage-load system in forward flight are obtained by appropriately combining the perturbation equations of the rotor in steady level flight [Section 4.3] with those of the fuselage and load [Section 3.4]. This results in an 18th order model of the system which is used to examine the stability of the vehicle-load configuration. Subsequently a lower order [12th] model of the system is obtained by assuming the rotor to be quasi-static. Stability of the system as predicted by this model is compared with corresponding results obtained by using the model with complete rotor dynamics. It has been shown that the quasi-static model of the rotor is adequate for determining stability characteristics of the configuration. Comparing these characteristics with corresponding results predicted previously by the RVDR model, it is observed that the disc rotor model is a good approximation to an articulated rotor and it is sufficient for analyzing the characteristic behavior of the system in forward flight.

CHAPTER VI

STABILITY AUGMENTATION USING AN OPTIMAL CONTROLLER

6.1 Introduction

The preceding stability analyses of a helicopter/load system indicate that in the presence of a load the inherent motion of the vehicle in forward flight could become unstable and that the load dynamics induces additional oscillatory motion of the helicopter which may or may not be stable. Consequently it is desirable that the system stability be satisfactorily augmented by artificial means. In this chapter a stability augmentation scheme is developed in the form of a linear optimal regulator. The method of synthesis for such a scheme is well established (BR1, page 163), (KW1 page 247). In this study a regulator is designed using a sixth order model of the helicopter, obtained from RVDR model. A relation between the rotor disc controls (ϕ_D, θ_D, v_i) and the articulated rotor controls (θ_0, θ_s, θ_c) is subsequently derived and used to obtain an equivalent steady state control law that is applicable to the RVAR model of the helicopter. The performance of such a regulator in the presence of a suspended load is examined for various design and flight conditions.

6.2 Optimal Controller for RVDR Helicopter

In order to synthesize a linear regulator which would augment the stability of the helciopter motion in forward flight, it is convenient to consider the linearized equations of motion of the vehicle about an equilibrium point corresponding to uniform translation. Such a system of equations is obtained here from the vehicle-load perturbation equations, derived in Chapter III, by omitting the effects of the suspended load. For the sake of simplicity the motion of the helicopter in forward, lateral, pitch and roll only are considered. This seems reasonable since the vertical and yawing motion of the helicopter are usually well damped and have favorable effects on the other motion (SE1, page 380). Following these modifications, the perturbation equations of motion of the helicopter are obtained in the form

$$\dot{\bar{X}} = \underline{A}\bar{X} + \underline{B}\bar{U} \tag{7.1}$$

where

$$\bar{X}^T = [u \; v \; \phi_v \; p_v \; \theta_v \; q_v]$$

$$\bar{U}^T = [\phi_D \; \theta_D]$$

Regulator Synthesis

The general problem of designing a regulator for a linear, time-invariant system,

$$\dot{\bar{X}} = \underline{A}\bar{X} + \underline{B}\bar{U} \tag{7.2}$$

where $\bar{X}$ is an n-vector, $\bar{U}$ is an m-vector, involves determining a linear, steady state control law

$$\bar{U} = - \underline{F}\bar{X} \tag{7.3}$$

such that

(a) the closed loop system $\dot{\bar{X}} = (\underline{A} - \underline{BF})\ \bar{X}$ is stable

(b) the control input is optimal and minimizes the sum of integrated square regulating error and the integrated square input, which are described by the quadratic cost function

$$\int_{t_0}^{t_1} [\bar{X}^T\ \underline{R_1}\ \bar{X} + \bar{U}^T\ \underline{R_2}\ \bar{U}]\ dt$$

where $\underline{R_1}$ is a non-negative definite and symmetric weighting matrix and $\underline{R_2}$ is a positive definite weighting matrix. Consider the above system of differential equations (7.2) together with its adjoint in the form

$$\dot{\bar{Z}} = \underline{S}\bar{Z} \tag{7.4}$$

where

$$Z = \begin{Bmatrix} \bar{X} \\ \bar{P} \end{Bmatrix}, \quad \underline{S} = \begin{bmatrix} \underline{A} & -\underline{B}\ \underline{R_2}^{-1}\ \underline{B}^T \\ -\underline{R_1} & -\underline{A}^T \end{bmatrix}$$

The following theorem (KW1) holds good for the augmented system in Equation 7.4.

Theorem

Suppose the given system in Equation (7.2) is completely controllable (rank of the controllability matrix is n) and $\underline{S}$ has 2n distinct characteristic values. Then,

(a) If λ is an eigenvalue of $\underline{S}$, $-\lambda$ is also an eigenvalue.

(b) $\underline{S}$ has no eigenvalue with zero real part

(c) The eigenvalues of the steady state closed loop optimal regulator are those characteristic values of $\underline{S}$ that have negative real parts.

(d) If $\underline{S}$ is diagonalized in the form

$$\underline{S} = \underline{W} \begin{bmatrix} \underline{\Lambda} & \underline{0} \\ \underline{0} & \underline{\Lambda} \end{bmatrix} \underline{W}^{-1} \tag{7.5}$$

where the diagonal matrix $\underline{\Lambda}$ has as diagonal elements the eigenvalues of $\underline{S}$ with positive real parts, then the steady state solution of the algebraic Riccati equation

$$\underline{0} = \underline{R_1} - \underline{P}\ \underline{B}\ \underline{R_2}^{-1}\ \underline{B}^T\ \underline{P} + \underline{A}^T\ \underline{P} + \underline{P}\ \underline{A} \tag{7.6}$$

can be written as

$$\underline{\tilde{P}} = \underline{W_{22}}\ \underline{W_{12}^{-1}} \tag{7.7}$$

The proof of this theorem can be found in reference (KW1). As a consequence of the above theorem, the steady state control law is given by

$$\bar{U} = -\underline{F}\bar{X} = -\underline{R_2}^{-1}\underline{B}^T \tilde{\underline{P}}\ \bar{X} \tag{7.8}$$

It is important to note that one can obtain the closed loop modes of a given system (7.2) for a specified set of weighting matrices $\underline{R_1}$ and $\underline{R_2}$, without explicitly solving the matrix Riccati equation.

It is observed that for nominal parameter values, the openloop eigenvalues of the helicopter system matrix in Equation 7.1 are all distinct and that the vehicle is completely controllable. Table (XV) shows the gain matrix obtained for a typical set of weighting matrices $\underline{R_1}$ and $\underline{R_2}$ that were selected after several trials. The resulting closed loop eigenvalues of the helicopter augmented system matrix are shown in Table (XVI) along with the corresponding openloop eigenvalues. It is found that satisfactory damping of the oscillatory modes can be obtained by using the same set of gains for other forward speeds.

6.3 Equivalent Regulator for RVAR Helicopter Model

In order that the steady state control law determined here by using a simplified model of the helicopter be

Table XV - Typical Weighting Matrices and the Corresponding Gain Matrix for RVDR Helicopter in Forward Flight

$$\underline{R}_1 = \text{Diag.}\ [0.1 \quad 0.1 \quad 0.01 \quad 0.01 \quad 0.01 \quad 0.01]$$

$$\underline{R}_2 = \text{Diag.}\ [1000 \quad 1000]$$

$$\underline{G} = \begin{bmatrix} -0.156\text{E-}02 & 0.933\text{E-}02 & 0.179 & 0.956\text{E-}01 & 0.310\text{E-}01 & 0.169\text{E-}01 \\ 0.756\text{E-}02 & 0.133\text{E-}02 & 0.369\text{E-}01 & -0.231\text{E-}02 & -0.285 & -0.353 \end{bmatrix}$$

Table XVI - Open and Closed Loop Modes of RVDR Helicopter in Forward Flight. [Nominal Parameter Values]

Mode	Open Loop Modes	Closed Loop Modes
S_3	-0.543	-0.719
S_4	-1.011	-1.319
S_6	0.0957 ±0.314i	-0.285 ±0.563i
S_7	0.0129 ±0.149i	-0.557 ±0.832i

utilized in analyzing a more complex model of the vehicle, that includes an articulated rotor as well [RVAR model], a relation between the rotor control in both the models of the helicopter is desirable. Such a relation is obtained by considering identical changes in the rotor force components, produced by a set of control inputs in the two models. Mathematically,

$$J_{\underline{A}}\ \bar{U}_A = J_{\underline{D}}\ \bar{U}_D$$

or

$$\bar{U}_A = J_{\underline{A}}^{-1}\ J_{\underline{D}}\ \bar{U}_D \tag{7.9}$$

where

$$\bar{U}_D^T = [v_i \quad \phi_D \quad \theta_D]$$

$$\bar{U}_A^T = [\theta_0 \quad \theta_c \quad \theta_s]$$

$$J_{\underline{D}} = \left[\begin{array}{ccc} \frac{dF_x}{dv_i} & \frac{dF_x}{d\phi_D} & \frac{dF_x}{d\theta_D} \\ \frac{dF_y}{dv_i} & \frac{dF_y}{d\phi_D} & \frac{dF_y}{d\theta_D} \\ \frac{dF_Z}{Dv_i} & \frac{dF_Z}{d\phi_D} & \frac{dF_Z}{d\theta_D} \end{array}\right]_e$$

and

$$J_{\underline{A}} = \begin{bmatrix} \frac{dF_x}{d\theta_0} & \frac{dF_x}{d\theta_c} & \frac{dF_x}{d\theta_s} \\ \frac{dF_y}{d\theta_0} & \frac{dF_y}{d\theta_c} & \frac{dF_y}{d\theta_s} \\ \frac{dF_Z}{d\theta_0} & \frac{dF_Z}{d\theta_c} & \frac{dF_Z}{d\theta_s} \end{bmatrix}$$

The rotor force derivatives in Equation 7.9 are evaluated at the equilibrium condition. For example,

$$\frac{dF_x}{d\theta_s} = \left[\frac{\partial F_x}{\partial \theta_s} + \frac{\partial F_x}{\partial \beta_0} \frac{\partial \beta_0}{\partial \theta_s} + \frac{\partial F_x}{\partial \phi_R} \frac{\partial \phi_R}{\partial \theta_s} + \frac{\partial F_x}{\partial \theta_R} \frac{\partial \phi_R}{\partial \theta_s} \right]_e$$

where the derivatives $(\partial \beta_0/\partial \theta_s)$, $(\partial \phi_R/\partial \theta_s)_e$ and $(\partial \theta_R/\partial \theta_s)_e$ are obtained from Equation 4.17.

For the nominal flight condition of the helicopter/load system the control equivalence matrix $(J_{\underline{A}}^{-1} J_{\underline{D}})$ between the helicopter models with a disc rotor and an articulated rotor, is computed and given below.

$$\begin{Bmatrix} \Delta\theta_0 \\ \Delta\theta_c \\ \Delta\theta_s \end{Bmatrix} = \begin{bmatrix} 0.151E\text{-}01 & 0.549E\text{-}02 & 0.652E\text{-}01 \\ -0.664E\text{-}04 & -0.968 & 0.575E\text{-}01 \\ -0.567E\text{-}02 & -0.724E\text{-}01 & -0.839 \end{bmatrix} \begin{Bmatrix} \Delta v_i \\ \Delta\phi_D \\ \Delta\theta_D \end{Bmatrix} \tag{7.10}$$

It is observed that for a given collective pitch angle of the articulated rotor, changes in the longitudinal and lateral cyclic pitch angles correspond to greater changes in the rotor disc control angles ϕ_D, θ_D than the rotor inflow velocity. Consequently it is reasonable to use this control relation to transform the steady state control law designed previously, such that it is applicable to a helicopter model with articulated rotor. From Equations 7.8 and 7.9:

$$\bar{U}_A = J_{\underline{A}}^{-1} J_{\underline{D}} (-\underline{R_2}^{-1} \underline{B}^T \tilde{\underline{P}}) \bar{X} \qquad (6.11)$$

where $\bar{X}$ is defined in Equation 7.1. Using the gains in Table (XV) in conjunction with the transformation matrix (7.10), the steady state control law (7.11) was computed and the corresponding closed loop modes of the RVAR model of the vehicle/load system were obtained and are shown in Table [XVII(a),(b)] together with corresponding openloop modes. It is observed that this regulator is adequate for augmenting the vehicle-load stability in forward flight for other design and flight conditions, examined previously in the openloop stability analysis of this configuration.

6.4 Summary

A steady state control law is designed for stability augmentation of a helicopter in forward flight by using a vehicle model that has a rigid body fuselage and a conceptual

Table XVII(a) - RVAR: Open and Closed Loop Modes of Helicopter/Load System in Forward Flight - ℓ = 4m

Mode	Open Loop Modes	Closed Loop Modes
1	-0.414 ±2.726i	-0.769 ±2.439i
2	-0.0247 ±2.053i	-0.0741 ±2.024i
3	-0.774	-1.912
4	-3.108	-4.278
5	-1.320	-1.232
6	0.135 ±0.509i	-0.259 ±0.533i
7	-0.188 ±0.376i	-0.461 ±0.966i
8	-0.485	-0.807
9	-14.513 ±42.392i	-15.167 ±42.557i
10	-13.150 ±4.826i	-9.822 ±6.099i
11	-14.482 ±18.297i	-14.446 ±18.499i

Table XVII(b) - RVAR: Open and Closed Loop Modes of Helicopter/Load System in Forward Flight - ℓ = 64m

Mode	Open Loop Modes	Closed Loop Modes
1	-0.728 ±1.762i	-1.333 ±1.645i
2	0.0265 ±0.978i	-0.373 ±0.848i
3	-0.731	-1.686
4	-3.027	-4.238
5	-1.315	-1.198
6	0.0179 ±0.302i	-0.0722 ±0.339i
7	-0.00265 ±0.211i	-0.0269 ±0.369i
8	-0.228	-0.632
9	-14.513 ±42.393i	-15.168 ±42.556i
10	-13.148 ±4.828i	-9.818 ±6.107i
11	-14.483 ±18.297i	-14.447 ±18.449i

rotor in the form of an actuator disc, which has pitch and roll degrees of freedom with respect to the fuselage. Only forward, lateral pitch and roll motion of the helicopter are considered in this design. A relation between the rotor disc pitch and roll angles, rotor induced velocity and the collective, cyclic pitch angles of an articulated rotor has been developed so that the regulator designed here can be modified to an equivalent steady state control law for applications in more complex vehicle models that include an articulated rotor as well. By using RVAR model of the helicopter/load system it has been shown that the inherent instability of the helicopter in forward flight and that induced by the suspended load can be alleviated by using a regulator that feeds back only some of the vehicle states.

CHAPTER VII

RESULTS AND CONCLUSIONS

7.1 Results

An analysis of the dynamic stability of a helicopter-load configuration in forward flight, as predicted by the most complex model [RVAR] developed in this study, indicates that the modes of such a system consist of high frequency oscillations associated with dynamics of the articulated rotor, inherent oscillatory and aperiodic motion of the fuselage, and longitudinal and lateral oscillations of the vehicle/load system that are induced by the suspended load. It is found that the stability of the fuselage and load induced modes of the system are strongly dependent on the values of the system parameters $\hat{m}$, u_e, ℓ_p, h_p and ℓ. The degree of coupling between the rigid body motion of the fuselage, and pitch and azimuthal motion of a suspended load is characteristically influenced by the length of the suspension cable; greater coupling for longer cable length. Since the instabilities of the system are primarily associated with motion of the fuselage and load, the quasi-static model of the rotor is found to be adequate in representing the coupled motion of the rotor and fuselage. Modes of the system predicted by this lower order model [RVARQ] are also observed with the RVDR model of the configuration. It is

found that the conceptual disc model of the rotor is a good approximation to the quasi-static articulated rotor model and it is adequate for predicting trends towards instability in fuselage-load motion. The point mass representation of the configuration is found to be sufficient for analyzing the stability of the load induced modes in a case where $\hat{m}$ is small and the load is suspended from a point close to the $(cm)_v$, by a short cable. Consequently it is too restricted for any realistic analyses of the system stability. However this simple model serves as a convenient reference in an analysis such as considered here.

7.2 Conclusions

The principal conclusions of this study are:

1) The dynamic instabilities associated with the motion of helicopter-load configuration in forward flight, are primarily in the form of unstable, inherent oscillations of the helicopter as well as those induced by the suspended load. The length of suspension cable is an important parameter in determining the extent of coupling between the vehicle and load motion.

2) RVDR model of the configuration adequately represents the dynamics of the system in forward flight. This model is sufficient for predicting the instabilities observed

in this study.

3) A simple model [sixth order] of the helicopter that considers only the forward, lateral, pitch and roll motion of the vehicle is sufficient for designing a stability augmentation scheme for the helicopter in forward flight. Such a scheme is also found to be adequate for alleviating the instabilities of the vehicle motion, induced by the suspended load.

Although the above results and conclusions are based on a systematic analysis, it is important to remember that it did not consider the rigid body dynamics of the load and other sling configurations with multiple tethers.

7.3 Recommendations for Further Study

Some of the analytical models of the helicopter-load system developed in this work should be helpful in further analyzing the motion of such a configuration. It is recommended that subsequent studies should examine the following aspects of the motion of the vehicle-load system.

Considering the dynamics and aerodynamics of the load modeled appropriately as a rigid body, the effect of aerodynamic instabilities of the load on the motion of the configuration should be determined. An analysis of the dynamic stability of such a system in forward flight, in a turbulent

atmosphere, is suggested. Configurations in which the load is suspended by multiple tethers should be examined, using better models than in the past, to determine the merits of such suspension schemes.

REFERENCES

AB 1 Abzug, M. J., "Equations of Motion for a Helicopter with a Two Cable Sling Load", Rept. 99900-7026-RO-00, TRW Systems Group, Aug. 1969, TRW, Inc., Redondo Beach, Calif.

BI 1 Biggers, J. C., "Some Applications to the Flapping Stability of Helicopter Rotors", NASA SP-352, Feb. 13-15, 1974.

BO 1 Boeing Vertol Company, "Active Arm [External Cargo] Stabilization System Flight Demonstration", USAAMRDL-TR-76-23, Boeing Vertol Company, Philadelphia, Pa.

BR 1 Bryson, A. E. and Ho, Y. C., Applied Optimal Control, Xerox Publishing Company, Lexington, Mass., 1969.

CL 1 Cliff, E. M. and Bailey, D. B., "Dynamic Stability of a Translating Vehicle with a Simple Sling Load", Journal of Aircraft, Vol. 12, No. 10, Oct. 1975, pp 773-777.

DU 1 Dukes, Theodore, "Maneuvering Heavy Slung Loads near Hover. Part I: Damping the Pendulous Motion, Journal of American Helicopter Society [JAHS], Vol. 18, No. 2, April 1973; Part II: Some Elementary Maneuvers, Vol. 18, No. 3, July 1973.

ET 1 Etkins, B. and MacWorth, J.C., "Aerodynamic Instability of Non-Lifting Bodies Towed Beneath an Aircraft", TN65, Jan. 1963, Institute of Aerophysics, University of Toronto, Toronto, Ontario.

ET 2 Etkin, B, Dynamics of Atmospheric Flight, John Wiley & Sons, Inc., New York, 1972.

GA 1 Gable, R and Wilson, G. J., "Test Approaches to External Sling Load Instabilities", American Helicopter Society Journal, Vol. 13, July 1968, pp 44-55.

REFERENCES [CONT'D]

GE 1 Gessow, Alfred and Myers, Garry, Aerodynamics of the Helicopter, Frederick Ungar Publishing Co., New York, 1952.

GU 1 Gupta, N. K. and Bryson, A. E., "Automatic Control of a Helicopter with a Hanging Load", SUDAAR NO. 459, Stanford University, Stanford, Calif.

HA 1 Hall, E. W., "Computational Methods for the Synthesis of Rotary Wing VTOL Aircraft Control Systems", Stanford University, Aug. 1971.

HO 1 Houghton, E. L. and Brock, A. E., Aerodynamics for Engineering Students, Edward Arnold Ltd., London, 1960.

HO 2 Hohenemser, K., "Contribution to the Problem of Helicopter Stability", Proceedings of the Fourth Annual Forum, 1948, American Helicopter Society.

HU 1 Hutto, A. J., "Qualitative Report on Flight Test of a Two Point External Load Suspension System, Reprint 473, 26th Annual National Forum of the American Helicopter Society, May 1970, Washington, D.C..

KW 1 Kwakernaac and Sivan, Linear Optional Control Systems,

LI 1 Liu, D. T., "In-Flight Stabilization of Externally Slung Helicopter Loads" USAAMRDL Tech. Rept. 73-5, May 1973, U.S. Army Air Mobility Research and Development Labs, Fort Eustis Directorate, Fort Eustis, Va.

LU 1 Lucassen, L. B., and Sterk, F. J., "Dynamic Stability Analysis of a Hovering Helicopter with a Sling Load, American Helicopter Society Journal, Vol. 10, April 1965, pp 6-12.

ME 1 Meirovitch, Leonard, Methods of Analytical Dynamics, McGraw-Hill Book Co., New York, 1970.

REFERENCES [CONT'D]

MI 1 Miele, Angelo, Flight Mechanics, Vol. 1, Theory of Flight Paths, Addison-Wesley Publishing Co., Inc., Palo Alto, 1962.

NI 1 Nikolsky, A. A., Helicopter Analysis, John Wiley & Sons, Inc., New York, 1961.

PO 1 Poli, C. and Cromack, D., "Dynamics of Slung Bodies Using a Single Point Suspension", Journal of Aircraft, Vol. 10, Feb. 1973, pp 80-86.

SE 1 Seckel, E., Stability and Control of Airplanes and Helicopters, Academic Press, New York, 1964.

ZA 1 Zadeh, DeSoer, Linear System Theory, McGraw-Hill, New York, 1963.

APPENDIX A - SYSTEM DEFINITION MATRICES

The elements of the matrices defined in the following equations are given below. The zero elements in these matrices have been omitted for simplicity.

Equation 2.7

$$\underline{B}\,\dot{\overline{X}} = \underline{A}\,\overline{X} + \overline{F}$$

$$\overline{X}^T = [u\ w\ \theta_L\ q_L\ v\ \lambda\ r]$$

$$\overline{F}^T = [T_x\ T_z\ 0\ 0\ T_y\ 0\ 0]$$

Matrix B

$B(1,1) = (m_v + m_L)$

$B(1,4) = -m_L \ell \cos\theta_L^e$

$B(2,2) = (m_v + m_L)$

$B(2,4) = -m_L \ell \sin\theta_L^e$

$B(3,3) = 1$

$B(4,1) = -m_L \ell \cos\theta_L^e$

$B(4,2) = -m_L \ell \sin\theta_L^e$

$B(4,4) = m_L \ell^2$

$B(5,5) = (m_v + m_L)$

$B(5,7) = -m_L \ell \sin\theta_L^e$

$B(6,6) = 1$

$B(7,5) = -m_L$

$B(7,7) = m_L \ell \sin\theta_L^e$

APPENDIX A [Cont'd]

Matrix A

$A(1,1) = -2\,(K_v + K_L)\,u_e$

$A(1,4) = 2\,K_L u_e \ell \cos\theta_L^e$

$A(2,2) = -\,(K_v + K_L)\,u_e$

$A(2,4) = K_L u_e \ell \sin\theta_L^e$

$A(3,4) = 1$

$A(4,1) = 2\,K_L u_e \ell \cos\theta_L^e$

$A(4,2) = K_L u_e \ell \sin\theta_L^e$

$A(4,3) = -m_L g \ell / \cos\theta_L^e$

$A(4,4) = -K_L u_e \ell^2\,(1 + \cos^2\theta_L^e)$

$A(5,5) = -(K_v + K_L)\,u_e$

$A(5,7) = K_L u_e \ell \sin\theta_L^e$

$A(6,7) = 1$

$A(7,5) = K_L u_e$

$A(7,6) = -K_L u_e^2$

$A(7,7) = -K_L u_e \ell \sin\theta_L^e$

Equation 2.11

$$\dot{\bar{X}} = \underline{A}\,\bar{X}$$

$$\bar{X}^T = [v\ \gamma\ \theta_L\ q_L\ \beta\ \lambda\ r]$$

$$\underline{A} = \underline{B}^{-1}\,\underline{C}$$

Matrix B

$B(1,1) = (m_v + m_L)$

APPENDIX A [Cont'd]

Matrix B [Con'td]

$$B(1,4) = m_L \ell \cos\beta^e \cos\theta_L^e$$

$$B(1,7) = -m_L \ell \sin\beta^e \sin\theta_L^e$$

$$B(2,2) = (m_v + m_L)\, u_e$$

$$B(2,4) = m_L \ell \sin\theta_L^e$$

$$B(3,3) = 1$$

$$B(4,4) = m_L \ell \sin\beta_e \cos\theta_L^e$$

$$B(4,5) = -(m_v + m_L)\, u_e$$

$$B(4,7) = m_L \ell \cos\beta_e \sin\theta_L^e$$

$$B(5,1) = m_L \sin\beta_e$$

$$B(5,5) = m_L u_e \cos\beta_e$$

$$B(5,7) = -m_L \ell \sin\theta_L^e$$

$$B(6,6) = 1$$

$$B(7,1) = m_L \cos\theta_L^e \cos\beta_e$$

$$B(7,2) = m_L u_e \sin\theta_L^e$$

$$B(7,4) = m_L \ell$$

$$B(7,5) = -m_L u_e \sin\beta_e \cos\theta_L^e$$

Matrix C

$$C(1,1) = -\left[2K_L u_e + K_L V_L^e + \frac{K_L}{V_L} (u_e - \ell c \sin\theta_L^e \sin\beta^e)^2 \right]$$

$$C(1,2) = -(m_v + m_L)\, g$$

$$C(1,3) = -\left[-m_L \ell c^2 \cos\beta_e \cos\theta_L^e - K_L \ell c V_L^e \sin\beta_e \cos\theta_L^e \right.$$

$$\left. + \frac{K_L}{V_L^e} (u_e - \ell c \sin\theta_L^e \sin\beta_e) (\ell^2 c^2 \sin\theta_L^e \cos\theta_L^e \right.$$

APPENDIX A [Cont'd]

$$- \ell c u_e \cos\theta_L^e \sin\beta_e)\Big]$$

$$C(1,4) = -\Big[-2m_L \ell c \sin\beta_e \cos\theta_L^e + K_L \ell V_L^e \cos\theta_L^e \cos\beta_e + \frac{K_L}{V_L^e}(u_e - \ell c \sin\theta_L^e \sin\beta_e)\, \ell u_e \cos\theta_L^e \cos\beta_e\Big]$$

$$C(1,5) = -\Big[m_L \ell c^2 \sin\beta_e \sin\theta_L^e - K_L \ell c V_L^e \sin\theta_L^e \cos\beta_e - \frac{K_L \ell c}{V_L^e} u_e \sin\theta_L^e \cos\beta_e (u_e - \ell_c \sin\theta_L^e \sin\beta_e)\Big]$$

$$C(1,7) = -\Big[-2m_L \ell c \cos\beta_e \sin\theta_L^e - K_L \ell V_L^e \sin\theta_L^e \sin\beta_e + \frac{K_L}{V_L^e}(u_e - \ell c \sin\theta_L^e \sin\beta_e)(\ell^2 c \sin^2\theta_L^e - \ell u_e \sin\theta_L^e \sin\beta_e)\Big]$$

$$C(2,2) = -(m_L \ell c^2 \cos\beta_e \sin\theta_L^e + K_L \ell c V_L^e \sin\beta_e \sin\theta_L^e)$$

$$C(2,4) = -K_L \ell V_L^e \sin\theta_L^e$$

$$C(3,4) = 1$$

$$C(4,1) = -\Big[(m_v + m_L)\, c - \frac{K_L \ell c}{V_L^e} \sin\theta_L^e \cos\beta_e (u_e - \ell c \sin\theta_L^e \sin\beta_e)\Big]$$

APPENDIX A [Cont'd]

Matrix C [Cont'd]

$$C(4,3) = -\left[-m_L \ell c^2 \sin\beta_e \cos\theta_L^e + K_L \ell c V_L^e \cos\theta_L^e \cos\beta_e + \frac{K_L \ell c}{V_L^e} \sin\theta_L^e \cos\beta_e \left(\ell^2 c^2 \sin\theta_L^e \cos\theta_L^e - \ell c u_e \cos\theta_L^e \sin\beta_e\right)\right]$$

$$C(4,4) = -\left[2m_L \ell c \cos\beta_e \cos\theta_L^e + K_L \ell V_L^e \cos\theta_L^e \sin\beta_e + \frac{K_L \ell^2 c}{V_L^e} u_e \sin\theta_L^e \cos\theta_L^e \cos^2\beta_e\right]$$

$$C(4,5) = \left[m_L \ell c^2 \sin\theta_L^e \cos\beta_e + K_L \ell c V_L^e \sin\theta_L^e \sin\beta_e + \frac{K_L \ell^2 c^2}{V_L^e} u_e \sin^2\theta_L^e \cos^2\beta_e\right]$$

$$C(4,7) = -\left[(m_v + m_L) u_e - 2m_L \ell c \sin\beta_e \sin\theta_L^e + K_L \ell V_L^e \sin\theta_L^e \cos\beta_e + \frac{K_L \ell c}{V_L^e} \sin\theta_L^e \cos\beta_e \left(\ell^2 c^2 \sin^2\theta_L^e - \ell u_e \sin\theta_L^e \sin\beta_e\right)\right]$$

$$C(5,1) = -\left[-m_L c \cos\beta_e + K_L V_L^e \sin\beta_e + \frac{K_L}{V_L^e} \left(u_e \sin\beta_e - \ell c \sin\theta_L^e\right)\left(u_e - \ell c \sin\theta_L^e \sin\beta_e\right)\right]$$

APPENDIX A [Cont'd]

Matrix C [Cont'd]

$$C(5,3) = -\left[-K_L\, cV_L^e \cos\theta_L^e + \frac{K_L}{V_L^e}\,(u_e \sin\beta_e - \ell c \sin\theta_L^e)\,(\ell^2 c^2 \sin\theta_L^e \cos\theta_L^e - \ell c u_e \cos\theta_L^e \sin\beta_e)\right]$$

$$C(5,4) = -\left[-2m_L \ell c \cos\theta_L^e + \frac{K_L}{V_L^e}\,\ell u_e \cos\theta_L^e \cos\beta_e\,(u_e \sin\beta_e - \ell c \sin\theta_L^e)\right]$$

$$C(5,5) = -\left[m_L c u_e \sin\beta_e + K_L V_L^e u_e \cos\beta_e - \frac{K_L \ell c}{V_L^e}\, u_e \sin\theta_L^e \cos\beta_e\,(u_e \sin\beta_e - \ell c \sin\theta_L^e)\right]$$

$$C(5,7) = -\left[m_L u_e \cos\beta_e - K_L \ell V_L^e \sin\theta_L^e + \frac{K_L}{V_L^e}\,(u_e \sin\beta_e - \ell c \sin\theta_L^e)\,(\ell^2 c \sin^2\theta_L^e - \ell u_e \sin\theta_L^e \sin\beta_e)\right]$$

$$C(6,7) = 1$$

$$C(7,1) = -\left[m_L c \sin\beta_e \cos\theta_L^e + K_L V_L^e \cos\beta_e \cos\theta_L^e + \frac{K_L u_e}{V_L^e} \cos\beta_e \cos\theta_L^e\,(u_e - \ell c \sin\theta^e \sin\beta_e)\right]$$

$$C(7,2) = -K_L u_e V_L^e \sin\theta_L^e$$

APPENDIX A [Cont'd]

Matrix C [Cont'd]

$$C(7,3) = -\Big[-m_L c u_e \sin\beta_e \sin\theta_L^e - m_L \ell c^2 \cos 2\theta_L^e + m_L g \cos\theta_L^e - K_L V_L^e u_e \cos\beta_e \sin\theta_L^e + \frac{K_L u_e}{V_L^e} \cos\beta_e \cos\theta_L^e (\ell^2 c^2 \sin\theta_L^e \cos\theta_L^e - \ell c u_e \cos\theta_L^e \sin\beta_e)\Big]$$

$$C(7,4) = -\Big[K_L V_L^e \ell + \frac{K_L \ell}{V_L} u_e^2 \cos^2\theta_L^e \cos^2\beta_e\Big]$$

$$C(7,5) = -\Big[m_L c u_e \cos\theta_L^e \cos\beta_e - K_L u_e V_L^e \cos\theta_L^e \sin\beta_e - \frac{K_L \ell}{V_L^e} c u_e^2 \sin\theta_L^e \cos\theta_L^e \cos^2\beta_e\Big]$$

$$C(7,7) = -\Big[m_L u_e \sin\beta_e \cos\theta_L^e - m_L \ell c \sin 2\theta_L^e + \frac{K_L u_e}{V_L^e} \cos\beta_e \cos\theta_L^e (\ell^2 c \sin^2\theta_L^e - \ell u_e \sin\theta_L^e \sin\beta_e)\Big]$$

NOTE: $V_L^e = (u_e^2 + \ell^2 c^2 \sin^2\theta_L^e - 2\ell c u_e \sin\theta_L^e \sin\beta_e)^{\frac{1}{2}}$

APPENDIX A [Cont'd]

Equation 3.41

$$\dot{\overline{X}} = \underline{A}\,\overline{X} + \underline{B}\,\overline{U}$$

$$\overline{X}^T = [u\ w\ \theta_v\ q_v\ \theta_L\ q_L\ v\ \phi_v\ p_v\ r_v\ \lambda\ r_L]$$

$$\overline{U}^T = [\theta_R\ \phi_R\ \theta_t\ \theta_{tr}]$$

$\underline{A}$ and $\underline{B}$ are defined in terms of $\underline{P}$, $\underline{Q}$ and $\underline{R}$ as

$$\underline{A} = \underline{P}^{-1}\underline{Q},\quad \underline{B} = \underline{P}^{-1}\underline{R}$$

Matrix P

$P(1,1) = m_v + m_L$

$P(1,4) = m_L h_P$

$P(1,6) = -m_L \ell \cos\theta_L$

$P(2,7) = m_v + m_L$

$P(2,9) = -m_L h_p$

$P(2,11) = -m_L \ell \sin\theta_L$

$P(2,12) = m_L \ell_p$

$P(3,2) = m_v + m_L$

$P(3,4) = -m_L \ell_P$

$P(3,6) = -m_L \ell \sin\theta_L$

APPENDIX A [Cont'd]

Matrix P [Cont'd]

$P(4,7) = -m_L h_P$

$P(4,9) = I_{xx} + m_L h_P^2$

$P(4,11) = m_L h_P \ell \sin\theta_L$

$P(4,12) = -m_L h_P \ell_P$

$P(5,1) = m_L h_P$

$P(5,2) = -m_L \ell_P$

$P(5,4) = I_{yy} + m_L (h_P^2 + \ell_P^2)$

$P(5,6) = m_L \ell (\ell_P \sin\theta_L - h_P \cos\theta_L)$

$P(6,7) = m_L \ell_P$

$P(6,9) = -m_L \ell_P h_P$

$P(6,11) = -m_L \ell_P \ell \sin\theta_L$

$P(6,12) = I_{zz} + m_L \ell_P^2$

$P(7,1) = -m_L \ell \cos\theta_L$

$P(7,2) = -m_L \ell \sin\theta_L$

$P(7,4) = -m_L \ell (h_P \cos\theta_L - \ell_P \sin\theta_L)$

APPENDIX A [Cont'd]

Matrix P [Cont'd]

$P(7,6) = m_L \ell^2$

$P(8,7) = -m_L \ell \sin\theta_L$

$P(8,9) = m_L \ell h_P \sin\theta_L$

$P(8,11) = m_L \ell^2 \sin^2\theta_L$

$P(8,12) = -m_L \ell \ell_P \sin\theta_L$

$P(9,5) = 1$

$P(10,10) = 1$

$P(11,3) = 1$

$P(12,8) = 1$

Matrix Q

$\bar{a} = \frac{1}{2} \rho b c \Omega^2 R^3$

$TX1 = -2 \rho A_D v_i \cos^2\phi_R \sin^2\theta_R - \bar{a} C_{d_o}/2\Omega R$

$TX2 = -\rho A_D v_i \sin 2\phi_R \sin\theta_R$

$TX3 = \rho A_D v_i \cos^2\phi_R \sin 2\theta_R$

$TX4 = -h\rho A_D v_i \sin 2\phi_R \sin\theta_R$

APPENDIX A [Cont'd]

Matrix Q [Cont'd]

$$TX5 = 2H\rho A_D v_i \cos^2\phi_R \sin^2\theta_R + h\bar{a} C_{d_o}/2\Omega R$$

$$TY1 = -\rho A_D v_i \sin 2\phi_R \sin\theta_R$$

$$\bar{V} = (c\Omega^2 R^3)_{tr}/(c\Omega^2 R^3)_R$$

$$PN = \bar{V} (m_v + n_L) g/(2C_T/a\sigma)$$

$$PP = PN (\mu\theta_{tr})/(\Omega R)_{tr}$$

$$TY2 = -2\rho A_D v_i \sin^2\phi_R - \bar{a} C_{d_o}/2\Omega R$$

$$TY3 = \rho A_D v_i \sin 2\phi_R \cos\theta_R$$

$$TR2 = PN/2(\Omega R)_{tr}$$

$$TY4 = -2h\rho A_D v_i \sin^2\phi_R - h\bar{a} C_{d_o}/2\Omega R$$

$$\underline{S} = \underline{K}^{-1} \underline{L}$$

$$K(1,1) = -1.5\bar{e} \Omega^2/(1 - \bar{e})$$

$$K(1,2) = (\gamma\Omega^2/8) (1 - 0.5\mu^2)$$

$$K(2,1) = (-\gamma\Omega^2/8) (1 + 0.5\mu^2)$$

$$K(2,2) = K(1,1)$$

$$L(1,1) = \gamma\Omega/8$$

$$L(1,2) = -2\Omega [1 + 1.53\bar{e}/(1 - \bar{e})]$$

$$L(2,1) = -L (1,2)$$

$$L(2,2) = L(1,1)$$

APPENDIX A [Cont'd]

Matrix Q [cont'd]

$DT1 = -T\,[\sin\phi_R \sin\theta_R\, S(1,1) + \cos\phi_R \cos\theta_R\, S(2,1)]$

$DT2 = -T\,[\sin\phi_R \sin\theta_R\, S(1,2) + \cos\phi_R \cos\theta_R\, S(2,2)]$

$TR3 = (PN)\, \ell_{tr}/2\, (\Omega R)_{tr}$

$TR4 = \bar{V}\, z_{tr}/2\, (\Omega R)_{tr}$

$TY5 = h\rho A_D\, v_i \sin 2\phi_R \sin\theta_R$

$PQ = (PN)\, \mu\theta_{tr}\, z_{tr}/(\Omega R)_{tr}$

$TZ1 = \rho A_D\, v_i \cos^2\phi_R \sin 2\theta_R$

$TZ2 = \rho A_D\, v_i \sin 2\phi_R \cos\theta_R$

$TZ3 = -2\rho A_D\, v_i \cos^2\phi_R \cos^2\theta_R$

$TZ4 = h\rho A_D\, v_i \sin 2\phi_R \cos\theta_R$

$TZ5 = -h\rho A_D\, v_i \cos^2\phi_R \sin 2\theta_R$

$Q(1,1) = TX1 - 2u_e\, (K_v + K_L)$

$Q(1,2) = TX3$

$Q(1,3) = -(m_v + m_L)g$

$Q(1,4) = TX5 - 2K_L\, u_e\, h_P = DT2$

$Q(1,6) = 2K_L\, u_e \ell \cos\theta_L$

$Q(1,7) = TX2$

$Q(1,9) = TX4$

APPENDIX A [Cont'd]

Matrix Q [Cont'd]

$Q(2,1) = TY1 + PP$

$Q(2,2) = TY3$

$Q(2,4) = TY5 - PQ + T^e \cos\phi_R \; S(1,2)$

$Q(2,7) = TY2 - (K_v + K_L)\, u_e - TR2$

$Q(2,8) = (m_v + m_L)\, g$

$Q(2,9) = TY4 + K_L u_e h_P - TR4 + T^e \cos\phi_R \; S(1,1)$

$Q(2,11) = K_L u_e \ell \sin\theta_L$

$Q(2,12) = -K_L u_e \ell_P + TR3$

$Q(3,1) = TZ1$

$Q(3,2) = TZ3 - (K_v + K_L)\, u_e$

$Q(3,4) = TZ5 + K_L u_e \ell_P$

$Q(3,6) = K_L u_e \ell \sin\theta_L$

$Q(3,7) = TZ2$

$Q(3,9) = TZ4$

$Q(4,1) = h(TY1) + z_{tr}(PP)$

$Q(4,2) = h(TY3)$

$Q(4,4) = h(TY5) - z_{tr}(PQ) + hT^e \cos\phi_R \; S(1,2)$

$Q(4,7) = h(TY2) - z_{tr}(TR2) + K_L u_e h_P$

APPENDIX A [Cont'd]

Matrix Q [Cont'd]

$$Q(4,8) = -m_L g h_P$$

$$Q(4,9) = h(TY4) - z_{tr}(TR4) - K_L u_e h_P^2 + hT^e \cos\phi_R \; S(1,1)$$

$$Q(4,11) = -K_L u_e h_P \ell \sin\theta_L$$

$$Q(4,12) = z_{tr}(TR3) + K_L u_e h_P \ell_P$$

$$Q(5,1) = -h(TX1) + C_m^f (\lambda + 2\mu\theta_R^e)/\Omega R - C_t [\lambda + 2\mu (\theta_R + \theta_t)]/\Omega R$$

$$Q(5,2) = -h(TX3) + \mu (C_m^f - C_m^t) + K_L u_e \ell_P$$

$$Q(5,3) = -m_L g h_P$$

$$Q(5,4) = -h(TX5) - h C_m^f (\lambda + 2\mu\theta_R)/\mu R + h C_m^t [\lambda + 2\mu (\theta_R + \theta_R)]/\Omega R$$

$$Q(5,6) = K_L u_e \ell (2h_P \cos\theta_L - \ell_P \sin\theta_L)$$

$$Q(5,7) = -h(TX2)$$

$$Q(5,9) = -h(TX4) - h(DT1)$$

$$Q(6,1) = -\ell_{tr}(PP)$$

$$Q(6,4) = \ell_{tr}(PQ)$$

$$Q(6,7) = \ell_{tr}(TR2) - K_L u_e \ell_P$$

$$Q(6,9) = \ell_{tr}(TR4) + K_L u_e \ell_P h_P$$

$$Q(6,11) = K_L u_e \ell_P \ell \sin\theta_L$$

APPENDIX A [Cont'd]

Matrix Q [Cont'd] .

$Q(6,12) = -\ell_{tr}(TR3) - K_L u_e \ell_P^2$

$Q(7,1) = 2K_L u_e \ell \cos\theta_L$

$Q(7,2) = K_L u_e \ell \sin\theta_L$

$Q(7,4) = K_L u_e \ell h_P \cos\theta_L$

$Q(7,5) = K_L u_e^2 \ell \sin\theta_L - m_L g \ell \cos\theta_L$

$Q(7,6) = (-K_L u_e \ell^2)(1 + \cos^2\theta_L^e)$

$Q(8,1) = K_L \ell u_e \sin\theta_L$

$Q(8,10) = -K_L u_e^2 \ell \sin\theta_L$

$Q(8,11) = -K_L u_e \ell^2 \sin^2\theta_L$

$Q(9,6) = 1$

$Q(10,11) = 1$

$Q(11,4) = 1$

$Q(12,9) = 1$

$TX7 = 2\rho A_D v_i (u_e \sin^2\theta_R \sin 2\phi_R - v_i \sin\phi_R \sin\theta_R)$

$TX8 = -2\rho A_D v_i (u_e \cos^2\phi_R \sin 2\theta_R - v_i \cos\phi_R \cos\theta_R)$

$TY7 = -2\rho A_D v_i (u_e \cos 2\phi_R \sin\theta_R - v_i \cos\phi_R)$

APPENDIX A [Cont'd]

Matrix Q [Cont'd]

$TY8 = -\rho A_D v_i u_e \sin 2\phi_R \cos\theta_R$

$TZ7 = 2\rho A_D v_i (v_i \sin\phi_R \cos\theta_R - u_e \sin 2\phi_R \cos\theta_R \sin\theta_R)$

$TZ8 = 2\rho A_D v_i (u_e \cos^2\phi_R \cos 2\theta_R + v_i \cos\phi_R \sin\theta_R)$

$R(1,1) = TX7$

$R(1,2) = TX8$

$R(2,1) = TY7$

$R(2,2) = TY8$

$PC = \overline{V} (m_v + m_L) g (1 + \frac{3}{2}\mu^2)/3 (2c_T/a\sigma)$

$R(2,4) = PC$

$R(3,1) = TZ7$

$R(3,2) = TZ8$

$R(4,1) = h(TY7)$

$R(4,2) = h(TY8)$

$R(4,5) = z_{tr}(PC)$

$R(5,1) = -h(TX7)$

$R(5,2) = -h(TX8)$

APPENDIX A [Cont'd]

Equation 5.2

$$\underline{SA} \begin{Bmatrix} \dot{\bar{X}}_v \\ \dot{\bar{X}}_L \end{Bmatrix} = \underline{SB}\ \bar{X}_R + \underline{SC}\ \dot{\bar{X}}_R + \underline{SD} \begin{Bmatrix} \bar{X}_v \\ \bar{X}_L \end{Bmatrix} + \underline{SE}\ \bar{U}$$

$\underline{SA}$ and $\underline{P}$ in Equation 3.41 [see in Appendix] are same and will not be defined here.

Matrix SB

$Z4 = \bar{a}/3\Omega$

$Z5 = -\bar{a}\mu/4\Omega R$

$Z7 = -(\bar{a}/\Omega R)\ (\frac{3}{4}\ \theta_s + \mu\theta_0)$

$Z8 = (-\bar{a}/\Omega R)\ (\frac{3}{4}\ \theta_c - \mu\beta_0)$

$Z9 = (-\bar{a}/\Omega R)\ [\frac{1}{2} + \lambda\ (\theta_0 - \theta_0 K)]$

$Z11 = (-\bar{a}\ \bar{h}/\Omega R)\ [\theta_c/2 + \phi_R/4 - \mu\beta_0/2 + \mu/4]$

$Z13 = (-\bar{a}\ \bar{h}/\Omega R)\ [-\phi_R/2 + \theta_R/4 - \mu\theta_0/2]$

$Z19 = -\bar{a}\ (\frac{1}{3} + \mu^2/2)$

$Z20 = -\bar{a}\ (\mu^2/4 + \mu/4)$

$X1 = \bar{a}\ (-\mu\beta_0/2 + \phi_R/6 + \theta_c/6)$

$X2 = \bar{a}\beta_0/6$

$X3 = F_z^e + \bar{a}\lambda/4 + \theta_R(Z3)$

$X4 = \theta_R(Z4)$

APPENDIX A [Cont'd]

Matrix SB [Cont'd]

$$X5 = \theta_R(Z5) + (\bar{a}/\Omega)\ (\theta_0/6 - \lambda/2)$$

$$X6 = \theta_R(Z6) + (\bar{a}/\Omega)\ \beta_0/6$$

$$Q8 = (-\bar{a}/\Omega R)\ [C_{d_o}/2a + \theta_0\lambda/2 + \beta_0{}^2/4]$$

$$X7 = Q8 + \theta_R(Z7)$$

$$Q9 = 1.5\ \bar{a}\beta_0\ (\theta_0/2 - \lambda)/\Omega R$$

$$X8 = Q9 + \theta_R(Z8)$$

$$X9 = \theta_R(Z9)$$

$$X11 = (\bar{a}/\Omega)\ (\theta_0/6 - \lambda/2) + \theta_R(Z11) + (\tfrac{3}{2})\ (\bar{a}\ \bar{h}/\Omega)\ \beta_0 \left(\frac{\theta_0}{2} - \lambda \right)$$

$$X13 = (\bar{a}\beta_0/6\Omega) + \theta_R(Z13) + (\bar{h}\ \bar{a}/\Omega)\ [C_{d_o}/2a + \theta_0\lambda/2 + \beta_0{}^2/4]$$

$$X19 = -\mu\bar{a}\lambda/2 + \theta_R(Z19)$$

$$X20 = -\bar{a}\lambda/4 + \theta_R(Z20)$$

$$X21 = \bar{a}\beta_0/6 + \theta_R(Z21)$$

$$Y1 = -\tfrac{3}{4}\ \mu\ \bar{a}\ (\theta_0/2 - \lambda) + \theta_R\ \bar{a}/6 - \theta_s\ \bar{a}/6$$

$$Y2 = -\phi_R(Z2) - F_z^e - \bar{a}\lambda/4$$

$$Y3 = \bar{a}\beta_0/6 - \phi_R(Z3)$$

$$Y4 = -\phi_R(Z4)$$

APPENDIX A [Cont'd]

Matrix SB [Cont'd]

$Y5 = -\phi_R(Z5) - \bar{a}\beta_0/6\Omega$

$Y6 = -\phi_R(Z6) + (\bar{a}/\Omega)\ (\theta_0/6 - \lambda/2)$

$Y7 = (-\frac{3}{4})\ \bar{a}\beta_0\ (\theta_0/2 - \lambda)/\Omega R - \phi_R(Z7)$

$Y8 = (-\bar{a}/\Omega R)\ [C_{d_o}/2a + \theta_0\lambda/2 + \beta_0{}^2/4] - \phi_R(Z8)$

$Y9 = -\phi_R(Z9)$

$Y11 = (-\bar{a}/\Omega)\ \beta_0/6 - \phi_R(Z11) - (\bar{h}\ \bar{a}/\Omega)\ [C_{d_o}/2a + \theta_0\lambda/2 + \beta_0/4]$

$Y13 = (\bar{a}/\Omega)\ (\theta_0/6 - \lambda/2) - \phi_R(Z13) + \frac{3}{4}\ \bar{h}\ \bar{a}\beta_0\ (\theta_0/2 - \lambda)$

$Y19 = -3\mu\bar{a}\ \beta_0/8 - \phi_R(Z19)$

$Y20 = -\phi_R\ (Z20) - \bar{a}\beta_0/6$

$Y21 = -\phi_R(Z21) - \bar{a}\lambda/4$

SB(1,1) = X1

SB(1,2) = X2

SB(1,3) = X3

SB(2,1) = Y1

SB(2,2) = Y2

SB2,3) = Y3

APPENDIX A [Cont'd]

Matrix SB [Cont'd]

SB(3,1) = Z1

SB(3,2) = Z2

SB(3,3) = Z3

SB(4,1) = h(Y1)

SB(4,2) = h(Y2)

SB(4,3) = h(Y3)

SB(5,1) = -h(X1)

SB(5,2) = -h(X2)

SB(5,3) = $-h(X3) + \mu^2 \ (C_m^f - C_t^t)$

Matrix SC

SC(1,1) = X4

SC(1,2) = X5

SC(1,3) = X6

SC(2,1) = Y4

SC(2,2) = Y5

SC(2,3) = Y6

SC(3,1) = Z4

APPENDIX A [Cont'd]

Matrix SC [Cont'd]

$SC(3,2) = Z5$

$SC(3,3) = Z6$

$SC(4,1) = h(Y4)$

$SC(4,2) = h(Y5)$

$SC(4,3) = h(Y6)$

$SC(5,1) = -h(X4)$

$SC(5,2) = -h(X5)$

$SC(5,3) = -h(X6)$

Matrix SD

$AX = \overline{V}\ (m_v + m_L)g/(2C_T/a\sigma)$

$SD(1,1) = X7 - 2\ (K_v + K_L)\ u_e$

$SD(1,2) = X8$

$SD(1,3) = X9$

$SD(1,5) = X11$

$SD(1,6) = -(m_v + m_L)g$

$SD(1,7) = X13 - 2K_L u_e h_P$

$SD(1,10) = 2K_L u_e \ell \cos\theta_L$

APPENDIX A [Cont'd]

Matrix SD [Cont'd]

$$Q14 = \overline{V}\,(m_v + m_L)g\,\theta_{tr}\,\mu/(\Omega R)_{tr}/(2C_T/a\sigma)$$

$$SD(2,1) = Q14 + Y7$$

$$SD(2,2) = Y8 - (K_v + K_L)\,u_e - AX/2(\Omega R)_{tr}$$

$$SD(2,3) = Y9$$

$$SD(2,4) = (m_v + m_L)g$$

$$SD(2,5) = K_L u_e h_P + Y11 - AX(z_{tr})/2(\Omega R)_{tr}$$

$$SD(2,7) = -(Q14)\,z_{tr} + Y13$$

$$SD(2,8) = -K_L u_e \ell_P + (AX)\,\ell_{tr}/2(\Omega R)_{tr}$$

$$SD(2,12) = K_L u_e \ell \sin\theta_L$$

$$SD(3,1) = Z7$$

$$SD(3,2) = Z8$$

$$SD(3,3) = Z9 - (K_v + K_L)\,u_e$$

$$SD(3,5) = Z11$$

$$SD(3,7) = Z13 + K_L u_e \ell_P$$

$$SD(3,10) = K_L u_e \ell \sin\theta_L$$

$$SD(4,1) = h(Y7) + z_{tr}(Q14)$$

$$SD(4,2) = h(Y8) + K_L u_e h_P$$

APPENDIX A [Cont'd]

Matrix SD [Cont'd]

$$SD(4,3) = h(Y9)$$

$$SD(4,4) = -m_L g h_P$$

$$SD(4,5) = h(Y11) - K_L u_e h_P^2 - z_{tr}^2 (AX)/2(\Omega R)_{tr}$$

$$SD(4,7) = h(Y13) - z_{tr}^2 (Q14)$$

$$SD(4,8) = K_L u_e h_P \ell_P + z_{tr}(AX)\, \ell_{tr}/2(\Omega R)_{tr}$$

$$SD(4,12) = -K_L u_e h_P \ell \sin\theta_L$$

$$SD(5,1) = -h(X7) + C_m^f (\lambda/\Omega R + 2\mu\theta_R/\Omega R) - (C_t^t/\Omega R)\,[\lambda + 2\mu\,(\theta_R + \theta_t)] - 2K_L u_e h_P$$

$$SD(5,2) = -h(X8)$$

$$SD(5,3) = (\mu/\Omega R)\,(C_m^f - C_t^t) - h(X9) + K_L u_e \ell_P$$

$$SD(5,5) = -h(X11)$$

$$SD(5,6) = -m_L g h_P$$

$$SD(5,7) = -h(X13) + C_m^f\,[-\lambda\bar{h}/\Omega - 2\theta_R\,\mu\bar{h}/\Omega] + (C_t/\Omega)\,[\lambda\bar{h} + 2\mu\bar{h}\,(\theta_R + \theta_t)] - K_L u_e\,(2h_P^2 + \ell_P^2)$$

$$SD(5,10) = K_L u_e \ell\,(2h_P \cos\theta_L - \ell_P \sin\theta_L)$$

$$SD(6,1) = -\ell_{tr}(Q14)$$

APPENDIX A [Cont'd]

Matrix SD [Cont'd]

$SD(6,2) = -K_L u_e \ell_P + \ell_{tr}(AX)/2(\Omega R)_{tr}$

$SD(6,5) = K_L u_e \ell_P h_P + \ell_{tr}(AX)\, z_{tr}/2(\Omega R)_{tr}$

$SD(6,7) = \ell_{tr}\, z_{tr}$ (Q14)

$SD(6,8) = -K_L u_e \ell_P^2 - \ell_{tr}^2\, (AX)/2(\Omega R)_{tr}$

$SD(6,12) = K_L u_e \ell_P \ell \sin\theta_L$

$SD(7,1) = 2\, K_L \ell\, u_e \cos\theta_L$

$SD(7,3) = K_L \ell\, u_e \sin\theta_L$

$SD(7,7) = K_L \ell\, u_e h_P \cos\theta_L$

$SD(7,9) = K_L u_e \ell^2 \sin\theta_L - m_L g \ell \cos\theta_L$

$SD(7,10) = -K_L u_e \ell^2 (1 + \cos^2\theta_L)$

$SD(8,2) = K_L u_e \ell \sin\theta_L$

$SD(8,11) = -K_L u_e^2 \ell \sin\theta_L$

$SD(8,12) = -K_L u_e \ell^2 \sin^2\theta_L$

$SD(9,5) = 1$

$SD(10,7) = 1$

$SD(11,10) = 1$

$SD(12,12) = 1$

APPENDIX A [Cont'd]

Matrix SE

SE(1,1) = X19

SE(1,2) = X20

SE(1,3) = X21

SE(2,1) = Y19

SE(2,2) = Y20

SE(2,3) = Y21

Q19 = $\overline{V}\ (m_v + m_L)g\ (1 + \frac{3}{2}\ \mu^2)/3(2C_T/a\sigma)$

SE(2,5) = Q19

SE(3,1) = Z19

SE(3,2) = Z20

SE(3,3) = Z21

SE(4,1) = h(Y19)

SE(4,2) = h(Y20)

SE(4,3) = h(Y21)

SE(4,5) = z_{tr} (-Q19)

SE(5,1) = -h(X19)

SE(5,2) = -h(X20)

APPENDIX A [Cont'd]

Matrix SE [Cont'd]

$SE(5,3) = -h(X21)$

$SE(5,4) = -C_t^t \mu^2$

$SE(6,5) = -\ell_{tr}$ (Q19)

Equation 5.3

$$\ddot{\bar{X}}_R = \underline{MB}\,\bar{X}_R + \underline{MC}\,\dot{\bar{X}}_R + \underline{MD}\,\bar{X}_v + \underline{ME}\,\dot{\bar{X}}_v + \underline{MF}\,\bar{U}$$

$$\bar{X}_R^T = [\beta_0 \ \phi_R \ \theta_R]$$

$$\bar{X}_v^T = [u \ v \ w \ \phi_v \ p_v \ \theta_v \ q_v \ r_v]$$

$$\bar{U}^T = [\theta_0 \ \theta_s \ \theta_c \ \theta_t \ \theta_{tr}]$$

Matrix MB

$$MB(1,1) = -\left[1 + \tfrac{3}{2}\frac{\bar{e}}{1-\bar{e}}\right]\Omega^2$$

$$MB(2,2) = -\tfrac{3}{2}\frac{\bar{e}}{1-\bar{e}}\,\Omega^2$$

$$MB(2,3) = \frac{\gamma\Omega^2}{8}(1 - \tfrac{1}{2}\Omega^2)$$

$$MB(3,1) = \frac{\gamma\Omega^2}{6}\mu$$

$$MB(3,2) = -\frac{\gamma\Omega^2}{8}(1 + \tfrac{1}{2}\mu^2)$$

APPENDIX A [Cont'd]

Matrix MB [Cont'd]

$$MB(3,3) = -\frac{3}{2}\frac{\bar{e}}{1-\bar{e}}\Omega^2$$

Matrix MC

$$MC(1,1) = -\frac{\gamma\Omega}{8}$$

$$MC(1,2) = \frac{\gamma\Omega}{12}\mu$$

$$MC(2,1) = \frac{\gamma\Omega}{6}\mu$$

$$MC(2,2) = -\frac{\gamma\Omega}{8}$$

$$MC(2,3) = 2\Omega$$

$$MC(3,2) = -2\Omega$$

$$MC(3,3) = -\frac{\gamma\Omega}{8}$$

Matrix MD

$$MD(1,1) = \frac{\gamma\Omega^2}{8}\,[4\mu\theta_0 + 2\theta_s]/\Omega R$$

$$MD(1,2) = \frac{\gamma\Omega^2}{8}\,[2\theta_c - 2\lambda k/3]/\Omega R$$

$$MD(1,3) = \frac{\gamma\Omega^2}{8}\,[\tfrac{4}{3} + 2\lambda\theta_0 + \tfrac{2}{3}\lambda k\theta_c]/\Omega R$$

$$MD(1,5) = \frac{\gamma\Omega}{12}\,[\mu - \lambda\bar{h}k]$$

APPENDIX A [Cont'd]

Matrix MD [Cont'd]

$$MD(2,1) = \frac{\gamma\Omega^2}{8} \left[-\mu\theta_c + 2\lambda - 4\theta_0 - 6\mu\theta_s\right]/\Omega R$$

$$MD(2,2) = \frac{\gamma\Omega^2}{8} \left[-\tfrac{4}{3}\beta_0 + \mu\phi_R - 2\mu\theta_c\right]/\Omega R$$

$$MD(2,3) = \frac{\gamma\Omega^2}{8} \left[-2\mu - 2\lambda\theta_s\right]/\Omega R$$

$$MD(2,5) = -\frac{\gamma\Omega}{8}$$

$$MD(2,7) = 2\Omega\left[1 + \tfrac{3}{2}\frac{\bar{e}}{1-\bar{e}}\right] \frac{\gamma\Omega}{4}\lambda\bar{h}$$

$$MD(3,1) = \frac{\gamma\Omega^2}{8} \left[\tfrac{4}{3}\beta_0 - \mu\phi_R - 2\mu\theta_c\right]/\Omega R$$

$$MD(3,2) = \frac{\gamma\Omega^2}{8} \left[-\mu\theta_R + 2\lambda - 4\theta_0 - 2\mu\theta_s\right]/\Omega R$$

$$MD(3,3) = \frac{\gamma\Omega^2}{8} \left[-\tfrac{4}{3}\lambda K_{vi}\theta_0 - 2\lambda\theta_c\right]/\Omega R$$

$$MD(3,5) = -2\Omega\left[1 + \tfrac{4}{3}\frac{\bar{e}}{1-\bar{e}}\right] + \frac{\gamma\Omega}{4}\lambda\bar{h}$$

$$MD(3,7) = -\frac{\gamma\Omega}{8}$$

Matrix ME

$$ME(2,5) = -\left[1 + \tfrac{3}{2}\frac{\bar{e}}{1-\bar{e}}\right]$$

APPENDIX A [Cont'd]

Matrix ME [Cont'd]

$$ME(3,7) = -\left(1 + \tfrac{3}{2} \frac{\bar{e}}{1 - \bar{e}} \right)$$

Matrix MF

$$MF(1,1) = \frac{\gamma \Omega^2}{8} [1 + 2\mu^2]$$

$$MF(1,2) = \frac{\gamma \Omega^2}{4} \mu$$

$$MF(2,1) = -\frac{\gamma \Omega^2}{2} \mu$$

$$MF(2,2) = \frac{\gamma \Omega^2}{8} [1 + 3\mu^2]$$

$$MF(3,3) = -\frac{\gamma \Omega^2}{8} [1 + \mu^2]$$

APPENDIX A [Cont'd]

Equation 5.4

$$\underline{A}\,\dot{\overline{X}} = \underline{B}\,\overline{X} + \underline{C}\,\overline{U}$$

Matrix A

$$\begin{bmatrix} [I(3,3)] & [0(3,15) &] \\ [0(3,3)] & [I(3,3)] & [-\ ME(3,12)] \\ \begin{bmatrix} \\ 0(12,6) \\ \\ \end{bmatrix} & & \begin{bmatrix} \\ SA(12,12) \\ \\ \end{bmatrix} \end{bmatrix}$$

Matrix B

$$\begin{bmatrix} [0(3,3)] & [I(3,3)] & [0(3,12) &] \\ [MB(3,5)] & [MC(3,3)] & [\ MD(3,12) &] \\ \begin{bmatrix} \\ SB \\ (3,12) \\ \\ \end{bmatrix} & \begin{bmatrix} \\ SC \\ (3,12) \\ \\ \end{bmatrix} & \begin{bmatrix} \\ SD \\ (12,12) \\ \\ \end{bmatrix} \end{bmatrix}$$

Matrix C

$$\begin{bmatrix} [0(3,5) &] \\ [MF(3,5)] & \\ \begin{bmatrix} \\ SE \\ (12,5) \\ \\ \end{bmatrix} & \end{bmatrix}$$

APPENDIX B - DESCRIPTION AND COMPUTATION OF MODES AND MODESHAPES OF A LINEAR SYSTEM

Consider a linear, time-invariant system

$$\dot{\overline{X}} = \underline{A}\overline{X} + \underline{B}\overline{U} \tag{B-1}$$

where $\overline{X}$ is an n-vector of state variables and $\overline{U}$ is an m-vector of control variables. In the absence of control inputs, $\overline{U} = 0$, the general solution to this system of equations can be expressed as

$$\overline{X}(t) = \sum_{r=1}^{n} \overline{X}_r(0) e^{\lambda_r t} \tag{B-2}$$

where λ_r are the eigenvalues of $\underline{A}$ [assumed distinct] and $\overline{X}_r(0)$ are the corresponding eigenvectors (ZA1). Each of these eigenvectors is a special set of initial conditions that result in special, simple motion called the mode of the system. Each eigenvalue characterizes the behavior of the system in the corresponding mode; when λ is real, the mode is exponential in form and is stable for $\lambda < 0$ [convergence] and is unstable for $\lambda > 0$ [divergence]. When λ is complex, for a real matrix $\underline{A}$, the system always has another mode corresponding to conjugate of λ. Such a conjugate pair, $\lambda_{1,2} = n \pm \omega i$, define an oscillatory mode

of period $T = 2\pi/\omega$. If $n > 0$ the oscillation is divergent and indicates dynamic instability, while $n < 0$ indicates damped oscillation. The eigenvectors corresponding to these eigenvalues are also conjugate complex pairs. In this analysis the eigenvector corresponding to the eigenvalue $\lambda_1 = n - \omega i$ of a complex pair $\lambda_{1,2} = n \pm \omega i$ is presented. Consequently, the phase angle of individual components of such an eigenvector is measured positive in the clockwise direction [see Table I].

Computation of Eigenvalues and Eigenvectors

Eigenvalues and corresponding eigenvectors of the system state matrix [$\underline{A}$ in Equation B-1] were evaluated using a digital computer routine, CIGMAT, that utilizes QR method for determining the eigenvalues. This method has been found to be insensitive to widely separated eigenvalues, which is typical of the configuration in this study. In all the results presented here, each of the eigenvectors has been normalized with respect to its largest element, for the sake of convenience.

During this research other digital computer routines that are similar to CIGMAT were used to check and compare the results obtained through the latter routine.

VITA

The author was born in Tiptur, Karnataka, India, on May 23, 1949. Following his higher-secondary education in NewDelhi, India, he joined Indian Institute of Technology, Madras, and completed the five-year program leading to Bachelor of Technology in Aeronautical Engineering. Upon graduation in 1971, he accepted a graduate assistantship offered to him by the Department of Aerospace and Ocean Engineering at Virginia Polytechnic Institute and State University, Blacksburg, Virginia, to pursue his graduate studies. He was awarded M.S. degree in Aerospace Engineering on March 1, 1973.

He is presently working in the Flight Dynamics Department at Goodyear Aerospace Corporation, Akron, Ohio.

B. L. Nagabhushan

[B. L. Nagabhushan]

SYSTEMATIC INVESTIGATION OF MODELS OF HELICOPTER WITH A SLUNG LOAD

by

B. L. Nagabhushan

(ABSTRACT)

The dynamics, stability and control of a helicopter carrying an externally suspended load have been studied. Several mathematical models are developed to describe the dynamics of such a configuration in varying complexity. The simplest model [seventh order] is obtained by assuming both the helicopter and load to be point masses. The vehicle has a thrust force generated by a rigid, disc rotor that has pitch and roll degrees of freedom. A twelfth order model that includes the rigid body motion of the fuselage has been developed. Further, the dynamics of an articulated rotor is also included in an eighteenth order model.

Stability of the helicopter-load configuration in forward flight and in a coordinated turn has been examined. The system behavior as predicted by the various models are compared to determine the regions in parameter space where the lower order models are adequate. The effects of varying load mass and aerodynamic characteristics, suspension geometry, on the stability of vehicle-load motions are

determined. System stability is satisfactorily augmented by an optimal controller that is designed by using a sixth order model of the helicopter.

A number of numerical experiments have been conducted to determine the effects of rotor dynamics, rotor-fuselage coupling, rigid body motion of the fuselage, on the dynamic stability of this configuration.